MODELLING OF PHOTONIC COMPONENTS BASED ON ÷(3) NONLINEAR PHOTONIC CRYSTALS

Ivan Maksymov

ISBN: 978-84-593-4072-1
Dipòsit Legal: T-1163-2010

ISBN:978-84-593-4072-1/DL:T-1163-2010

Table of contents

UNIVERSITAT ROVIRA I VIRGILI
MODELLING OF PHOTONIC COMPONENTS BASED ON ÷(3) NONLINEAR PHOTONIC CRYSTALS
Ivan Maksymov
ISBN:978-84-593-4072-1/DL:T-1163-2010

ISBN:978-84-593-4072-1/DL:T-1163-2010

ISBN:978-84-593-4072-1/DL:T-1163-2010

Acknowledgements

The author would like to take this opportunity to gratefully thank his scientific supervisor Dr. Lluís Marsal for the guidance throughout the years and support in all aspects of the work. He would like to acknowledge the Universitat Rovira i Virgili for the scholarship that made it possible to conduct the doctoral work. Many thanks are also given to the co-authors for their collaboration and the colleagues from NePhoS group for their friendship.

This work has been supported by Ministerio de Educación y Ciencia, projects No. TIC2002-04184-C05 and TEC2005-02038.

UNIVERSITAT ROVIRA I VIRGILI
MODELLING OF PHOTONIC COMPONENTS BASED ON ÷(3) NONLINEAR PHOTONIC CRYSTALS
Ivan Maksymov
ISBN:978-84-593-4072-1/DL:T-1163-2010

Preface

Photonic crystals are periodic dielectric or metal-dielectric nanostructures that are designed to affect the propagation of electromagnetic waves in the same way as the periodic potential in semiconductor crystals affects the electron motion by defining allowed and forbidden energy bands. If the photonic crystal consists of a material whose properties do not depend on the intensity of the propagating light, it is called linear. In contrast, if the properties of the constituent material depend on the intensity, the photonic crystal is called nonlinear. Nonlinear photonic crystals can be made from dielectrics, glasses, polymers or ferroelectrics.

This dissertation represents a summary of the author's work in the last four years in developing a numerical approach for designing and analysing Kerr nonlinear photonic crystal and all-optical devices based on them. The work carried out is theoretical in nature. It is concerned with such issues as numerical methods, calculations of dispersion characteristics, design and analysis of all-optical devices with possible applications to optical communication systems and optical chips.

The author hopes that his experience with the numerical method employed could be useful as a hint and a guide for other researchers working in the same field.

ISBN:978-84-593-4072-1/DL:T-1163-2010

Objectives of the dissertation, practical importance and author's contribution

The objectives of the work are:

- developing a finite-difference time-domain-based numerical approach to calculate dispersion characteristics of Kerr nonlinear photonic crystals;
- analysing the basic characteristics of the numerical approach such as the spatial resolution, stability, convergence, numerical errors, etc.;
- application of the numerical approach developed to study the characteristics of Kerr nonlinear photonic crystals both perfect and with defects;
- design and analysis of a novel all-optical switching structure for application in optical communication systems or optical chips.

The methods of investigation applied in the dissertation can be classified as follows. First, a novel numerical approach proposed by the author, based on the finite-difference time-domain (FDTD) simulation of the oscillating dipole

ISBN:978-84-593-4072-1/DL:T-1163-2010

radiation and combined with the Kerr nonlinear model, is used to calculate dispersion characteristics in the both linear and nonlinear regimes. In it, the Bloch periodic boundary conditions are imposed to simulate the periodic nature of photonic crystals and the super-cell technique is applied to simulate various defects introduced, for instance, by removing a row of scatterers. In addition, the plane wave expansion method is used as an auxiliary tool to calculate linear dispersion characteristics with the purpose of validating the FDTD-based approach. Secondly, another FDTD-based approach known in the literature as the Order-N method is used to analyse the dispersion characteristics of nonlinear photonic crystal slabs. Absorbing boundary conditions are combined with the Order-N method to take into account the confinement in the vertical direction. In the final part of the work, the information on physical processes in the studied nonlinear photonic crystals serves as a generator of ideas to be implemented in novel optical devices.

The scientific novelty of the work consists in proposing a novel approach for analysing dispersion characteristics of Kerr nonlinear photonic crystals and considering for the first time the behaviour of the oscillating dipole in infinite nonlinear periodic media. The super-cell technique is combined with the approach proposed to calculate dispersion characteristics of nonlinear photonic crystal waveguides and directional couplers. Regarding to the calculation of dispersion characteristics of nonlinear photonic crystal slabs, it is also proposed for the first time to combine the Order-N method with the models of the Kerr nonlinearity. The results achieved by analysing the dispersion characteristics have allowed to understand inherent physical processes in nonlinear photonic crystals. Such an understanding results in new ideas that can be implemented in promising solutions for novel optical devices.

ISBN:978-84-593-4072-1/DL:T-1163-2010

The viability of the results achieved in this dissertation is partially confirmed by comparison with the previous results reported by other authors. However, a few works related to the theme of this dissertation had been published when the work was started. Therefore, the correctness of the results presented in the dissertation is examined by means of the comparison between the results obtained by using different numerical approaches.

The practical importance of the work:

- the numerical approach proposed for analysing dispersion characteristics is a powerful tool that can be applied in designing novel photonic crystal integrated optical devices that will be widely used in the future in such areas as telecommunications and optical computing;
- the FDTD source code developed during the doctoral work can be used to simulate various optical devices and investigate their basic characteristics. It serves to design novel optical devices with such optimized characteristics as the size and the power consumption;
- from the theoretical point of view, the investigation of the dipole's behaviour in nonlinear periodic media helps to obtain the deeper understanding of physical processes in photonic crystal optical devices.

The basic results of the dissertation were presented and discussed at international and national conferences and published in papers in international referred journals. The author's contributions to the papers consist in formulation of the problem, choosing the numerical method, developing the source code and performing the calculations. The author would like to underline the help of Mr. M. Ustyantsev. During the author's previous work, he contributed to four scientific

works published in a national journal (both in Russian) and in two international conferences. The subject of these publications is closely related to that of the dissertation.

The dissertation is organised as follows:

In Chapter 1, a brief introduction to the photonic crystal technology is given. It is started with the discussion of the basic concepts of photonic crystals, the possible areas of application and the fabrication technologies. After that, the attention is focused on the nonlinear photonic crystals that, unlike their linear analogues, allow to control the propagation of light beams by means of other beams of light. An example of such a control is presented. The fabrication technologies that are used to create nonlinear photonic crystals are briefly reviewed.

Chapter 2 is of theoretical character. In it, a brief overview of the third-order nonlinear effect is presented and the impact of this effect on photonic crystal devices is discussed. This discussion starts with the Maxwell's equations for nonlinear media and in continuation several physical mechanism responsible for the intensity dependent change in the refractive index are reviewed. After that, the attention is paid to the light propagation in nonlinear waveguides. In particular, it is demonstrated that the capacity limit of these waveguides depends on the nonlinearity. The discussion on how to enhance the nonlinearity by light slowing in photonic crystal waveguides finishes this chapter.

Chapter 3 is devoted to the numerical methods. First, the methods of theoretical investigation of photonic crystals are presented and compared by taking into consideration the possibility of their application to different problems. Secondly, the FDTD method employed in the dissertation is described and

ISBN:978-84-593-4072-1/DL:T-1163-2010

discussed. The basics of the conventional FDTD algorithm are outlined including such important issues as the discretization of the computational domain, the stability condition, the initial and the boundary conditions, the approach for computing the transmission and reflection spectra and the models of Kerr nonlinearity. In what follows, one of the modifications of the FDTD – the numerical simulation of radiation of oscillating dipole embedded in photonic crystal – is presented. It is shown how this approach can be combined with a Kerr nonlinear model with the aim of analysing dispersion characteristics of nonlinear photonic crystals.

In Chapter 4, the FDTD method presented in Chapter 3 is applied to calculate dispersion characteristics of Kerr nonlinear photonic crystals. First, one-dimensional structures are considered. Apart from the dispersion characteristics, the energy density spectra calculated for both linear and nonlinear regimes are compared showing the impact of the nonlinearity. Such issues as the unit cell discretization and the convergence are presented. Secondly, two-dimensional structures are considered for which the same calculations as above have been performed for both TE and TM polarisations. In continuation, dispersion characteristics of such two-dimensional structures with defects as line-defect and coupled-cavity waveguides are calculated and the impact of the group velocity is discussed. Thirdly, the discussion switches to nonlinear photonic crystal slabs.

In Chapter 5, a novel all-optical switching device based on a nonlinear two-dimensional photonic crystal decoupler is presented and analyzed. In this device, an enhancement of nonlinear effects is achieved with a slow wave structure embedded into the coupling region. The behaviour of the device is examined by means of the FDTD method.

Chapter 6 presents an approach of taking the two-photon absorption effect

into account. This approach is applied to analyze the all-optical switch from Chapter 5 by means of the FDTD method. It is shown for a shortened model of the device that the impact of the two-photon absorption (TPA) on the functionality of the device is drastic.

The last Chapter 7 contains the summary and conclusions of the thesis. Some ideas on how the feature work could be carried out are formulated.

In the author's publications, both the SI and Gaussian systems of units are used. In Appendix A, the Maxwell's equations are presented in both these systems of units. In addition, it is shown for the SI system how the Kerr coefficient is related to the nonlinear refractive index.

UNIVERSITAT ROVIRA I VIRGILI
MODELLING OF PHOTONIC COMPONENTS BASED ON ÷(3) NONLINEAR PHOTONIC CRYSTALS
Ivan Maksymov
ISBN:978-84-593-4072-1/DL:T-1163-2010

Chapter 1

Introduction to photonic crystals

We are living in the information age with an over-abundance of information everywhere we turn. The use of optical fibres, wireless and computer technologies are now realized for anyone. The Internet enables a lot of information services to be accessed on a global basis and the demand for broad networks increases considerably as increases the number of users. In order to satisfy this demand, the search must be on for faster and more efficient components to increase the bandwidth of the existing networks. The current optoelectronic devices are expected to work at up 100 Gbit/s [1]. Beyond that speed, pure all-optical devices are needed [2]. Such devices can be achieved by using the photonic crystal technology [3-4] that is one of the most important scientific areas with a huge industrial potential. A combination of nanoscale photonic crystal devices with the nonlinearity in some materials is expected to provide a possibility to create all-optical devices with convenient characteristics.

ISBN:978-84-593-4072-1/DL:T-1163-2010

These devices can substitute their conventional optoelectronic analogues and they can become the basic element base of optics in the XXI century.

One of the main advantages of the photonic crystal technology is the possibility of the full integration of optical devices on all-optical chips that can operate at much higher frequency and consume less power than today's electronic silicon chips. The application of these chips together with optical interconnections makes it possible to create novel optical systems such as, for example, optical computers with extremely high speed of digital data processing [5]. In order to use the advantages of the photonic crystal technology, much theoretical and practical work must be carried out in the following areas: theoretical investigation, information recording, input/output devices, light sources, fabrication technology and measurements.

In the last decade, a considerable progress has been achieved in all these areas. In particular, theoretical investigations and developing of new fabrication technologies have allowed for the realization of new types of photonic crystal devices such as all-optical switches, two-state and many-state memories, all-optical limiters, all-optical modulators and all-optical transistors [2, 6]. Much of these activities are exploiting the nonlinear optical effects in polymers, glasses and semiconductors in order to achieve desired characteristics of the devices [7]. When designing these devices, a special attention should be paid to inherent physical limitations that hamper signal manipulation in the optical domain. Consequently, there is a need to find novel solutions that would improve the ability to manipulate the light.

In the quest for the optimal solutions, the numerical analysis, design and simulation play an important role. It is because they are able to make use of the advantages of the photonic crystal technology by predicting novel devices and

UNIVERSITAT ROVIRA I VIRGILI
MODELLING OF PHOTONIC COMPONENTS BASED ON ÷(3) NONLINEAR PHOTONIC CRYSTALS
Ivan Maksymov
ISBN:978-84-593-4072-1/DL:T-1163-2010

helping to understand their behaviour in realistic conditions [8]. Therefore, it is extremely important to improve the existing numerical techniques as well as develop novel ones.

1.1 Basic concepts of photonic crystals

Photonic crystals are periodic dielectric or metal-dielectric nanostructures that are designed to affect the propagation of electromagnetic waves in the same way as the periodic potential in semiconductors crystals affects the electron motion by defining allowed and forbidden energy bands. The simplest form of the photonic crystal is a one-dimensional periodic structure such as a multilayer film. The propagation of the electromagnetic wave in such structures was first studied

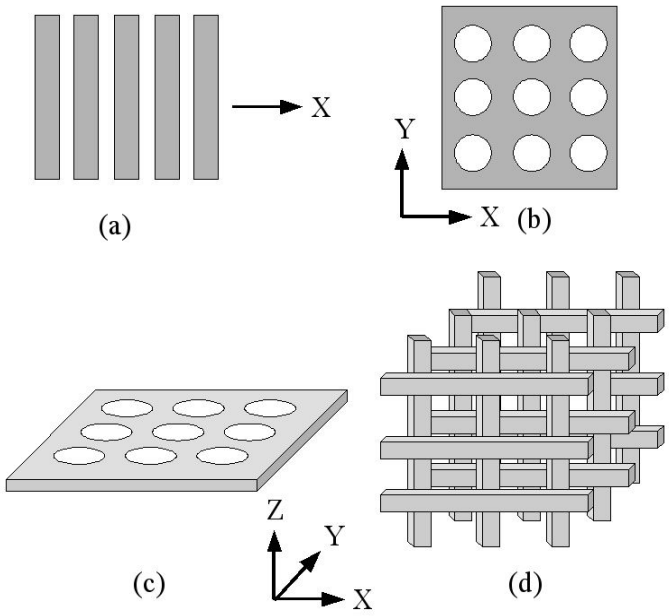

Fig. 1.1 Possible configurations of photonic crystals

by Rayleigh in 1887; it was shown that such a system has a forbidden band gap. The possibility to create two- and three-dimensional photonic crystal with two- and three-dimensional forbidden band gaps was suggested independently by Yablonovich and Jonh in 1987 [9-10]. However, a concept similar to that of photonic crystal was developed in 1950s and called the artificial dielectrics and metal-dielectrics [11-12]. The main difference between the photonic crystal and the artificial dielectric consists of the following: in photonic crystals the wavelength of the electromagnetic field interacting with the structure is comparable with the distance between the atoms, whereas in artificial dielectrics the distance between the atoms is much larger. At the present day, the concept of artificial dielectric is extended and called metamaterials [13] which are of great interest to researchers.

In order to illustrate the possible configurations of photonic crystals, Fig. 1.1 shows schematically the one-, two- and three-dimensional photonic crystals. As was mentioned, one-dimensional photonic crystals shown in Fig. 1.1(a) are simple multilayer films consisting of layers with high and low refractive index. The alternating of the layers takes place in only one direction. Fig. 1.1(b) shows a two-dimensional photonic crystal (top view), which is a system of air holes drilled in a high refractive index background material. This structure is periodic in two dimensions and infinite in the third one. A membrane of finite height shown in Fig. 1.1(c) with the same hole pattern is also classified as a two-dimensional photonic crystal. This structure is frequently referred to as the photonic crystal slab. Fig. 1.1(d) shows a three-dimensional photonic crystal, which is an arrangement of dielectric bulks of high refractive index situated in air. This is so-called “woodpile” photonic crystal structure [8]. It is periodic in all dimensions and, unlike the structures in Figs. 1.1 (a), (b) and (c), it demonstrates a complete

ISBN:978-84-593-4072-1/DL:T-1163-2010

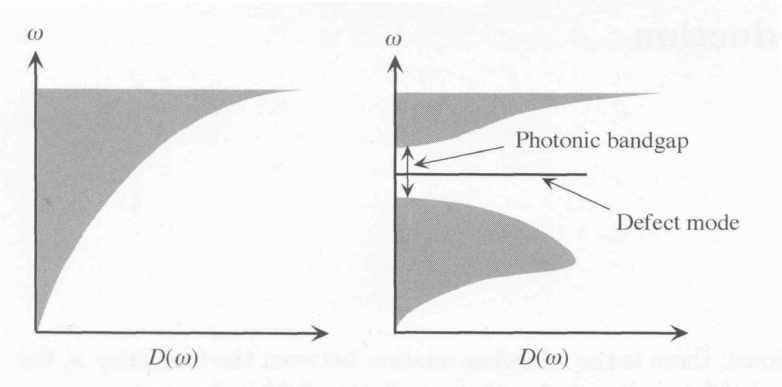

Fig. 1.2. Schematic illustration of the density of states of the radiation field (left) in free space and (right) in a photonic crystal. (After [14]).

forbidden band gap that means that the light concentrated within has no way to escape.

In order to discuss the concept of the forbidden band gap, the theory from Sakoda's book [14] can be adopted. As is well known, there is the following relation between the frequency f, the velocity c and the wavelength λ_0, of the radiation field in free space

$$c = \lambda_0 f \,. \tag{1.1}$$

When the wave number is defined as $k = 2\pi / \lambda_0$, the relation between the angular frequency and k is obtained as

$$\omega = ck \,. \tag{1.2}$$

This equation is called the dispersion relation of the radiation field. The density of

ISBN:978-84-593-4072-1/DL:T-1163-2010

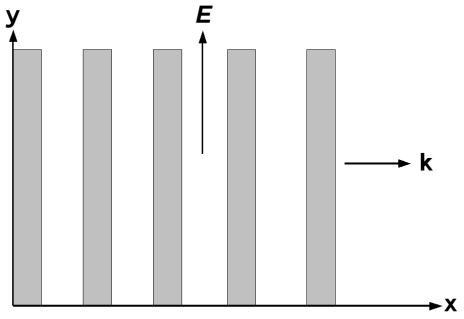

Fig. 1.3. Geometry of the calculation of the dispersion relation of a one-dimensional photonic crystal.

states of the radiation field in the volume V of free space is denoted as $D(\omega)$ and proportional to ω^2. It can be written as

$$D(\omega) = \frac{\omega^2 V}{\pi^2 c^3}. \tag{1.3}$$

The density of states in the uniform material is obtained by replacing c by v in this equation. The optical properties of atoms and molecules strongly depend on $D(\omega)$. It is possible to design and modify $D(\omega)$ by changing the optical properties of atoms and molecules. This is the key idea of photonic crystals and it is schematically illustrated in Fig. 1.2. Unlike the density of state of the radiation field in free space, the photonic crystal's one has a forbidden band gap for a range of angular frequency.

In textbooks, the one-dimensional photonic crystal shown in Fig. 1.1 (a) is usually examined in detail to gain an understanding of the origin of this forbidden photonic band gap. Fig. 1.3 shows the geometry of the calculation of the

ISBN:978-84-593-4072-1/DL:T-1163-2010

dispersion characteristic that demonstrates the forbidden band gap. Only the electromagnetic wave propagated in the *x* direction and polarized linearly is considered. The *y* axis is taken in the direction of the polarization. The electric field of the propagated wave is denoted by a complex function $E(x,t)$. The wave equation for $E(x,t)$ is given by

$$\frac{c^2}{\varepsilon(x)}\frac{\partial^2 E}{\partial x^2}=\frac{\partial^2 E}{\partial t^2}, \tag{1.4}$$

where $\varepsilon(x)$ denotes the position-dependent relative dielectric constant of the photonic crystal. In (1.4) it is assumed that the magnetic permeability of the photonic crystal is equal to that in free space. Because $\varepsilon(x)$ is a periodic function of *x*, the dielectric constant can be written as

$$\varepsilon(x+a)=\varepsilon(x), \tag{1.5}$$

where *a* is the lattice constant. The function $\varepsilon^{-1}(x)$ is also periodic and can be expanded in a Fourier series

$$\varepsilon^{-1}(x)=\sum_{m=-\infty}^{\infty}k_m\exp\left(i\frac{2\pi m}{a}x\right), \tag{1.6}$$

where *m* is an integer and $\{k_m\}$ are the Fourier coefficients. Since $\varepsilon(x)$ has been assumed to be real, $k_{-m}=k_m^*$. It is known from the solid-state theory [15] that the Bloch's theorem holds for the electronic eigenstates in ordinary crystals because

ISBN:978-84-593-4072-1/DL:T-1163-2010

of the spatial periodicity of the potential energy that an electron feels due to the regular array of atomic nuclei. The same theorem holds for electromagnetic waves in photonic crystals. Any eigenmode in the one-dimensional crystal is thus characterized by a wave number k and expressed as follows

$$E(x,t) \equiv E_k(x,t) = u_k(x)\exp\{i(kx - \omega_k t)\}, \tag{1.7}$$

where ω_k denotes the eigen-angular frequency and $u_k(x)$ is a periodic function

$$u_k(x+a) = u_k(x). \tag{1.8}$$

Therefore it can also be expanded in a Fourier series. As a result, (1.7) becomes

$$E_k(x,t) = \sum_{m=-\infty}^{\infty} E_m \exp\left\{i\left(k + \frac{2\pi m}{a}\right)x - i\omega_k t\right\}, \tag{1.9}$$

where $\{E_m\}$ are the Fourier coefficients.

In what follows, it is assumed for simplicity that only components with $m = 0$ and ± 1 are dominant in the expansion (1.6)

$$\varepsilon^{-1}(x) \approx k_0 + k_1 \exp\left(i\frac{2\pi}{a}x\right) + k_{-1}\left(-i\frac{2\pi}{a}x\right) \quad . \tag{1.10}$$

When (1.9) and (1.10) are substituted into the wave equation (1.4), one obtains

ISBN:978-84-593-4072-1/DL:T-1163-2010

$$k_1\left\{k+\frac{2(m-1)\pi}{a}\right\}^2 E_{m-1}+k_{-1}\left\{k+\frac{2(m+1)\pi}{a}\right\}^2 E_{m+1}\approx\left\{\frac{\omega_k^2}{c^2}-k_0\left(k+\frac{2m\pi}{a}\right)^2\right\}E_m\,. \quad (1.11)$$

Sakoda showed that E_0 and E_{-1} are dominant and all other terms can be neglected. Under this assumption one obtains the following coupled equations

$$(\omega_k^2-k_0c^2k^2)E_0-k_1c^2\left(k-\frac{2\pi}{a}\right)^2E_{-1}=0\,, \quad (1.12)$$

$$-k_{-1}c^2k^2E_0+\left\{\omega_k^2-k_0c^2\left(k-\frac{2\pi}{a}\right)^2\right\}E_{-1}=0\,. \quad (1.13)$$

These linear equations have a nontrivial solution when the determinant of coefficients vanishes

$$\begin{vmatrix}\omega_k^2-k_0c^2k^2 & -k_1c^2\left(k-\frac{2\pi}{a}\right)^2\\ -k_{-1}c^2k^2 & \omega_k^2-k_0c^2\left(k-\frac{2\pi}{a}\right)^2\end{vmatrix}=0\,. \quad (1.14)$$

If one introduces $h=k-\pi/a$, the solutions are then given by

$$\omega_\pm\approx\frac{\pi c}{a}\sqrt{k_0\pm|k_1|}\pm\frac{ac}{\pi|k_1|\sqrt{k_0}}\left(k_0^2-\frac{|k_1|^2}{4}\right)h^2\,, \quad (1.15)$$

as far as $|h|<<\pi/a$. So, there is no mode in the interval

ISBN:978-84-593-4072-1/DL:T-1163-2010

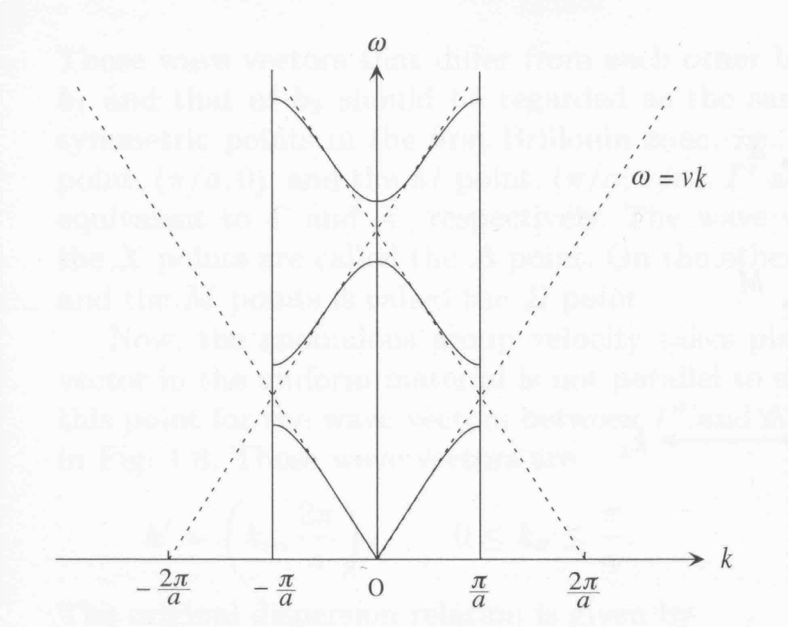

Fig. 1.4. Dispersion characteristic of a one-dimensional photonic crystal (solid lines). The boundary of the first Brillouin zone is denoted by two vertical lines. The dispersion lines in the uniform material are denoted by the dashed lines. When the dispersion lines cross, they repel each other and a forbidden photonic band gap appears. (After [14]).

$$\frac{\pi c}{a}\sqrt{k_0 - |k_1|} < \omega < \frac{\pi c}{a}\sqrt{k_0 + |k_1|}\,. \tag{1.16}$$

This gap disappears when $k_1 = 0$. This result can be interpreted that the modes with $k \approx \pi / a$ and $k \approx -\pi / a$ were mixed with each other in the presence of the periodic modulation of the dielectric constant and this mixing led to a frequency splitting.

In general, those wave vectors which differ from each other by a multiple of $2\pi / a$ should be regarded as the same because of the presence of the periodic spatial modulation of the dielectric constant. When the spatial modulation is

ISBN:978-84-593-4072-1/DL:T-1163-2010

small, the dispersion relation in the photonic crystal is not so far from $\omega = vk$, but it should thus be expected with the wave vector in the first Brillouin zone $[-\pi/a, \pi/a]$. In addition, if two dispersion lines cross each other, a frequency gap appears. All these things are schematically illustrated in Fig. 1.4. There are an infinite number of frequency gaps in the spectrum. However, one should note that

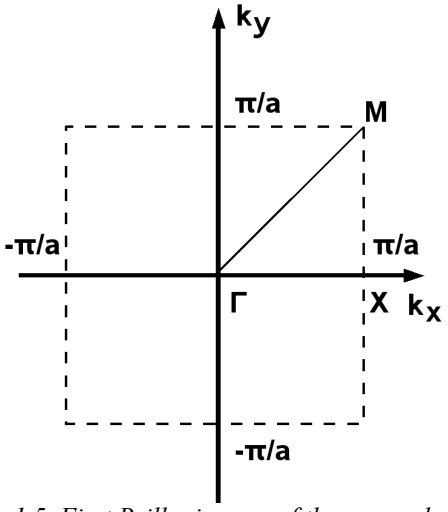

Fig. 1.5. First Brillouin zone of the square lattice.

this is true only as far one deals with electromagnetic waves travelling along the *x* direction and that there is no gap when one takes into consideration the modes travelling in other directions.

The dispersion relation of a two-dimensional photonic crystal is quite different because of the fact that all wave vectors are not parallel to each other in two dimensions [8, 14]. As the first example, Fig. 1.5 shows the reciprocal lattice space of a two-dimensional square lattice. The first Brillouin zone is surrounded by a dashed line. There are three highly symmetric points in the first Brilloun

ISBN:978-84-593-4072-1/DL:T-1163-2010

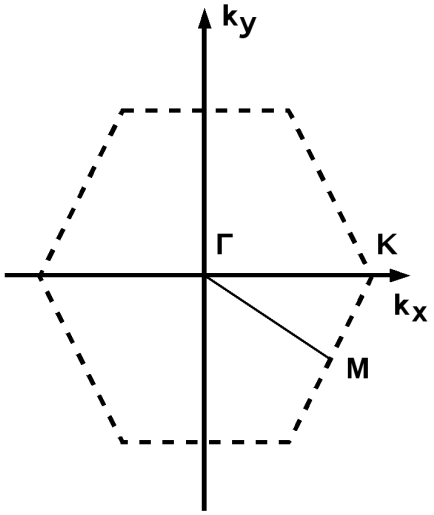

Fig. 1.6. First Brillouin zone of the hexagonal lattice.

zone, that is, the Γ point (0,0), the X point (π/a, 0) and the M point (π/a, π/a). The second example, the reciprocal lattice space of a two-dimensional hexagonal lattice, is presented in Fig. 1.6. The three highly symmetric points are the Γ point (0,0), the K point ($4\pi/3a$,0) and the M point (π/a, $-\pi/a\sqrt{3}$). The configuration of the first Brilloin zone of three-dimensional photonic crystals depends on the type of the lattice. For instance, it can be the simple cubic or the fcc lattice. It this dissertation, no calculation is made for three-dimensional photonic crystals and therefore any attention is paid to their dispersion relations.

1.2 Areas of application

The photonic crystal technology gave rise to a big group of novel optical devices that potentially can play a very important role in optical-communication

systems being integrated on optical chips [1]. The first example of photonic crystal-based optical devices are light-emitting diodes (LEDs). Usually, these devices are made from photoemissive materials that emit photons excited electrically or optically. These photons are typically emitted in many different directions and also have a range of wavelengths that is not ideal for communications applications. It possible to create an LED that only emits light in one direction by using a reflector. However, the efficiency of such an LED depends on that of the reflector. The photonic crystal technology can be used to design a mirror that reflects selected wavelengths of light with very high efficiency. In addition, such a mirror can be integrated within the photoemissive layer to create an LED that emits light of a specific wavelength and direction. Ideally, one needs to create a three-dimensional photonic crystal to achieve a full control of light in all three dimensions. In order to do this, the fabrication method proposed by Yablonovitch [16] can be employed. Alternatively, a "woodpile" structure shown in Fig. 1.1(d) can be used [8]. Fortunately, some of the properties of three-dimensional photonic crystals can be attained with two-dimensional photonic crystal slabs, where the light is confined by both the periodic structure

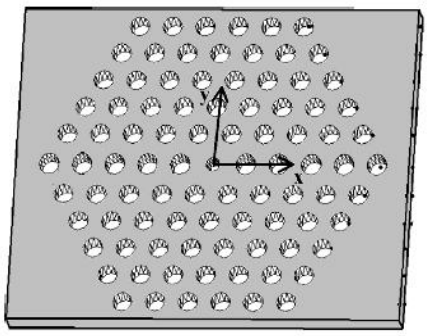

Fig. 1.7. Example of a microcavity made by decreasing the radius of the hole

UNIVERSITAT ROVIRA I VIRGILI
MODELLING OF PHOTONIC COMPONENTS BASED ON ÷(3) NONLINEAR PHOTONIC CRYSTALS
Ivan Maksymov
ISBN:978-84-593-4072-1/DL:T-1163-2010

and the bulk of the constitutive material. Their main advantage is the relative simplicity of the fabrication process and the possibility of to be easy incorporated within planar waveguides [17].

The second group of photonic crystal based devices are microcavities (see Fig. 1.7) [1, 8, 18], which are very important for creating photonic crystal lasers. These lasers [19] can be integrated with other components in optical communication systems or optical chips. They are made by introducing defects into the perfect lattice of the photonic crystal. It gives rise to a defect state situated within the forbidden photonic band gap. While the material emits light in a wide spectral range, only the wavelength that corresponds to that of the defect mode is amplified because only it can propagate freely in the photonic crystal. In the microcavity, the intensity of the propagated light increases as it undergoes lots of reflections and travels back. The light at other wavelengths is trapped within the photonic crystal and cannot escape. This means that the laser light is emitted in a narrow wavelength range that is directly related to the dimension of the cavity. The linewidth can be modified by searching for unusual geometries of the

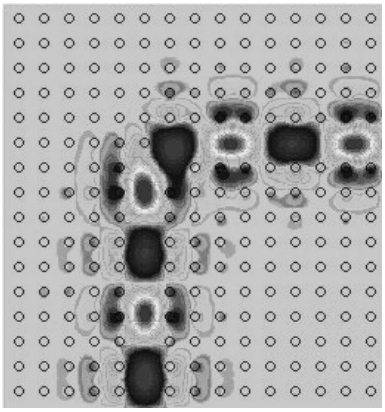

Fig. 1.8. Bend photonic crystal waveguide. (After [8])

UNIVERSITAT ROVIRA I VIRGILI
MODELLING OF PHOTONIC COMPONENTS BASED ON ÷(3) NONLINEAR PHOTONIC CRYSTALS
Ivan Maksymov
ISBN:978-84-593-4072-1/DL:T-1163-2010

photonic crystal lattice. In addition, apart from the lasers, such microcavities can improve the efficiency of LEDs.

Photonic crystal microcavities that are fabricated from passive materials can also be used to create filters that only transmit a very narrow range of wavelengths. Such filters can be used to select a wavelength channel in a WDM communications system. Indeed, arrays of these devices can be integrated onto an optical chip to form the basis of a channel demultiplexer that separates and sorts light pulses of different wavelengths [20].

Miniature waveguides that can be used to transmit light signals between different devices are a key component for integrated optical circuits. However, the development of such nanoscale optical interconnects was a difficult deal because of the problem of guiding light efficiently round very tight bends. Conventional optical fibres and waveguides work by the process of total internal reflection [1]. The contrast in refractive index between the glass core of the fibre and the surrounding cladding material determines the maximum radius through which the light can be bent without any losses. For conventional glass waveguides this bend

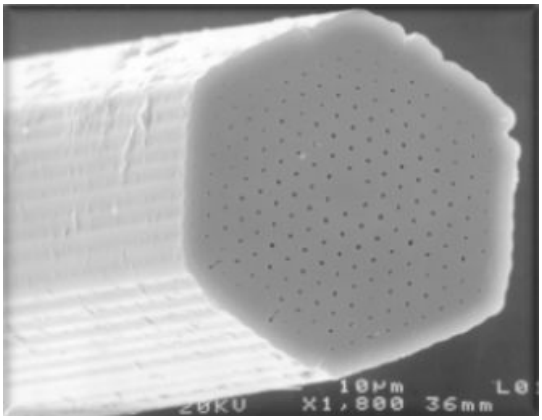

Fig. 1.9. SEM photograph of a holey fibre. (After [23])

ISBN:978-84-593-4072-1/DL:T-1163-2010

radius is about a few millimetres. However, the interconnects between the components in an integrated optical circuit require bend radii of 10 μm or less. In order to solve this problem, it is possible to form a narrow-channel waveguide within a photonic crystal by removing a row of holes or rods from an ideal photonic crystal lattice [21]. Light will be confined within the line of defects (see Fig. 1.8) for wavelengths that lie within the band gap of the surrounding photonic crystal. Under this condition one can introduce a pattern of sharp bends that will either cause the light to be reflected backwards or directed round the bend.

The advantages of the photonic crystal technology can help to speed up the Internet by improving the transmission of long-distance optical signals. In conventional optical fibres, the light of different wavelengths can travel through the material at different speeds. Over long distances, time delays can occur between signals that are encoded at different wavelengths. This phenomenon known as dispersion [22] is worse if the core is very large, as the light can follow different paths or modes through the fibre. A pulse of light travelling through such

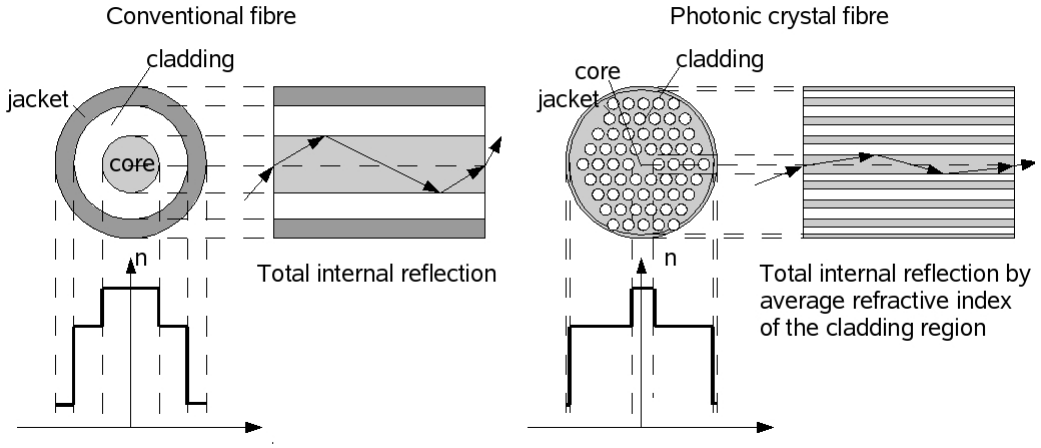

Fig. 1.10. Comparison of the functionality of a conventional and a holey fibres

ISBN:978-84-593-4072-1/DL:T-1163-2010

a fibre broadens out, thereby limiting the amount of data that can be sent. These problems can be solved by using a so-called "holey fibre" [23] shown in Figs. 1.9 and 1.10. This fibre has a regular lattice of air cores running along its length and transmits a wide range of wavelengths without suffering from dispersion. It is made by packing a series of hollow glass capillary tubes around a solid glass core that runs through the centre. This structure is then heated and stretched to create a long fibre that is only a few microns in diameter. The fibre has the unusual property that it transmits a single mode of light, even if the diameter of the core is very large.

1.3 Fabrication technologies

In this subsection, the general technologies for fabricating photonic crystals are discussed. It should be noticed that the key parameter here is the working wavelength $\lambda = 1.5\mu m$ used in optical communication systems. All the applications proposed for photonic crystal use the existence of the forbidden photonic band gap. The frequencies at which this band gap can be found are directly related to the dimensions of the scattering elements of photonic crystals (radii of holes or rods, height of slab, etc.). Specifically, the size of the features should be of the order of $\lambda_{PBG}/2$, where λ_{PBG} is the wavelength at which the band gap occurs. Consequently, in order to achieve a photonic crystal that can be used in optical communication systems, fabrication technologies to create lattice element of 0.25μm should be available.

One of the most general methods for fabricating photonic crystal is the lithography, which is used to pattern the substrate for two-dimensional lattices. In

ISBN:978-84-593-4072-1/DL:T-1163-2010

this case, the standard photolithography techniques are not applicable because the size of the lattice elements varies between 0.2 and 0.6 μm. The most popular alternative is the electron beam lithography (EBL), in which photons for resist exposure are replaced by electrons. Since the wavelength of an electron is much smaller than that of a photon, the resolution is not limited by the diffraction. Usually, a focused electron beam is scanned across the surface to generate the pattern. The quality of the resist and the properties of the substrate are the factors that limit the resolution of this process. EBL has been used by a variety of groups to generate patterns that are designated for use in devices for optical communication systems [24-26].

Another popular method for fabricating photonic crystals is dry etching. There are various versions of dry-etching processes, which have the following acronyms: RIE, DRIE, RIBE, CAIBE, ets. A comprehensive review of these techniques is very complicated and it is beyond the scope of this thesis. Generally, dry etching covers a family of methods by which a solid surface is etched in the gas or vapour phase physically by ion bombardment, chemically by a chemical reaction o by a combined mechanism. Most dry-etching techniques are plasma-assisted. They can be classified as chemical plasma etching (PE), synergetic reactive ion etching (RIE) and physical ion-beam etching (IBE). A special attention should be paid to chemically assisted ion beam etching (CAIBE) [25, 27-28], which is the most widely used dry-etching technique for fabricating two-dimensional planar photonic crystals, waveguides and microcavities. CAIBE is also used to fabricate photonic crystal based light emitting devices from GaAs. The InP systems can be fabricated by using inductively coupled plasma reactive ion etching (ICP-RIE) [29].

Soft lithography technique [30] is a nonphotolithographic technique based

ISBN:978-84-593-4072-1/DL:T-1163-2010

on self-assembly and replica moulding for nanofabrication. It is used to generate patterns with feature sizes ranging from 30 nm and 10 μm. This technique is useful in fabricating both two- and three-dimensional photonic crystal (by iterative processing).

The capillary plate is the first material used to successfully fabricate a two-dimensional photonic crystal in both near-IR and visible wavelength region [31]. The method consists of drawing a bundle of optical fibres in which the core (SiO_2) and the cladding (PbO) are selectively dissolved. Hundreds of glass fibres are bundled together to form a hexagonal lattice. The bundle is then heated and drawn out to reach the desired lattice parameters. Next, the core is selectively dissolved to leave a hexagonal lattice of air holes in glass. The attainable feature size is of 0.2 μm [32].

The next group of fabrication methods is usually called the anodization techniques. They are wet etching techniques that use selective etching phenomena that depend on the semiconductor crystal direction. Unlike dry etching methods, in which the anisotropy of the etching process is controlled by the plasma conditions, the anodic etching of a single crystal semiconductor formed from Si, InP or GaAs is a selective etching process and its selectivity depends on the nature of the crystal direction. By using this tecnique, both two- and three-dimensional photonic crystals can be created. In particular, the anodization of Si in acid solutions (for example HF) gives rise to macroporous silicon photonic crystals [33-34]. The etching process proceeds upon provision of positive carriers (holes), which takes part in the chemical dissolution reaction. In p-type Si, the holes are the majority carriers, while in n-type Si they must be generated by illumination. The sample characteristics (doping level, orientation), the applied voltage and the etching current are the main etching parameters that control the pore size and

morphology.

An alternative approach for producing two-dimensional photonic crystals that display bang gaps in the visible is the anodic growth of porous alumina [35]. After the anodic oxidation of alumina in an acid solution, a porous oxide film of vertical holes is formed on the surface. The covering film, known as anodic porous alumina, is the result of the formation of a regular structure, in which an amorphous state of alumina grows via self-organisation.

In addition, the both macroporous Si and porous alumina can be used as templates for creating photonic crystal consisting of pillars grown through the porosity [34].

1.4 Kerr nonlinear photonic crystals

Although there are many analogies between the semiconductors and photonic crystals, the full parallel cannot be drawn because photons, in contrast to electrons, are not easily tuneable. It prevents the use of ordinary photonic crystal as active components of optical chips and communication systems. This is the reason why the scientific community is looking for a possibility of controlling light with light [2] by means of material nonlinearities from which the photonic crystal are made. These photonic crystals are called nonlinear [36]. Their properties depend on the intensity of the interacting electromagnetic field or an additional (control) electromagnetic wave. In this dissertation, the attention will be only paid to the Kerr nonlinear photonic crystals, i.e., the photonic crystals consisting of Kerr nonlinear materials such as semiconductors, glasses and polymers [7]. This type of photonic crystals has been recently applied to such

ISBN:978-84-593-4072-1/DL:T-1163-2010

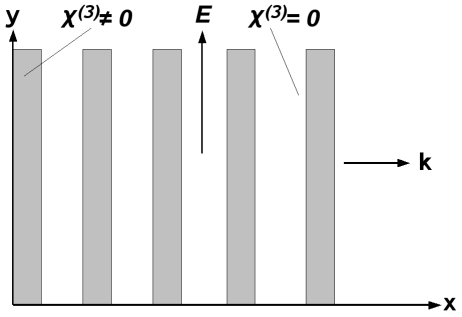

Fig. 1.11. Geometry of the calculation of the dispersion relation of a one-dimensional nonlinear photonic crystal.

nonlinear optical devices as low-threshold optical limiters [37], short pulse compressors [38], nonlinear optical diodes [39], all-optical switches and modulators [40] and others. In these devices, the refractive index is changed by the high-intensity control laser beam to dynamically control the transmission of the light.

In order to gain an understanding of the basic idea of nonlinear photonic crystals, one should consider the structure shown in Fig. 1.11 and solve the wave equation (1.17) where the dielectric constant depends on the Kerr coefficient and the intensity of the electric field. Eq. (1.17) is derived from Eq. (1.4) and it can be written as

$$\frac{c^2}{\left\{\varepsilon(x)+\chi^{(3)}(x)|E|^2\right\}}\frac{\partial^2 E}{\partial x^2}=\frac{\partial^2 E}{\partial t^2}, \tag{1.17}$$

with $\chi^{(3)}$ being the Kerr coefficient. As it can be seen, the wave equation (1.17) has become nonlinear and its solution is complicated considerably. In order to

ISBN:978-84-593-4072-1/DL:T-1163-2010

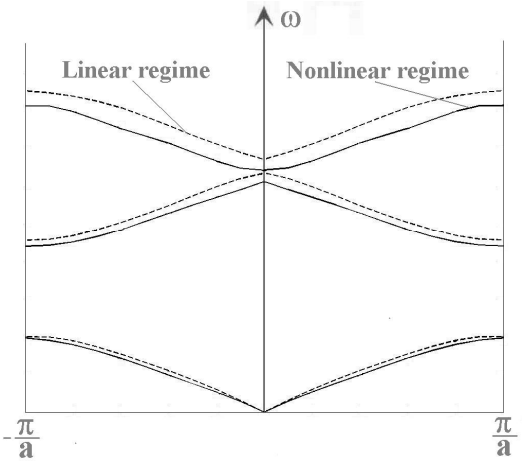

Fig. 1.12. Dispersion characteristic of a one-dimensional nonlinear photonic crystal operating in the (a) linear and (b) nonlinear regimes.

avoid some problems than one could encounter in solving it, a simple approach for estimating the change in the dispersion characteristic due to the incident intensity is proposed. In this approach, the term $\chi^{(3)}(x)|E|^2$ is assumed to be invariable. It is possible to make such an assumption because at some moment of time the field distribution stabilizes. In this dissertation and also in other works devoted to nonlinear photonic crystals this approach is successfully applied.

Under the assumption made, Eq. (1.17) can be written as

$$\frac{c^2}{\{\varepsilon(x)+\Delta\varepsilon\}}\frac{\partial^2 E}{\partial x^2}=\frac{\partial^2 E}{\partial t^2}\,. \tag{1.18}$$

Eq. (1.18) is solved using the same technique presented in [14].

Fig. 1.12 shows a qualitative evaluation of the dispersion characteristic for the nonlinear regime made by using the approach proposed above. In this

UNIVERSITAT ROVIRA I VIRGILI
MODELLING OF PHOTONIC COMPONENTS BASED ON ÷(3) NONLINEAR PHOTONIC CRYSTALS
Ivan Maksymov
ISBN:978-84-593-4072-1/DL:T-1163-2010

evaluation, the value of $\Delta\varepsilon$ is assumed to be positive. As it can be seen, in the nonlinear regime ($\Delta\varepsilon > 0$) the dispersion curves (solid lines) are red-shifted with regard to the linear regime (dashed lines). This shift can be qualified by the following argument. In the frequency domain, the band gap exists due to the difference between the dielectric constants of the material that forms the photonic crystal and that of the background. This difference can be expressed as

$$\Delta\varepsilon = \left[\varepsilon_{\text{Photonic Crystal}} + \chi^{(3)}|E|^2\right] - \varepsilon_{\text{Background}}\,, \tag{1.19}$$

where $\varepsilon_{Photonic\,\text{Crystal}}$ and $\varepsilon_{Background}$ are respectively the dielectric constants of the materials that form the photonic crystal and its background. The value of $\Delta\varepsilon$ increases as the intensity of the electric field increases if $\chi^{(3)} > 0$ and decreases if $\chi^{(3)} < 0$. As the electromagnetic wave excites the structure, the value of $\Delta\varepsilon$ changes and the position of the forbidden band gap dynamically shifts. This process is the basis for intensity-driven optical limiting and all-optical switching. Along with the shift of the band gap, other important characteristics such as defect modes and the density of state are changed. In this dissertation, these changes will be investigated in detail and a considerable use of them will be made.

In the following section, some examples of the devices based on the nonlinear photonic crystals will be presented.

1.4.1 Examples of application

In optical communication systems and optical chips, the active nonlinear photonic crystal-based devices can substitute their optoelectronic analogues. In

ISBN:978-84-593-4072-1/DL:T-1163-2010

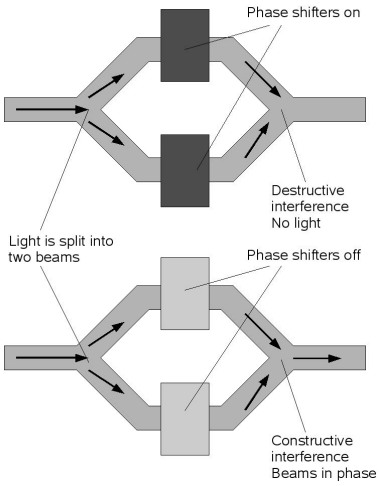

Fig. 1.13. Conventional optical modulator

order to provide an example of such a substitution, Figs. 1.11 and 1.12 show two optical modulators based on the Mach-Zehnder interferometers. The first of them is based on the conventional nonlinear dielectric waveguides whereas the second one is constructed using the nonlinear photonic crystal technology.

The optical modulator shown in Fig. 1.13 encodes 1s and 0s by first splitting a signal laser beam in two and then applying an electric field to the beams. One of the beams is delayed by half a wavelength relative to the other. When the beams recombine, both beams will be out of phase, and they will cancel out. When no electric field is applied, the beams remain in phase when recombined. Encoding the beam with 1s and 0s means making interfere (0) or keeping them in phase (1). The structure shown in Fig. 1.13 is usually made of $LiNbO_3$ and it occupies the area of 1-2 cm^2.

Fig. 1.14 schematically shows the photonic crystal device that was

ISBN:978-84-593-4072-1/DL:T-1163-2010

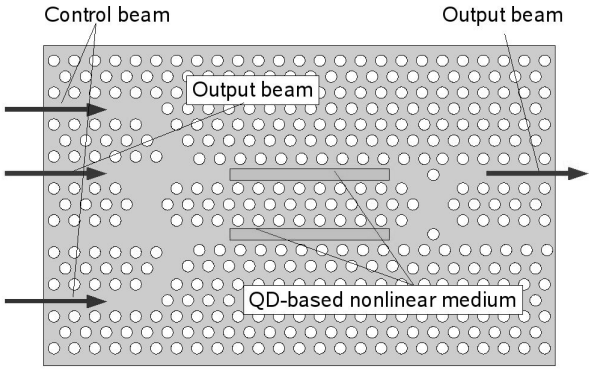

Fig. 1.14. Nonlinear photonic crystal based optical modulator

proposed to be used as an optical modulator [41-42]. It is composed of the two photonic crystal line-defect waveguides and nonlinear optical phase shift arms are selectively embedded with quantum dots that exhibit large nonlinear properties. A signal beam is split in two by using two bend photonic crystal waveguides. The rotated splitter is used to produce an output signal. Another two bend waveguides are used to launch control beams.

The principle of the functionality of the structure shown in Fig. 1.14 is the following. A switch-on control beam incident on the upper nonlinear arm causes a change in the refractive index, which leads to a phase shift for a signal beam. Similarly, another phase shift is generated in the lower arm by the second switch-off beam. When the beams recombine, they experience the same physical processes that take place in conventional optical modulators.

Thus, the optical modulator based on the nonlinear photonic crystal provides the same functionality as that in Fig. 1.13. In addition, it demonstrates several advantages over its conventional counterpart. The first of them arises from the fact that the photonic crystal technology dramatically downsizes the area that

ISBN:978-84-593-4072-1/DL:T-1163-2010

is of 1 mm^2 and reduces the optical switching energy. The second advantage is due to the possibility to integrate active and passive photonic crystal-based components on a chip. It also makes it possible to considerably increase the working frequency by excluding the electronic parts from the circuit and keeping all signals in the optical domain.

Other examples summarise the activity of different research groups working on numerical design and analysis of novel all-optical bistable devices based on nonlinear photonic crystals.

First, a high-contrast all-optical switching device based on a waveguide coupled to a cavity [43] is considered. Both the waveguide and the cavity are made in a square lattice rod-type nonlinear photonic crystal. The waveguide is made by removing a row of rods and the cavity is a point defect with an elliptical dielectric rod. The defect region possesses instantaneous Kerr nonlinear response

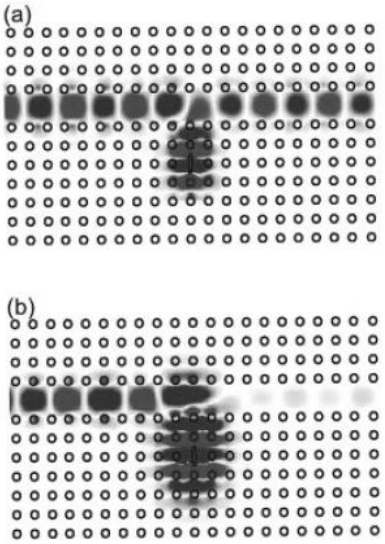

Fig. 1.15. Electric field distribution for (a) the high transmission state and (b) the low transmission state. (After [43])

ISBN:978-84-593-4072-1/DL:T-1163-2010

achievable in many semiconductors. A numerical simulation reveals that in the linear regime at a low incident power the structure behaves linearly. In the nonlinear regime, however, the structure shows bistable behaviour. Fig. 1.15 shows the field patterns for the two bistable states for the same level of the input power. Fig. 1.15 (a) corresponds to the high transmission state. In it, the field inside the cavity is low and thus the decaying field amplitude from the cavity is negligible. Fig. 1.15 (b) corresponds to the low transmission state. Here, the field intensity inside the cavity is higher, shifting the cavity resonance frequency down to the excitation frequency of the incident field. Therefore there exists the interference between the wave propagating in the waveguide and the decaying amplitude from the cavity that results in the high contrast ratio in transmission.

A structure based on the concept similar to that of the device presented above, was proposed in [44]. Here, a waveguide is directly coupled to a cavity. In such a system, the ratio of outgoing to incoming power displays a hysteresis loop even when the photonic crystal is made from an instantaneous-response material. This relationship can be used for many applications: logic gates, memory,

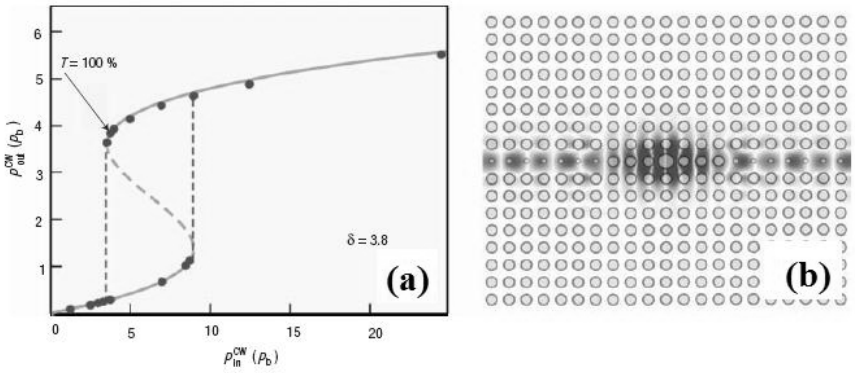

Fig. 1.16. (a) Ratio of outgoing to incoming power and (b) the electric field at 100 % transmission. (After [44])

ISBN:978-84-593-4072-1/DL:T-1163-2010

amplification, noise reduction and so on. The relationship between the outgoing and the incoming power and the field pattern of the devices are shown in Fig. 1.16.

The following exemplifies a structure that could be suitable for performing an optical transistor [44]. The structure consists of a cavity weakly coupled to four single-mode waveguides. It is up-down and left-right symmetric.

The cavity supports two dipole-type states. One state is odd with respect to the *x* axis and the other one is even. The mode propagating in the left or right waveguide can couple only to the cavity state that is even with respect to the *x* axis. The mode propagating in the up or down waveguide can couple only to the odd cavity state. Thus no portion of the signal travelling along the *x*-direction can be transferred into the *y*-direction. By making the central rod elliptical one can break the degeneracy between the two states and have different resonant frequencies for them. When light is present in only a single direction, it does not travel through the structure. But when the signals are present in the both

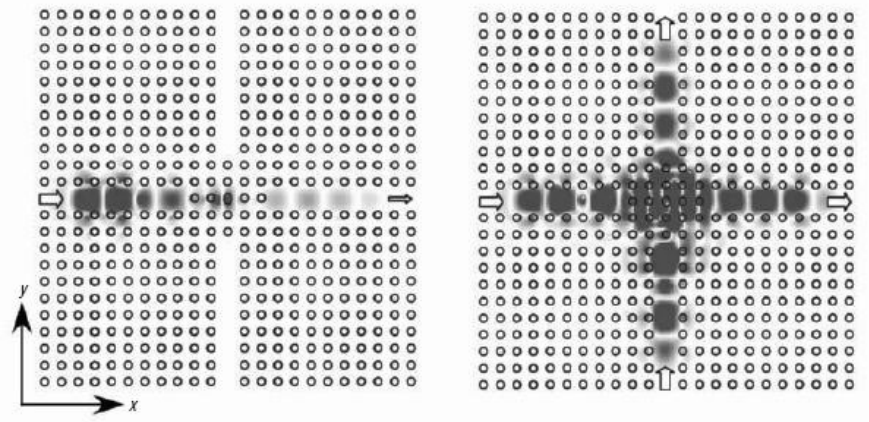

Fig. 1.17. (Left panel) Ratio of outgoing to incoming power and (right panel) the electric field at 100 % transmission. (After [44])

ISBN:978-84-593-4072-1/DL:T-1163-2010

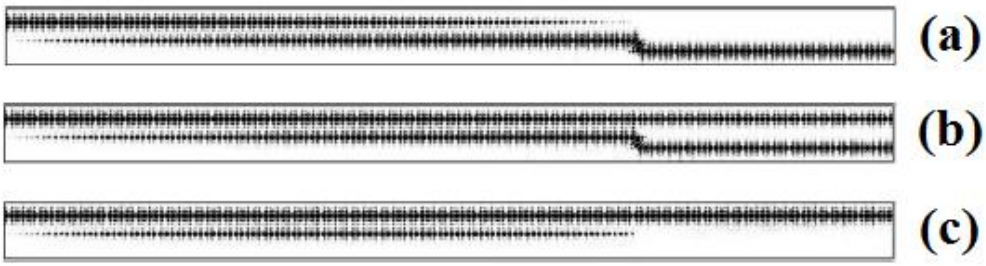

Fig. 1.18. Nonlinear directional coupler operating (a)in the cross state, (b) as a power splitter and (c) in the bar state. (After [50])

directions, they can control each other. Fig. 1.17 shows how this device can operate as an all-optical logical AND gate. The results similar to those presented above are also obtained by other researchers [45-49].

A special attention is also paid to the devices based on parallel nonlinear photonic crystal waveguides [49-54]. The examples are nonlinear directional couplers whose functionality depends on the intensity of the input signal or a control beam. When this intensity is low, the device functions in the cross state and its behaviour is similar to that of the linear directional coupler. As the intensity increases, the coupling condition worsens and the device becomes a 50% power splitter. At a high incident intensity, however, the device switches to the bar state. The field patters corresponding to these regimes are shown in Fig. 1.18. In articles [50] and [54], a similar device is proposed where a control beam of high intensity controls the propagation of the low-intensity input signal.

ISBN:978-84-593-4072-1/DL:T-1163-2010

1.4.2 Fabricating nonlinear photonic crystals

Before describing the technologies for fabricating nonlinear photonic crystal, it should be stressed that, in the general case, the technologies available for linear photonic crystals are still valid for their nonlinear counterparts. These technologies are described in one of the previous subsections and the following will describe the details that are only related to fabrication of Kerr nonlinear photonic crystals.

The first technology described here is related to the example given in the previous subsection. The nonlinear photonic crystal based optical modulator presented in [41-42] is created as an air-bridge-type two-dimensional photonic crystal slab. It consists of a GaAs core layer with three stacked layers of InAs quantum dots grown on top of a $Al_{0.6}Ga_{0.4}As$ clad layer that, in turn, is situated on a GaAs substrate. The molecular beam epitaxy technology is used to perform these steps. The quantum dots are formed in Stranski-Krastanov mode growth by a two-step growth technique [55]. The air-bridge photonic crystal structure is fabricated using high-resolution electron-beam lithography, dry etching and selective wet etching techniques [56].

The next fabrication technology - the anodization for creating porous silicon [34] - is also widely used to create both linear and nonlinear photonic crystals. For example, one-dimensional photonic crystals and cavities based on the porous silicon can be created for generating the third harmonic [57]. The control of the porosity of silicon allows to achieve both high quality factors and reflectance. The samples prepared in [57] are fabricated by the conventional electro-chemical etching procedure [34] using p-type Si wafers with resistivity of

ISBN:978-84-593-4072-1/DL:T-1163-2010

0.005 Ωcm. The modulation of the refractive index is achieved by the time variation of the etching current. The thickness is controlled with the etching time. The typical pore size achieved is of 30 nm.

Nonlinear optical polymers (NLO) are very useful materials that can be used to fabricate nonlinear photonic crystals optical devices because they exhibit high nonlinear properties over a wide frequency range. In order to fabricate a nonlinear photonic crystal waveguide [58], the following steps are made. Disperse Red 1 (DR1) doped poly(methylmethacrylate) (PMMA) is the nonlinear optical polymer used as the waveguide core layer. It is deposited on the metal cladding by spin coating and curing techniques. To pattern the nonlinear optical polymer, a 150 nm spin-on glass hard mask is used. Resist patterns formed by electron beam lithography are transferred to the hard mask by inductively coupled plasma (ICP) etching [29] in plasma. Finally, the polymer in waveguide core is patterned by ICP using hard mask pattern.

Recently, it has been shown that all-optical switching with high switch efficiency can be observed in two-dimensional organic nonlinear photonic crystals made of polystyrene [59-60]. In the fabrication process, polystyrene powder is dissolved in toluene with a weight ratio of 1:14. Completely dissolved polystyrene solution is obtained in about 40 hours. In order to prevent formation of microbubbles in the solution, additional shaking is needed. The spin coating method is used to fabricate the thin film slab of polystyrene on silica substrates, which should be precleaned. Ion-beam etching is employed to prepare the periodic patterns of two-dimensional photonic crystals. The lattice constant and the radius of the air holes achieved are 220 and 90 nm, respectively.

ISBN:978-84-593-4072-1/DL:T-1163-2010

References

[1] A. Yariv, *Optical Electronics in Modern Communications* (Oxford University Press, New York, 1997).

[2] H. M. Gibbs, *Optical bistability: Controlling light with light* (Academic Press, Orlando, 1985).

[3] J.-M. Lourtioz, *Photonic crystals. Towards nanoscale photonic devices* (Springer, Berlin, 2005).

[4] K. Busch, *Photonic crystals. Advances in design, fabrication and characterization* (Wiley, 2004).

[5] A. D. McAulay, *Optical computer architectures: the application of optical concepts to next generation computers* (Wiley, New York, 1991).

[6] S. John and M. Florescu, "Photonic band gap materials: towards an all-optical micro-transistor", J. Opt. A: Pure Appl. Opt. **3** ,103 (2001).

[7] R. W. Boyd, *Nonlinear Optics* (Academic Press, Boston, 1992).

[8] J. D. Joannopoulos, *Photonic crystals. Molding the flow of Light* (Princeton University Press, New Jersey, 1995).

[9] E. Yablonovich, "Inhibited Spontaneous Emission in Solid-State Physics and Electronics", Phys. Rev. Lett. **58**, 2059 (1987).

[10] S. John, "Strong localization of photons in certain disordered dielectric superlattices", Phys. Rev. Lett. **58**, 2486 (1987).

[11] J. Brown, "Artificial dielectrics having refractive indices less than unity", Proceedings J.E.E., May 1953, p. 51.

[12] N. A. Khizhiak, "Artificial anisotropic dielectrics", Zh. Eksp. Teor. Fiziki **27**, 2006–2038 (1957) (in Russian).

ISBN:978-84-593-4072-1/DL:T-1163-2010

[13] V. G. Veselago, “Left-handed materials”, Usp. Fiz. Nauk **92**, 517-526 (1967) (in Russian).

[14] K. Sakoda*, Optical properties of photonic crystals* (Springer Verlag, Berlin, 2001).

[15] C. Kittel, *Quantum theory of solids* (Wiley, 1963).

[16] E. Yablonovich, T. J. Gmitter and K. M. Leung, “Photonic band structure: the face-centered-cubic case employing nonspherical atoms”, Phys. Rev. Lett. **67**, 2295 (1991)

[17] S. G. Johnson and J. D. Joannopoulos, *Photonic crystals. The road from theory to practice* (Kluwer, Boston, 2002).

[18] A. Yariv, Y. Xu, R. K. Lee, A. Scherer, “Coupled-resonator optical waveguide: a proposal and analysis”, Opt. Lett. 24, 711-713 (1999).

[19] H. Altug and J. Vuckovic, “Photonic crystal nanocavity laser”, Opt. Express **13**, 8819 (2005).

[20] S. Haykin, *Communication systems* (Wiley, 2001).

[21] A. Mekis, J. C. Chen, I. Kurland, S. Fan, P. R. Villeneuve and J. D. Joannopoulos, “High transmission through sharp bends in photonic crystal waveguides”, Phys. Rev. Lett. **77**, 3787 (1996).

[22] T. Schneider, *Nonlinear optics in Telecommunications* (Springer-Verlag, Berlin, 2004).

[23] P. Russell, “Holey fiber concept spawns optical-fiber renaissance”, Laser Focus World **38**, 77 (2002).

[24] M. D. B. Charlton, S. W. Roberts and G. J. Parker, “Guided mode analysis and fabrication of a 2-dimensional visible photonic crystal band structure confined within a planar semiconductor waveguide”, Mater. Sci. Eng. B **49**, 155 (1997).

[25] T. F. Krauss, Y. P. Song, S. Thoms, C. D. W. Wilkinson and R. M. de la Rue,

ISBN:978-84-593-4072-1/DL:T-1163-2010

"Fabrication of 2-D photonic bandgap structures in GaAs/AlGaAs", Electron. Lett. **30**, 1444 (1994).

[26] J. M. Gerard, A. Izrael, J. Y. Marzin, R. Padjen and F. R. Ladan, "Photonic bandgap of two-dimensional dielectric photonic crystal", Solid-State Electron. **37**, 1341 (1994).

[27] T. F. Krauss, R. M. de la Rue and S. Brand, "Two-dimensional photonic bandgap structures operating at near-infrared wavelengths", Nature **383**, 699 (1996).

[28] J. O'Brien, O. Painter, R. Lee, C. C. Cheng, A. Yariv and A. Scherer, "Laser incorporating 2D photonic bandgap mirrors", Electron. Lett. **32**, 2243 (1996).

[29] T. Baba, K. Inoshita, H. Tanaka, J. Yonekura, M. Ariga, A. Matsutani, T. Miyamoto, F. Koyama and K. Iga, "Strong enhancement of light extraction efficiency in GaInAsP 2-D-arranged microcolumns", IEEE J. Lightwave Tech. **17**, 2113 (1999).

[30] Y. Xia and G. M. Whitesides, "Soft lithography", Annu. Rev. Mater. Sci. **28**, 153 (1998).

[31] K. Inoue, M. Wada, K. Sakoda, A. Yamanaka, M. Hayashi and J. W. Haus, "Fabrication of two-dimensional photonic band structure with near-infrared band gap", Jpn. J. Appl. Phys. 33, Part2 L1463 (1994).

[32] A. Rosenberg, R. J. Tonucci and E. A. Bolden, "Photonic band-structure effects in the visible and near ultraviolet observed in soli-state dielectric arrays", Apll. Phys. Lett. **69**, 2638 (1999).

[33] V. Lehmann and H. Föll, "Formation mechanism and properties of electrochemically etched trenches in n-type silicon", J. Electrochem. Soc. **137**, 653 (1990).

[34] T. Trifonov, "Photonic bandgap analysis and fabrication of macroporous

ISBN:978-84-593-4072-1/DL:T-1163-2010

silicon by electrochemical etching", Ph. D. thesis (Universitat Rovira i Virgili, Tarragona, 2005).

[35] H. Masuda, H. Yamada, M. Satoh, H. Asoh, M. Nakao and T. Tamamura, "Highly ordered nanochannel-array architecture in anodic alumina", Appl. Phys. Lett. **71**, 2770 (1997).

[36] R. E. Slusher and B. J. Eggleton, *Nonlinear Photonic Crystals* (Springer Verlag, Berlin, 2003).

[37] B.Y. Soon, W. Haus, M. Scalora, C. Sibilia, "One-dimensional photonic crystal optical limiter", Opt. Express **11**, 2007 (2003).

[38] N.I. Koroteev, S.A. Magnitskii, A.V. Tarasishin, A.M. Zheltikov, "Compression of ultrashort light pulses in photonic crystals: when envelopes cease to be slow", Opt. Commun. **159**, 191 (1999).

[39] M.D. Tocci, M.J. Bloemer, M. Scalora, J.P. Dowling, C.M. Bowden, "Thin-film nonlinear optical diode", Appl. Phys. Lett. **66**, 2324 (1995).

[40] M. Scalora, J.P. Dowling, C.M. Bowden, M.J. Bloemer, "Optical limiting and switching of ultrashort pulses in nonlinear photonic band gap materials", Phys. Rev. Lett. **73**, 1368 (1994).

[41] Y. Tanaka, Y. Sugimoto, N. Ikeda, H. Nakamura, K. Kanamoto and K. Asakawa, "Design, fabrication, and characterization of a two-dimensional photonic-crystal symmetric Mach-Zehnder interferometer for optical integrated circuits", Appl. Phys. Lett. **86**, 141104 (2005).

[42] H. Nakamura, Y. Sugimoto, K. Kanamoto, N. Ikeda, Y. Tanaka, Y. Nakamura, S. Ohkouchi, Y. Watanabe, K. Inoue, H. Ishikawa and K. Asakawa, "Ultra-fast photonic crystal/quantum dot alloptical switch for future photonic networks", Opt. Express. **12**, 6606 (2004).

[43] M. F. Yanik, S. Fan and M. Soljačíc, "High-contrast all-optical bistable

ISBN:978-84-593-4072-1/DL:T-1163-2010

switching in photonic crystal microcavities", Appl. Phys. Lett. **83,** 2739 (2003).

[44] M. Soljačíc and J. D. Joannopoulos, "Enhancement of nonlinear effects using photonic crystals", Nature Materials **3**, 211 (2004).

[45] N. Panoiu, M. Bahl, and R. Osgood, Jr., "All-optical tunability of a nonlinear photonic crystal channel drop filter," Opt. Express **12**, 1605 (2004).

[46] S. F. Mingaleev and Yu. S. Kivshar, "Nonlinear photonic crystals: Toward all-optical technologies", Opt. Photon. News **13**, 48 (2002).

[47] S. F. Mingaleev and Yu. S. Kivshar, "Nonlinear transmission and light localization in photonic-crystal waveguides", J. Opt. Soc. Am. B **19**, 2241 (2002).

[48] D. Vujic and S. John, "Pulse reshaping in photonic crystal waveguides and microcavities with Kerr nonlinearity: critical issues for all-optical switching", Phys. Rev. A **72**, 013807 (2005).

[49] K. Komatsu, T. Fujisawa and M. Koshiba, "Optical bistable switching in a channel-rejection photonic-crystal directional coupler", Electron. and Commun. In Japan, **89-2**, 9 (2006).

[50] F. Cuesta-Soto, A. Martínez, J. García, F. Ramos, P. Sanchis, J. Blasco, and J. Martí, "All-optical switching structure based on a photonic crystal directional coupler," Opt. Express **12,** 161 (2004),

[51] A. Locatelli, D. Modotto, D. Paloshi and C. De Angelis, "All optical switching in ultrashort photonic crystal couplers," Opt. Commun. **273**, 97 (2004).

[52] T. Fujisawa and M. Koshiba, "Finite-element modelling of nonlinear Mach-Zehnder interferometers based on photonic-crystal waveguides for all-optical signal processing", IEEE J. Lightwave Technol. **24**, 617 (2006).

[53] M. Soljačíc, S. Johnson, S. Fan, M. Ibanescu, E. Ippen and J. D. Joannopoulos, "Photonic-crystal slow-light enhancement of nonlinear phase sensitivity", J. Opt. Soc. Am. B **19**, 2052 (2002).

ISBN:978-84-593-4072-1/DL:T-1163-2010

[54] F. Cuesta-Soto, A. Martínez, B. García-Baños and J. Martí, "Numerical analysis of all-optical switching based on a 2-D nonlinear photonic crystal directional coupler", IEEE J. Select. Top. Quantum. Electron. **5**, 1101 (2004).

[55] Y. Nakamura, H. Nakamura, S. Ohkouchi, N. Ikedca, Y. Sugimoto and K. Asakawa, "Selective formation of high-density and high-uniformity InAs/GaAs quantum dots for ultra-small and ultra-fast all-optical switches," In Proc. 29th Int. Symp. Compound Semiconductors, Lausanne, Switzerland, **174**, 133 (2002).

[56] Y. Sugimoto, N. Ikeda, N. Carlsson, K. Asakawa, N. Kawai, and K. Inoue, "Fabrication and characterization of different types of two-dimensional AlGaAs photonic crystal slabs," J. Appl. Phys. **91**, 922-929 (2002).

[57] M. G. Martemyanov, E. M. Kim, T. V. Dolgova, A. A. Fedyanin, and O. A. Aktsipetrov, "Third-harmonic generation in silicon photonic crystals and microcavities", Phys. Rev. B **70**, 073311 (2004).

[58] S. Inoue, K. Kajikawa and Y. Aoyagi, "Dry-etching method for fabricating photonic-crystal waveguides in nonlinear-optical polymers", Appl. Phys. Lett. **82**, 2966 (2003).

[59] X. Hu, Y. Liu, J. Tian, B. Cheng and D. Zhang, "Ultrafast all-optical switching in two-dimensional organic photonic crystal", Appl. Phys. Lett. **86**, 121102 (2005)

[60] X. Hu and Q. Gong, Y. Liu, B. Cheng, and D. Zhang, "All-optical switching of defect mode in two-dimensional nonlinear organic photonic crystals", Appl. Phys. Lett. **86**, 231111 (2005).

ISBN:978-84-593-4072-1/DL:T-1163-2010

Chapter 2

Third-order nonlinear effect: physics and impact on photonic crystal devices

This chapter presents a brief overview of the third-order nonlinear effect and its impact on photonic crystal-based optical devices. First, the Maxwell's equations for nonlinear media are presented and several physical mechanisms responsible for the intensity-dependent change in the refractive index are reviewed. Secondly, the attention is paid to the electromagnetic wave propagation in nonlinear waveguides. In particular, it is shown how the capacity limit of these waveguides depends on nonlinearity. The chapter is finished with discussion on how to enhance the nonlinearity by light slowing in photonic crystal waveguides.

UNIVERSITAT ROVIRA I VIRGILI
MODELLING OF PHOTONIC COMPONENTS BASED ON ÷(3) NONLINEAR PHOTONIC CRYSTALS
Ivan Maksymov
ISBN:978-84-593-4072-1/DL:T-1163-2010

2.1 Third-order nonlinearity

2.1.1 Nonlinear refractive index

Nonlinear optics studies phenomena that take place as a result of the modification of the optical properties of a material by the presence of light. Only laser light is sufficiently intense to modify the optical properties of a material and this was the reason why the beginning of the nonlinear optics is dated back to the creation of lasers narrated in detail in [1]. In order to describe the optical nonlinearity, the theoretical consideration is started with the Maxwell's equation that in SI units are written as [2]

$$\nabla \times \vec{E} = -\frac{\partial \vec{B}}{\partial t}, \tag{2.1}$$

$$\nabla \times \vec{H} = \frac{\partial \vec{D}}{\partial t} + \vec{J}, \tag{2.2}$$

$$\nabla \cdot \vec{B} = 0, \tag{2.3}$$

$$\nabla \cdot \vec{D} = \rho, \tag{2.4}$$

where ρ and $\vec{J}$ are the free electric charge and the current density, respectively, and c is the speed of light. The relations among the four electromagnetic field vectors are known as the constitutive relations. These relations, even in presence of nonlinearities, have the form

$$\vec{D} = \varepsilon_0 \vec{E} + \vec{P}_E, \tag{2.5}$$

ISBN:978-84-593-4072-1/DL:T-1163-2010

$$\vec{B} = \mu_0 \vec{H} + \vec{P}_M \ . \tag{2.6}$$

In linear optics the polarisation $\widetilde{P}_E(t)$ depends linearly upon the electric field strength $\widetilde{E}(t)$ (the tilde is used to denote a quantity that varies rapidly in time) and can often be expressed as

$$\widetilde{P}_E(t) = \varepsilon_0 \chi^{(1)} \widetilde{E}(t), \tag{2.7}$$

where $\chi^{(1)}$ is known as the linear susceptibility. In nonlinear optics, however, the optical response can often be described by expressing the polarisation $\widetilde{P}_E(t)$ as a power series in the field strength $\widetilde{E}(t)$ as

$$\widetilde{P}_E(t) = \varepsilon_0 \left(\chi^{(1)} \widetilde{E}(t) + \chi^{(2)} \widetilde{E}^{(2)}(t) + \chi^{(3)} \widetilde{E}^{(3)}(t) + \ldots \right), \tag{2.8}$$

where $\chi^{(2)}$ and $\chi^{(3)}$ are known as the second- and third-order nonlinear optical susceptibility, respectively. $\widetilde{P}^{(2)}(t) = \varepsilon_0 \chi^{(2)} \widetilde{E}^{(2)}(t)$ is refereed as the second-order nonlinear polarisation and $\widetilde{P}^{(3)}(t) = \varepsilon_0 \chi^{(3)} \widetilde{E}^{(3)}(t)$ as the third-order nonlinear polarisation, respectively.

In the general case, $\widetilde{E}(t)$ is made up of several different frequency components and the expression for $\widetilde{P}^{(3)}(t)$ is very complicated. For this reason, a simple case in which the applied field is monochromatic, is only considered

$$\widetilde{E}(t) = E\cos(\omega t). \tag{2.9}$$

ISBN:978-84-593-4072-1/DL:T-1163-2010

If the formula $\cos^3(\omega t)=\frac{1}{4}\cos(3\omega t)+\frac{3}{4}\cos(\omega t)$ is used, one can obtain

$$\widetilde{P}^{(3)}(t)=\frac{1}{4}\varepsilon_0\chi^{(3)}E^3\cos(3\omega t)+\frac{3}{4}\varepsilon_0\chi^{(3)}E^3\cos(\omega t). \qquad (2.10)$$

The first term of Eq. (2.10) describes a response at the frequency 3ω that is due to an applied field at frequency ω. This term leads to the process of third-harmonic generation. The second term of Eq. (2.10) describes a nonlinear contribution to the polarisation at the frequency of the incident field. It leads to a nonlinear contribution to the refractive index experienced by a wave at frequency ω. The refractive index in the presence of this type of nonlinearity can be represented as

$$n = n_0 + n_2 I\ , \qquad (2.11)$$

where n_0 is the usual (linear) refractive index, $n_2=\frac{\chi^{(3)}}{n_0^2 c\varepsilon_0}$ is an optical constant that characterises the strength of the optical nonlinearity and $I=\frac{1}{2}\varepsilon_0 n_0 cE^2$ is the intensity of the incident wave.

2.1.2 Physical mechanisms

Several physical mechanisms [3] that contribute to the intensity-dependent refractive index are discussed below.

ISBN:978-84-593-4072-1/DL:T-1163-2010

Electronic polarization. This mechanism involves a distortion of the electron cloud about an atom or molecule by the optical field. If the atom or molecule is highly polarizable, then it can exhibit significant electron nonlinearity. The nonlinear susceptibility is related to the second hyperpolarizability, which is a microscopic parameter and can be computed from quantum mechanics using perturbation theory. These computational methods are beyond the scope of this thesis, but they are described in the literature [4]. For nonresonant electronic processes in dielectrics, a typical value for second hyperpolarizability is $\gamma \sim 10^{-61} C - m^4 / V^3$ and $\chi^{(3)} \sim 10^{-22} m^2 / V^2$. Nonresonant electronic processes are very fast with typical time response $\tau \sim 10^{-15} sec$.

Raman induced Kerr effect. This effect is related to stimulated Raman scattering and is an example of a strong beam inducing a refractive index change for a weak probe beam. The strong beam incident on a Raman active medium is from a laser at frequency ω_2. A weak probe beam of frequency ω_s is also incident on the medium. The weak beam is referred to as a Stokes beam with $\omega_s < \omega_2$.

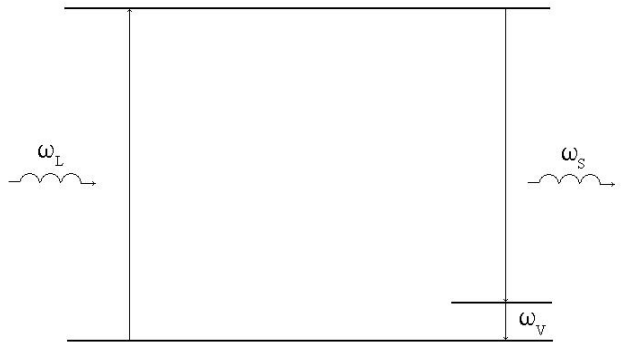

Fig. 2.1. Schematic diagram of Raman scattering.

UNIVERSITAT ROVIRA I VIRGILI
MODELLING OF PHOTONIC COMPONENTS BASED ON ÷(3) NONLINEAR PHOTONIC CRYSTALS
Ivan Maksymov
ISBN:978-84-593-4072-1/DL:T-1163-2010

Linear Raman scattering is a two-photon process wherein a laser photon scatters into a Stokes photon, which is down-shifted in frequency from the laser frequency by an amount equal to a Raman active mode in the medium, for example, molecular vibration quantum (see Fig. 2.1).

Stimulated Raman scattering is a four photon process wherein a Stokes beam incident on the Raman active medium is amplified. The gain in the Stokes beam is at the expense of photons lost from the laser beam. However, for a strong laser beam and weak Stokes beam, the laser field can be treated as approximately constant (nondepleted pump approximation).

The real part of the third order Raman susceptibility has a typical value of $\mathrm{Re}\left\{\chi_R^{(3)}\right\} \sim 10^{-20} m^2/V^2$. This is about two orders of magnitude larger than typical nonresonant electronic processes because of the resonant nature of the Raman effect. The response times of these effects are of the order of the lifetime of the Raman induced material excitations and is typically $\tau \sim 10^{-12} sec$.

Molecular orientational effects. Anisotropic molecules tend to exhibit an

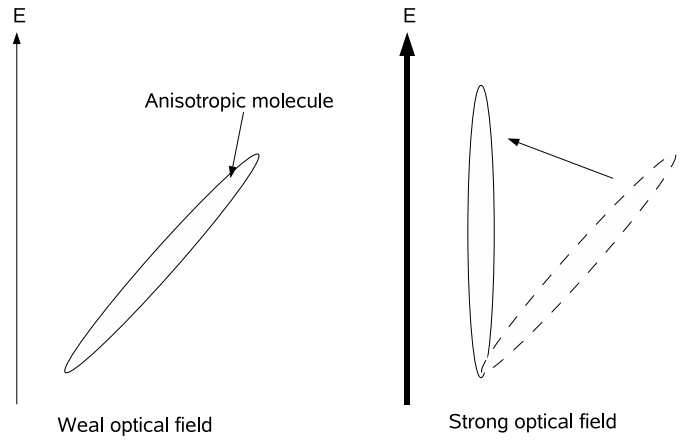

Fig. 2.2. Anisotropic molecular reorientation by a strong electric field.

ISBN:978-84-593-4072-1/DL:T-1163-2010

optically isotropic behaviour in the bulk when they are disordered, i.e., when their orientations are randomly distributed. This is true of several liquids (e.g., CS_2) and of liquid crystals. When a strong electric field is applied to such system (see Fig. 2.2), the induced dipole moments of the molecules experience a torque attempting to align the most polarizable axis with the applied field, working against the thermal fluctuation forces (i.e., molecular collisions).

When the applied field is dc, the effect is called the Kerr effect. Similarly, the field could be due to a strong optical field. The system then responds not to the instantaneous field but to the time averaged field squared and the effect is then termed the ac optical Kerr effect. When the alignment field and the incident optical field are one and the same, this leads to a self-induced refractive index change expressible by an n_2 as long as the induced dipole – electric field interaction energy is small compared to the thermal energy, which is typically the case.

Typical nonlinearities associated with small anisotropic molecular systems are $\chi^{(3)} \sim 10^{-22} - 10^{-21} m^2 / V^2$. The response time is $\tau \sim 10^{-12} sec$.

Electrostriction. This is a phenomenon that depends on the presence of an inhomogeneous intensity, i.e., a spatially varying, time averaged electric field. This would occur, for example, in the superposition of coherent waves to form an interference pattern of light and dark fringes, or along the transverse direction to a propagating Gaussian shaped beam. Such an inhomogeneous field produces a force on the molecules or atoms comprising a system called the electrostrictive force. This force can be understood from the fact that the induced dipoles in the medium will experience a translational force in a nonuniform field that is proportional to the gradient of the field. The force is such as to move the dipoles

ISBN:978-84-593-4072-1/DL:T-1163-2010

into a region of higher intensity. This produces an increase in the local density resulting in an increase of the refractive index locally. For this physical mechanism, the typical nonlinearity is $\chi^{(3)} \sim 10^{-20} m^2 / V^2$. The response time is $\tau \sim 10^{-9} sec$.

Thermal contributions. The change in index due to a temperature rise ΔT can be expressed as

$$\Delta n = \frac{dn}{dT} \Delta T , \tag{2.12}$$

where dn / dT is called the thermooptic coefficient. In most liquids and solids it is due to the density change (i.e., expansion) with the temperature. Since the density decrease in expansion and the refractive index is proportional to density, this contribution to dn / dT is generally negative. In some semiconductors, the absorption band edge will red-shift with temperature (Franz-Keldish effect). This produces a positive thermooptic coefficient.

Population redistribution. When the frequency of incident radiation is near a resonant energy transition of an atom or molecule, then real transitions are induced. This means that electrons can occupy real excited states for a finite period of time. This is called population redistribution. Since the optical polarization is ordinarily determined by the total number of atoms or molecules in the ground electronic state (for low intensity light), this population redistribution produces a change in the index of refraction. This effect can be seen in atomic vapours, molecular gases, liquid solutions of organic molecules, transparent dielectric solids doped with metal ions or colour centres, and semiconductors.

ISBN:978-84-593-4072-1/DL:T-1163-2010

In some situations, the near resonant interaction can be described as if the material had only two energy levels. This is because the resonant interaction between the radiatively connected ground and excited states is so strong that other nonresonant interactions can be ignored. It is assumed that the resonant frequency for a transition from the excited state to a higher lying state is far removed from that of the ground and excited states. The situation of semiconductors, with finite valence and conduction energy bands, is somewhat different depending on the time scale of the optical interaction.

A simple two-level system is illustrated in Fig. 2.3. It consists of the two levels are the ground (g) and excited (e). The resonant transition frequency connecting these states is defined by ω_{eg}. The system is also characterized by a transition dipole moment, μ_{eg}, and an equilibrium population difference $\Delta N^{eq} = \left(N_g - N_c\right)^{eq}$, where N_g and N_c are the number densities of atoms or molecules in the ground and excited states, respectively, long after or before the radiation is incident on the medium.

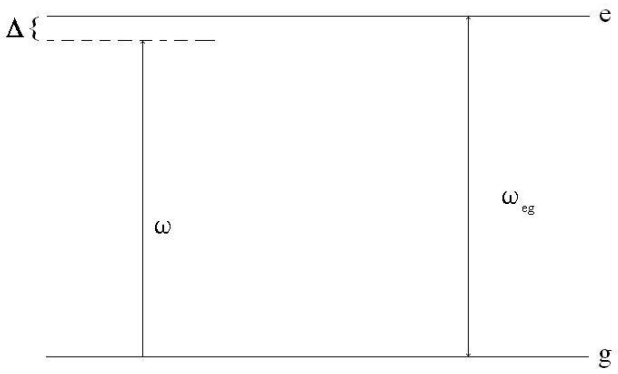

Fig. 2.3. Two-level system.

UNIVERSITAT ROVIRA I VIRGILI
MODELLING OF PHOTONIC COMPONENTS BASED ON ÷(3) NONLINEAR PHOTONIC CRYSTALS
Ivan Maksymov
ISBN:978-84-593-4072-1/DL:T-1163-2010

The average dipole moment of such a system described above is usually derived by density matrix theory. The polarization is then given as the average dipole moment per unit volume. In two particular time regimes, defined as the steady-state and the adiabatic following regimes, the resulting polarization P can be written as a constant times the applied field E. The susceptibility of the system is then given by $\varepsilon_0 \chi = P/E$.

The steady-state regime is the typical case of the response of a two-level system to a CW laser. The applied optical field is close to resonance, and a detuning parameter is defined by

$$\Delta = \omega - \omega_{eg} . \tag{2.13}$$

Since the frequency is near resonance, the susceptibility will be complex, with its real part related to the index of refraction and its imaginary part related to the absorption coefficient. The susceptibility is also proportional to the nonequilibrium population difference, which is itself dependent on the intensity of the incident radiation due to optically induced resonant transitions from the ground to excited states (i.e., absorption). Typical values are $\chi^{(3)} \sim 10^{-17} - 10^{-16} m^2/V^2$.

2.2 Wave propagation in nonlinear optical waveguides

2.2.1 Capacity limit of nonlinear optical waveguides

The performance of a practical transmission system depends on a large

ISBN:978-84-593-4072-1/DL:T-1163-2010

number of factors such as the detection method, the choice of the modulation format and so on. But the most fundamental factor is the channel capacity. The channel capacity is the maximum possible bit rate at which the information can be transmitted without errors over a channel with a certain noise level. The capacity (C) is determined by the usable bandwidth (B) of the channel and the spectral efficiency. The spectral intensity usually depends only on the ratio between the signal and the noise power, that is on the signal to noise ratio (S/N). The Shannon formula (sometimes called Kotelnikov-Shannon formula because Kotelnikov passed ahead of Shannon) [5-6] for a linear transmission system with the additive Gaussian noise gives

$$C = B \cdot E = B \cdot \log_2(1 + S/N). \tag{2.14}$$

In order to provide an example, the following case is considered. If the usable bandwidth (in the wavelength range) is 7.5 nm and it is centred at the wavelength 1.55 μm, the frequency bandwidth is calculated as

$$\Delta f \approx \frac{\Delta\lambda \cdot c}{\lambda^2} \approx 100 GHz\ . \tag{15}$$

For a signal ratio of 25 dB it gives the channel capacity of about 470 Gbit/s.

In the information theory, the channel is considered as linear where the noise is additive and independent on the signal power. The capacity of the channel increases as the power of the signal increases. But the realistic waveguides, like for example optical fibres, are nonlinear. If the signal power is increased, the intensity and therefore the efficiency of nonlinear effects will be increased. Thus

ISBN:978-84-593-4072-1/DL:T-1163-2010

the signal power and the noise are not independent of each other because an increase in the signal power leads to an increase of the noise. In addition, there is a power threshold which means that no additional power can enter into the waveguide. Therefore, the equations used to determine the capacity cannot be used.

In a nonlinear channel, the capacity cannot be increased up to infinity with the signal power and an optimum signal power should exist at which the capacity of the channel reaches its maximum. If the intensity is increased further, the stronger nonlinear effects will lead to a higher noise power and hence, to a reduction of the channel capacity.

Nonlinear effects in nonlinear waveguides can be divided into two groups [7]. The origin of the first group is the nonlinear refractive index. The origin of the second group are nonlinear scattering effects [2-3] (the Raman and the Brillouine scattering). The effects related to the nonlinear change in the refractive index can be estimated by using the third order nonlinear polarisation as

$$\vec{P}^{(3)} = \varepsilon_0 \chi^{(3)} ABC \,, \tag{16}$$

where A, B and C are the three different electric fields that can be coupled with each other by means of the nonlinear susceptibility $\chi^{(3)}$. An example is a WDM system where the bandwidth is divided into separately modulated sub bands. The two most important cases should be considered:

- In the case of self-phase modulation (SPM) [7-8], all three electric fields A, B and C come from the same channel and act back on this channel. For the SPM, the phase of the pulse is changed by its own intensity. This

ISBN:978-84-593-4072-1/DL:T-1163-2010

change leads to a frequency change (chirp) and, together with the dispersion of the fibre, can affect the temporal width of the pulse. Thus the SPM determines the minimal guard time between adjacent time channels. But if the pulses are injected with an opposite chirp, the temporal broadening due to SPM can be compensated.

- In the case of cross-phase modulation (XPM) [7-8], two fields of another channel in the system (for instance *B* and *C*) act on the channel *A*. As in the case of SPM, this can lead to a temporal broadening of the pulses and to the additional noise in the system and, therefore, a reduction of the capacity. Unlike SPM, this effect cannot be suppressed because the information in the other channels is independent of the information in channel *A*.

SPM effect has a very small influence on the parameters of the channel. The XPM, however, must be borne in mind when designing all-optical devices.

2.2.2 Nonlinear pulse propagation in slow wave structures

Light waves at different wavelength can interact by means of nonlinearities of the propagation medium. The development of all-optical devices has traditionally been focused on materials with strong nonlinearities. But for most of materials the nonlinearity is weak and it is followed by high absorption rate, which means that long devices or very high optical powers are required for creating efficient devices.

ISBN:978-84-593-4072-1/DL:T-1163-2010

It is known that nonlinear interactions can be enhanced inside optical resonators such as Fabry-Pérot cavities and microrings [9]. For a single resonator, a high level of enhancement implies narrow bandwidth. It does not permit developing of devices based on single resonators because of low operating efficiency. This problem disappears when a series of directly coupled resonators is cascaded to produce an optical slow wave structure (SWS) [10]. In optical SWS, additional resonators can be cascaded to increase nonlinear interaction length without affecting bandwidth. Spectral response can also be optimized to allow efficient optical signal processing on wideband channels.

The idea of direct-coupled resonators comes from the microwave field. Since such structures support waves with a group velocity that is significantly slower that the phase velocity of the wave, they are generally referred to as slow wave structures.

The SWS can be employed at optical frequencies. As in the case of microwave devices, optical SWS can be realized by forcing an optical wave to bounce back and forth through a number of direct-coupled resonators inserted into an optical waveguide. An optical SWS can be made by using Bragg gratings, by coupling of a sequence of microdisk resonators or by introducing defects in a photonic crystal [10-11]. Fig. 2.4 shows these three examples: direct-coupled Fabry-Pérot SWS (a), direct-coupled microring SWS (b) and photonic crystal SWS (c). The main property of SWS is the strong reduction of the group velocity [10] v_{gr} compared to that of the group velocity $v = c/n_0$ of the wave in the same, but unloaded waveguide and expressed by the slowing factor $S = v/v_{gr}$.

Inside a SWS the internal power P_m is increased by the resonant propagation with respect to the input power P_{inp} . According to the conservation of

ISBN:978-84-593-4072-1/DL:T-1163-2010

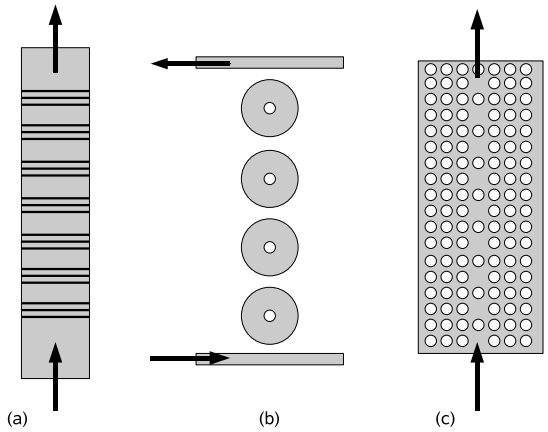

Fig. 2.4. Slow wave structures.

the energy flux, the enhancement factor P_m / P_{inp} results once more equal to the slowing ratio S. The nonlinear effective phase shift φ_{eff} can be related to the input power P_{inp} as [12]

$$\frac{d\varphi_{eff}}{dP_{inp}} = \frac{d\varphi_{eff}}{d\varphi}\frac{d\varphi}{dP_m}\frac{dP_m}{dP_{inp}}. \tag{2.17}$$

In Eq. (2.17), the first and the last derivatives are both equal to the slowing ratio S. The second term of this equation expresses the dependence of the nonresonant phase shift $d\varphi$ of the internal power P_m and it is proportional to the nonlinear constant $\gamma = \omega n_2 / cA_{eff}$, where A_{eff} is the effective mode area. Now the nonlinear effect in SWS can be described by defining an effective nonlinear constant γ_{eff} as

$$\gamma_{eff} = \frac{1}{d}\frac{d\varphi_{eff}}{dP_{inp}} = c_n \gamma S^2 , \qquad (2.18)$$

where the constant c_n depends on the particular kind of the structure and the values to be used in the case of SPM and XPM in SWS. It is evident from Eq. (2.18) that the slow wave propagation enhances both SPM and XPM by a factor proportional S^2

References

[1] R. D. Dupuis, “The diode laser – the first thirty days forty years ago”, LEOS Newsletter, vol. 17, no. 1, Feb. 2003.

[2] R. W. Boyd, *Nonlinear Optics* (Academic Press, Boston, 1992).

[3] R. L. Sutherland, *Handbook of nonlinear optics* (Marcel Dekker, New York, 1996).

[4] P.N. Prasad and D.J. Williams, *Introduction to Nonlinear Optical Effects in Molecules and Polymers* (John Wiley, New York, 1991).

[5] C. E. Shannon, “Communication in the presence of noise”, Proceedings of Institute of Radio Engineers, vol. 37, no. 1, pp. 20-21, Jan. 1949.

[6] V. A. Kotelnikov, “On the carrying capacity of the ether and wire in telecommunications”, Materials of the 1st All-Union Conference on Questions of Communications, Izd. Red. Upr. Svyazi RKKA, Moscow, 1933 (in Russian).

[7] T. Schneider, *Nonlinear optics in Telecommunications* (Springer-Verlag, Berlin, 2004).

[8] G. P. Agrawal, *Nonlinear fiber optics* (Academic Press, 1989).

[9] A. Yariv, *Optical Electronics in Modern Communications* (Oxford University Press, New York, 1997).

[10] A. Melloni, F. Morichetti and M. Martinelli, “Linear and nonlinear pulse propagation in coupled resonator slow-wave optical structures”, Opt. Quantum. Electron. **35**, 365 (2003).

[11] S. Mookherjea and A. Yariv, “Coupled resonator optical waveguides”, IEEE J. Select. Topics Quant. Electron. **8**, 448 (2002).

[12] J. E. Heebner and R. W. Boyd, “'Slow' and 'fast' light in resonator-coupled waveguides”, J. Modern Opt. **49**, 2629 (2002)..

UNIVERSITAT ROVIRA I VIRGILI
MODELLING OF PHOTONIC COMPONENTS BASED ON ÷(3) NONLINEAR PHOTONIC CRYSTALS
Ivan Maksymov
ISBN:978-84-593-4072-1/DL:T-1163-2010

Chapter 3

Numerical methods

This chapter describes and discusses the numerical methods that are employed in the dissertation. The description starts with the presentation and discussion of the methods of theoretical investigation of photonic crystals. These methods are compared by taking into consideration the possibility of their application to different problems. In this chapter, the main attention is devoted to the finite-difference time-domain (FDTD) method. The discussion is commenced by outlining the basic concepts of the method, existing types of boundary conditions and also some of its modifications and extensions including models of nonlinearity. In what follows, the special attention is paid to one of the specific applications of the FDTD method – numerical simulation of radiation of oscillating dipole embedded in photonic crystals. In this dissertation, the behaviour of oscillating dipoles embedded in nonlinear photonic crystal is studied for the first time. The finite-difference expression for the nonlinear regime are

ISBN:978-84-593-4072-1/DL:T-1163-2010

derived and presented in this chapter. A brief review of secondary numerical details finishes the chapter.

3.1 Methods of theoretical investigation of photonic crystals

As it was notices in the introduction, the theoretical investigation of photonic crystal's properties is one of the up-to-date tasks of the scientific community. The calculation of characteristics of the nonlinear photonic crystals is extremely important if all-optical devices are to be designed and analysed. In this section, existing approaches used for analysing photonic crystals are classified by considering their mathematical apparatus and then discussed taking into account the applicability to solve different classes of problems. First, these approaches can be mainly divided into four big groups that include the analytical, numerical-analytical, numerical grid and hybrid grid methods. Secondly, the secondary classification can be made by considering what kind of parameters has to be calculated. For example, the calculation of transmission and reflection consists in exploring analytically or numerically the propagation of the electromagnetic waves in finite structures like waveguides, cavities or photonic crystal lattices consisting of finite number of periods. By taking the Fourier transform of the temporal evolution of the field, one obtains the transmission and reflexion spectra. Such an approach corresponds to that used in realistic measurement techniques. In contrast, the dispersion characteristic calculation is carried out for infinite

structures where the periodic boundary conditions are imposed to model the periodicity. It is evident that in the reality no measurements can be made to verify theoretical results. However, the information on the structure obtained through the dispersion characteristic calculation really helps in developing optical devices. The following describes and discusses the approaches used for analysing the characteristics of nonlinear photonic crystals.

The first approach discussed here is analytical. It is borrowed from the solid-state theory where it was widely used to solve the Schrödinger equation [1]. This equation is one of the basics of the solid-state theory and it describes the behaviour of a particle in an arbitrary potential. Contrary to that, the photonic crystal analysis is based on the classical Maxwell theory that describes the behaviour of a wave packet in a medium. But under particular circumstances wave packets behave like particles thus justifying the application of the analytical approach to solve Maxwell's equations. However it can only be made in one-dimensional case where, due to the complexity of calculations, a lot of simplifications are made to achieve a result. In the linear regime, it is used to obtain both the transmission/reflexion spectra and the dispersion characteristics. In the nonlinear regime this approach is still very useful, but a lot of simplifications should be made [2-4].

The numerical-analytical approaches for investigating nonlinear photonic crystals are very useful in calculating dispersion characteristics. The plane wave expansion method is the brightest representative member of this group. It was also widely used in the solid-state theory and its application to photonic crystals is the result of the already mentioned analogy between them and semiconductors. The algorithm of the plane wave expansion method has lots of modifications [5-9]. Their goal is to solve the master equation for the magnetic modes of the photonic

ISBN:978-84-593-4072-1/DL:T-1163-2010

crystal. Doing so allows to determine the allowed mode frequencies for a given photonic crystal and also define which wave vectors $\vec{k}$ are associated with these modes. In other words, it determines the dispersion characteristic. Usually, the master equation is written as

$$\nabla \times \left[\frac{1}{\varepsilon(\vec{r})} \nabla \times \vec{H}_{\omega}(\vec{r}) \right] = \left(\frac{\omega}{c} \right)^2 \vec{H}_{\omega}(\vec{r}), \tag{3.1}$$

where $\vec{H}_{\omega}(\vec{r})$ is the magnetic field vector, $\varepsilon(\vec{r})$ is the position-dependent dielectric constant, c is the light speed and ω is the angular frequency. The subscript ω in $\vec{H}_{\omega}(\vec{r})$ means that the magnetic field pattern is different at each angular frequency. In addition to Eq. (3.1), the transversality requirement forces $\nabla \cdot \vec{H}_{\omega}(\vec{r}) = 0$.

The next step consists in expanding the field pattern into a set of plane waves. This converts the differential equation into a system of linear equations that can be solved numerically with one of the known methods [10]. Requiring that $\vec{H}(\vec{r})$ shares the periodicity of $\varepsilon(\vec{r})$ amounts to only including the reciprocal lattice $\vec{G}$ of the photonic crystal in the expansion

$$\vec{H}_{\omega}^{\vec{k}}(\vec{r}) = \sum_{\vec{G}\lambda} h_{\vec{G}\lambda} \hat{e}_{\lambda} e^{|i(\vec{k}+\vec{G})\vec{r}|}. \tag{3.2}$$

By means of Eq. (3.2) each mode with a wave vector $\vec{k}$ is identified and each mode is built out of plane waves with wave vector $\vec{k}+\vec{G}$ for all reciprocal lattice vectors $\vec{G}$. The polarization of each plane wave is one of the two unit vectors $\hat{e}_{\lambda}$, indexed by the label λ. The transversality requirement forces to consider only

ISBN:978-84-593-4072-1/DL:T-1163-2010

plane waves with $\hat{e}_{\lambda} \cdot \left(\vec{k} + \vec{G}\right) = 0$.

Before inserting this expansion into the master equation, the dielectric function $\varepsilon(\vec{r})$ should be also expanded in plane waves. As before, only plane waves whose wave vectors are reciprocal lattice vectors are considered because of the periodicity. Here, $\varepsilon\left(\vec{G},\vec{G}'\right)$ is called as the coefficient on the plane wave with wave vector $\left(\vec{G}'-\vec{G}\right)$. Inserting both expansions into the master equation (3.1), a system of linear equations is obtained

$$\sum_{(\vec{G}\lambda)'} \vec{\Theta}^{\vec{k}}_{(\vec{G}\lambda),(\vec{G}\lambda)'} \cdot h_{(\vec{G}\lambda)} = \left(\frac{\omega}{c}\right)^2 h_{(\vec{G}\lambda)}, \tag{3.3}$$

where the $\vec{k}$ -dependent matrix Θ is defined as the following quantity

$$\vec{\Theta}^{\vec{k}}_{(\vec{G}\lambda),(\vec{G}\lambda)'} = \left|\left(\vec{k} + \vec{G}\right) \times \hat{e}_{\lambda}\right| \cdot \left|\left(\vec{k} + \vec{G}'\right) \times \hat{e}_{\lambda'}\right| \varepsilon^{-1}\left(\vec{G}, \vec{G}'\right). \tag{3.4}$$

After that a technique to solve Hermitian eigenvalue problems is employed [11]. The following procedure is based on a complex expression for the variational energy of the eigenvalue problem [5]. Beginning with some guess for $h\left(\vec{G},\lambda\right)$, the program calculates the variational energy and updates its guess so as to lower the variational energy. The guesses are enforced to be orthogonal to any eigenvectors that were found previously. In this manner, all the eigenvalues $(\omega/c)^2$ can be obtained for a given value of $\vec{k}$. This information allows to plot dispersion characteristics.

In this dissertation, the author uses a freely available package MIT MPB

Table 3.1. Numerical-analytical approaches.

Method	**T/R**	**Disp. charact.**	**Nonlinearity**
Mode expansion [14]	Yes	Yes	Yes
Korringa-Kohn-Rostoker [15]	Yes	Yes	No
Fourier [16-17]	No	Yes	Yes
Modal [18]	Yes	No	Yes
Integral equation [19-22]	Yes	No	Yes
Spherical-wave [23-26]	No	Yes	Yes
Transfer matrix [27-28]	Yes	Yes	Yes

[12] based on the PWM to validate his codes in the linear regime. However, some of the modifications of the plane wave expansion method can be used to calculate dispersion characteristics of nonlinear photonic crystals [13]. In this case, an auxiliary iteration process is introduced to evaluate the amplitude of the electric field together with its influence on the intensity-dependent refractive index. Other representatives in the group of numerical-analytical approaches are presented in Table 3.1, which gives the information on their usability.

Considering the popularity of approaches from the following group – the group of the numerical grid methods -, the description here should be started with the finite-difference method [29]. This method is used to analyse both finite and infinite structures of all kinds and geometries. This fact makes it one of the most robustness numerical approaches for analysing characteristics of photonic crystals. There are two modifications of the finite-difference method. The type of the modification depends on whether the time derivative is considered in the

calculation or not. If it is considered, the method should be called by its very famous acronym FDTD [29], which means the “finite-difference time-domain”. This acronym was introduced by A. Taflove in 1980. At the present day, the word “FDTD” means an independent numerical method with tens of modifications and extensions [29]. However, if the time derivative is omitted, the acronym FD or finite-difference is used.

In the FDTD, the Maxwell's equations are discretized in both time and space and then iteratively solved for a finite number of iterations. All the dimensions can be considered. The simplest case is when a wave propagates in only one direction. In the two-dimensional case, when a wave propagates in a plane, the Maxwell's equations are divided into two sets for the TM and TE polarisations. Consequently, one should perform two independent calculations for each polarisation. In the three-dimensional case, all the field components and all the direction in space are considered, which means that the difference between the calculation and the natural electromagnetic field propagation is only due to discretization errors and computation limitations.

Unlike the FDTD method, the FD does not take into account the time derivatives and its algorithm is limited to solution of the Helmholtz equations. One equation contains the electric field vector and another one deals with the magnetic field vector. Here, no iteration process is made because the solution consists in solving a matrix equation, which takes into account the geometry of the photonic crystal and the boundary conditions. The main disadvantage arises when one tries to apply the FD method for computing dispersion characteristics of nonlinear photonic crystals. It is evident, that there is no manner to deal with nonlinearity if the basic equation does not include the electric field vector.

The second representative of the group of numerical grid methods is the

finite element method [30-31]. It is known to be a very flexible and powerful numerical tool due to the possibility to discretize arbitrary computation domains with fine grids of arbitrary configuration. The finite element method is used to calculate both dispersion characteristics and transmission spectra of nonlinear photonic crystal [32]. It was shown [33] that at the same memory requirements the finite element method is 10 times more complex than the FDTD method. It is the reason why a hybrid approach based on these two methods was proposed. In it, the central part of the computation domain is calculated with the FDTD and the finite element method is applied at the boundaries with a "complex" geometry.

The last group of the approaches for analysing the characteristics of nonlinear photonic crystal consists of hybrid grid methods. This group includes the method-of-lines [34], the beam propagation method [35-36], the finite-volume time-domain method [37] and the transmission line method [38-39]. The main attention should be paid to the beam propagation and the transmission line methods. The first of them is known to be a very efficient numerical tool, which is widely used in calculating the characteristic of nonlinear optical devices including photonic crystals. The second method, to the author's knowledge, was only implemented in one-dimensional nonlinear photonic crystal. Nevertheless, it can be extended to be applied to any geometry.

The comparison of the methods that belong to these four groups reveals that many of them can be applied to analyse nonlinear photonic crystals. However, each of them suffers from some disadvantages that arise from differences in algorithms and aims for which they were created. There is also one problem common for almost all the methods connected with a lack of universality. For example, the Fourier method was applied only for calculating dispersion characteristics of one-dimensional nonlinear photonic crystals. The Korringa-

Kohn-Rostoker (KKR) method has a very complex mathematical apparatus and its program realisation is a difficult task. The spherical-wave method is only valid for three-dimensional photonic crystals. Although the plane wave expansion method and the transfer matrix method are very suitable for calculating dispersion characteristics and transmission spectra, their application is limited because a change in geometry results in a change in the analytical expression in their algorithms. It prevents their application to structures with complex geometries, which cannot be described analytically. The finite element method seems to be universal, but its program realisation is difficult because very sophisticated mesh generators must be used.

Unlike all these methods, the finite-difference time-domain method looks like the most universal numerical tool for analysing nonlinear photonic crystals. A review of the up-to-date scientific software market reveals that this method is employed in the most powerful commercial programs such as FULLWAVE, OptiFDTD, Lumerical FDTD, XFDTD, CrystalWave and others. All these packages include models of nonlinear effects in various materials. In addition, they use the FDTD algorithm for analysing dispersion characteristics of photonic crystals. However, all they have the same problem in doing it. The procedure of dispersion characteristic calculation consists in computing energy spectra for each wave vector of the first Brilloune zone of a photonic crystal. The resonant peaks in these energy spectra give the eigenfrequencies, which are used to plot dispersion characteristics. Sometimes the amplitudes of the peaks can be very small or more than one peak can be situated in a narrow frequency interval as it frequently happens at the edges of the first Brilloune zone. It results in difficulties in plotting the dispersion characteristics that means that some parts of dispersion curves or even whole curves are not displayed. In the nonlinear regime, additional

ISBN:978-84-593-4072-1/DL:T-1163-2010

problems occur because a noise is produced by the nonlinear calculation. Tran [40], who was the first to calculate dispersion characteristics of Kerr nonlinear photonic crystals, encountered this problem and tried to explain it reasonably.

In order to avoid these problems, the developers complete their programs with band structure solvers based on the plane wave expansion method [6, 41]. These solvers are very efficient in the linear regime and some of them [42] can deal with nonlinear materials. But the question on the accuracy of the calculation is still open. The comparison of results obtained with the nonlinear plane wave expansion method [13, 43] and, for example, the nonlinear finite element method [44] shows a discrepancy when estimating intensities that induce the nonlinearity. Apart from the accuracy, there is also a difference between the mathematical apparatus of the FDTD and the plane wave expansion methods. For example, sometimes it is desirable to compare the positions of the forbidden bang gap defined via the dispersion characteristic with that taken from the transmission spectrum. In the most of the linear calculations the difference is negligible. In the nonlinear regime, however, it does exist due to the difference in treating the impact of the light intensity.

Many of these problems would be solved if the band structure solvers were based on the FDTD method. This method is very popular now and as the computer power rises it becomes possible to solve more and more complex problems with it. The accuracy of the FDTD method depends on only the CPU speed and amount of RAM available for calculation. In addition, a considerable effort in developing material models for use with this method makes it possible to employ the FDTD for a wide set of optical problems.

ISBN:978-84-593-4072-1/DL:T-1163-2010

3.2 Finite-difference time-domain method

3.2.1 Basics of the method

The finite-difference time-domain (FDTD) method is extensively explained in book of A. Taflove [29], which can be called the FDTD Bible. The explanation of the method should be started with the Maxwell's equations (2.1) – (2.4). Here, a linear and isotropic material and no free charges or currents are assumed for simplicity. In the FDTD method, the notation proposed by Yee [45] is used. Following his notation, a space point in a uniform rectangular lattice can be represented as

$$(i, j, k) = (i\Delta x, j\Delta y, k\Delta z). \tag{3.5}$$

Here Δx, Δy and Δz are, respectively, the lattice space increments in the x, y and z coordinate directions, and i, j and k are integers. Further, any function u of space and time evaluated at a discrete point in the grid and at a discrete point in time can be written as

$$u(i\Delta x, j\Delta y, k\Delta z, n\Delta t) = u^{n}{}_{i,j,k}, \tag{3.6}$$

where Δt is the time increment and n is an integer. The time increment must satisfy the Courant stability condition

ISBN:978-84-593-4072-1/DL:T-1163-2010

$$\Delta t \le \frac{c}{\sqrt{\frac{1}{(\Delta x)^2}+\frac{1}{(\Delta y)^2}+\frac{1}{(\Delta z)^2}}}. \tag{3.7}$$

The first partial space derivative of u in the x-direction evaluated at time $t_n = n\Delta t$ is then expressed as

$$\frac{\partial u}{\partial x}(i\Delta x, j\Delta y, k\Delta z, n\Delta t) = \frac{u^n{}_{i+1/2,j,k} - u^n{}_{i-1/2,j,k}}{\Delta x} + O\left[(\Delta x)^2\right]. \tag{3.8}$$

Yee's expression for the first time partial derivative of u evaluated at a fixed space point (i, j, k) follows by an analogy

$$\frac{\partial u}{\partial t}(i\Delta x, j\Delta y, k\Delta z, n\Delta t) = \frac{u^{n+1/2}{}_{i,j,k} - u^{n-1/2}{}_{i,j,k}}{\Delta t} + O\left[(\Delta t)^2\right]. \tag{3.9}$$

Yee chose this notation because he wished to interleave his $\vec{E}$ and $\vec{H}$ components in time at intervals of $(1/2)t$ for purposes of implementing a leapfrog algorithm.

Eqs. (2.1) – (2.4) in two-dimensions immediately reduce to two sets of equations for the TE polarisation (E_x, E_y and H_z are nonzero) and TM polarisation (H_x, H_y and E_z are nonzero). In the TE case, one obtains

$$-\mu\mu_0 \frac{\partial H_z}{\partial t} = \frac{\partial E_y}{\partial x} - \frac{\partial E_x}{\partial y}, \tag{3.10}$$

UNIVERSITAT ROVIRA I VIRGILI
MODELLING OF PHOTONIC COMPONENTS BASED ON ÷(3) NONLINEAR PHOTONIC CRYSTALS
Ivan Maksymov
ISBN:978-84-593-4072-1/DL:T-1163-2010

$$\frac{\partial D_x}{\partial t} = \frac{\partial H_z}{\partial y}, \tag{3.11}$$

$$-\frac{\partial}{\partial t} D_y = \frac{\partial H_z}{\partial x}, \tag{3.12}$$

The E_x and E_y components are found by using the constitutive relations $E_x = D_x/(\varepsilon\varepsilon_0)$ and $E_y = D_y/(\varepsilon\varepsilon_0)$, respectively, where ε is the dielectric constant and ε_0 is the electric permittivity of free space. In the TM case, one has the following formulae

$$\frac{\partial D_z}{\partial t} = \frac{\partial H_y}{\partial x} - \frac{\partial H_x}{\partial y}, \tag{3.13}$$

$$\mu\mu_0 \frac{\partial H_y}{\partial t} = \frac{\partial D_z}{\partial y}, \tag{3.14}$$

$$-\mu\mu_0 \frac{\partial H_x}{\partial t} = \frac{\partial D_z}{\partial x}, \tag{3.15}$$

where the E_z component is found by using the constitutive relation $E_z = D_z/(\varepsilon\varepsilon_0)$.

The finite-difference equations corresponding to Eqs. (3.10)-(3.12) are

$$H_z^{n+1/2}\left(i+\frac{1}{2}, j+\frac{1}{2}\right) = H_z^{n-1/2}\left(i+\frac{1}{2}, j+\frac{1}{2}\right) - \frac{\Delta t}{\mu\mu_0} \cdot \left[\frac{E_y^n\left(i+1, j+\frac{1}{2}\right) - E_y^n\left(i, j+\frac{1}{2}\right)}{\Delta x} - \frac{E_x^n\left(i+\frac{1}{2}, j+1\right) - E_x^n\left(i+\frac{1}{2}, j\right)}{\Delta y} \right], \tag{3.16}$$

UNIVERSITAT ROVIRA I VIRGILI
MODELLING OF PHOTONIC COMPONENTS BASED ON ÷(3) NONLINEAR PHOTONIC CRYSTALS
Ivan Maksymov
ISBN:978-84-593-4072-1/DL:T-1163-2010

$$D_x^{n+1}\left(i+\frac{1}{2},j\right)=D_x^{n}\left(i+\frac{1}{2},j\right)+\frac{\Delta t}{\Delta y}\cdot\left[H_z^{n+\frac{1}{2}}\left(i+\frac{1}{2},j+\frac{1}{2}\right)-H_z^{n+\frac{1}{2}}\left(i+\frac{1}{2},j-\frac{1}{2}\right)\right], \quad (3.17)$$

$$D_y^{n+1}\left(i,j+\frac{1}{2}\right)=D_y^{n}\left(i,j+\frac{1}{2}\right)-\frac{\Delta t}{\Delta x}\cdot\left[H_z^{n+\frac{1}{2}}\left(i+\frac{1}{2},j+\frac{1}{2}\right)-H_z^{n+\frac{1}{2}}\left(i-\frac{1}{2},j+\frac{1}{2}\right)\right]. \quad (3.18)$$

The constitutive relations are $E_x^{n+1}\left(i+\frac{1}{2},j\right)=D_x^{n+1}\left(i+\frac{1}{2},j\right)/\varepsilon\varepsilon_0$ and $E_y^{n+1}\left(i,j+\frac{1}{2}\right)=D_y^{n+1}\left(i,j+\frac{1}{2}\right)/\varepsilon\varepsilon_0$. The finite-difference expressions for Eqs. (3.13)-(3.15) are

$$D_z^{n+1}(i,j)=D_z^{n}(i,j)+\Delta t\cdot\left[\frac{H_y^{n+1/2}\left(i+\frac{1}{2},j\right)-H_y^{n+1/2}\left(i-\frac{1}{2},j\right)}{\Delta x}-\frac{H_x^{n+1/2}\left(i,j+\frac{1}{2}\right)-H_x^{n+1/2}\left(i,j-\frac{1}{2}\right)}{\Delta y}\right], \quad (3.19)$$

$$H_x^{n+1/2}\left(i,j+\frac{1}{2}\right)=H_x^{n-1/2}\left(i,j+\frac{1}{2}\right)-\frac{\Delta t}{\Delta y\mu\mu_0}\cdot\left[E_z^{n}(i,j+1)-E_z^{n}(i,j)\right], \quad (3.20)$$

$$H_y^{n+1/2}\left(i+\frac{1}{2},j\right)=H_y^{n-1/2}\left(i+\frac{1}{2},j\right)+\frac{\Delta t}{\Delta x\mu\mu_0}\cdot\left[E_z^{n}(i+1,j)-E_z^{n}(i,j)\right]. \quad (3.21)$$

The constitutive relation is $E_z^{n+1}(i,j)=D_z^{n+1}(i,j)/\varepsilon\varepsilon_0$. Eqs. (3.16)-(3.21) are iteratevly solved for the total number of time steps N_t, which defines the total simulated time.

ISBN:978-84-593-4072-1/DL:T-1163-2010

3.2.2 Boundary conditions

Obviously, the FDTD method cannot be used to describe electromagnetic fields in an infinite area in space. If a propagating wave reaches the unbounded edge of the grid, the calculation becomes unstable and the program “hangs up”. The problem of free surrounding space can be solved by using the absorbing boundary conditions that can be of two types: the analytical (for example, Mur [46] or Liao [47] approaches) and the numerical (various modifications of PML originally proposed by Berenger [48]). The analytical approaches absorb well only the electromagnetic waves incident on the boundary at about 90^{o}. Therefore their implementation is not acceptable if an accurate modelling is required. However, in some cases it turns out that their implementation results in satisfying absorption and simple realisation in the program. This is true for example for the Mur's second order absorbing boundary conditions imposed only in one of the directions. The author uses it in one of his programs [49]. Regarding to the PML, the author implements one of the modifications called the convolutional PML or simply CPML [50]. The CPML has been known to be one of the robustness implementations of the PML because of simplicity in coding and extremely high ability to absorb wave propagating at all angles and of almost all frequencies. All the approaches mentioned here are well-known by the scientific community and their implementation with the FDTD method is widely discussed in the literature [29, 51-53].

Another type of boundary conditions consists in assuming that the structure modelled is infinite. These boundary conditions are called periodic and come directly from the Bloch theorem [54]. They are widely used in analysing the

ISBN:978-84-593-4072-1/DL:T-1163-2010

photonic crystal while calculating their dispersion characteristics. If the structure is infinite in only one or two dimensions, the periodic boundary condition can be combined with absorbing boundary conditions. Here, the applications of the periodic boundary conditions will be considered for the two most common lattices of photonic crystal: the square and the triangle.

The most common form to express the periodic boundary conditions is the following

$$\Phi(\vec{r}+\vec{a},t)=\Phi(\vec{r},t)\exp\left(\hat{j}\vec{k}\vec{a}\right), \tag{3.22}$$

where $\vec{\Phi}$ is any field component ($\vec{E}$ or $\vec{H}$), $\vec{a}$ is the period, $\vec{k}$ is the wave vector in the first Brillouin zone and $\hat{j}=\sqrt{-1}$. The FDTD implementation of Eq. (3.22) is graphically shown for the square lattice (Fig. 3.1) and triangular lattice (Fig. 3.2). In this work, only the orthogonal finite-difference grid is used and, if even the

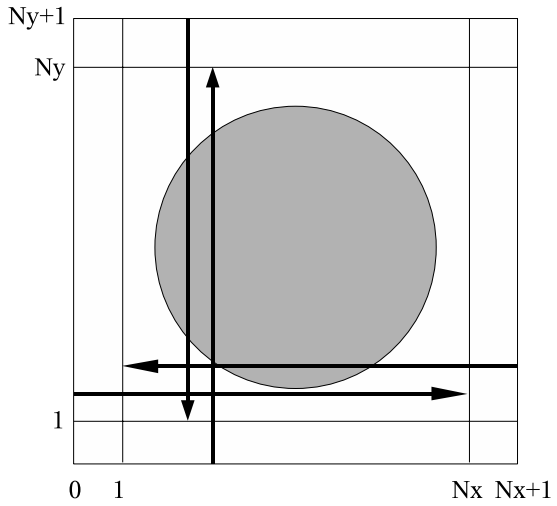

Fig. 3.1. Periodic boundary conditions for the square lattice.

triangular lattice is considered, it remains useful.

In Fig. 3.1, the computation domain is a square area discretised by the finite-difference grid. The circle corresponds to the area of high refractive index while the white area is the background with $\varepsilon = 1$. Only the first two and the last two nodes of the grid are meaningful in implementing Eq. (3.22). The black arrows show how the field components at the edges of the computation domain are updated. Considering the two-dimensional case and the TM polarisation, one should only impose the boundary conditions for the electric field components E_x and E_y because only they lie in the plane of periodicity. One has

$$E_x(i, ny+1) = E_x(i,1)\exp\left(\hat{j}k_y a\right), \tag{3.23}$$

$$E_x(i,0) = E_x(i, ny)\exp\left(-\hat{j}k_y a\right), \tag{3.24}$$

$$E_y(nx+1, j) = E_y(1, j)\exp\left(\hat{j}k_x a\right), \tag{3.25}$$

$$E_y(0, j) = E_y(nx, j)\exp\left(-\hat{j}k_x a\right). \tag{3.26}$$

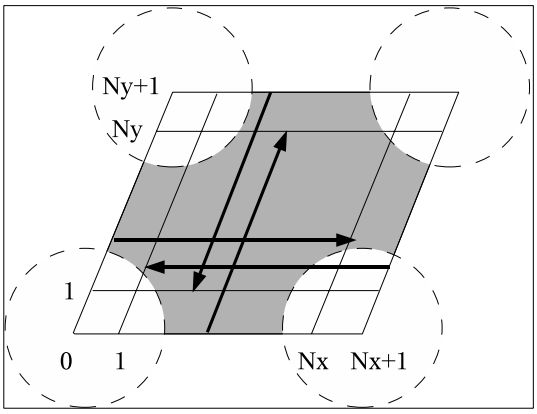

Fig. 3.2. Periodic boundary conditions for the triangular lattice.

ISBN:978-84-593-4072-1/DL:T-1163-2010

where i and j run from 0 to Nx or Ny, and k_x and k_y are the components of the wave vector.

In dealing with the TE polarisation, one should use H_x and H_y instead of E_x and E_y. If a dispersion characteristic is calculated for all directions of the first Brillouin zone, one should take into account the following points: $\Gamma(0,0)$, $X(\pi/a,0)$ and $M(\pi/a,\pi/a)$, where the first and the second values in parenthesis correspond to k_x and k_y, respectively.

In Fig. 3.2, the computation domain is a rectangular area, which includes a rhombus corresponding to the triangular lattice [29]. The grey area corresponds to the area of the background (high refractive index). The circles show the position of the holes drilled in the background. The black arrows show how the field components at the edges of the computation domain are updated. Both the rectangular area and rhombus are on the same orthogonal finite-difference grid, but the periodic boundary conditions are imposed only on the sides of the rhombus. In this case, the analogues of Eqs. (3.23)-(2.26) can be written as

$$E_x(i,ny+1) = E_x(i+a/2,1)\exp(\hat{j}k_y a), \tag{3.27}$$

$$E_x(i+a/2,0) = E_x(i,ny)\exp(-\hat{j}k_y a), \tag{3.28}$$

$$E_y(ny/\cos(60^o)+a/2,j) = E_y(ny/\cos(60^o),j)\exp(\hat{j}k_x a), \tag{3.29}$$

$$E_y(ny/\cos(60^o),j) = E_y(ny/\cos(60^o)+a/2,j)\exp(-\hat{j}k_x a). \tag{3.30}$$

As before, in dealing with the TE polarisation, one should use H_x and H_y instead

ISBN:978-84-593-4072-1/DL:T-1163-2010

of E_x and E_y. If a dispersion characteristic is calculated for all directions of the first Brillouin zone, one should take into account the following points: $\Gamma(0,0)$, $K\left(\pi/a, \pi/a\sqrt{3}\right)$ and $M(4\pi/3a,0)$.

3.2.3 Order-N method

Order-N is the name of an FDTD-based approach for analysing dispersion characteristics of photonic crystals [29, 55]. This method uses the same finite-difference time-domain scheme and boundary conditions as those described in the previous sections. However, it differs from the standard FDTD in the initial condition and postprocessing operations.

In the original Order-N [55], a set of plane waves that include all wave number taken into account in the simulation is used as the initial condition. In this dissertation, however, the incident intensity is simulated with the Dirac delta pulse of amplitude I_{inc} whose value varies depending on the goal of the simulation [49]. In the first step of the calculation process, only field components situated in randomly chosen nodes of the finite-difference grid are excited, while all field components in other nodes are set to be zero. Fig. 3.3 schematically shows an example of such an initial distribution. Here, the open circles correspond to those nodes that are chosen with a random number generator and excited.

The calculation is limited by two factors: the total simulated time T and the step in time Δt. The first factor is connected with the total number of time steps, which should be sufficiently large to obtain high resolution in the frequency domain. Usually, the number of time steps varies between $2^{14} \div 2^{16}$ and it defines

ISBN:978-84-593-4072-1/DL:T-1163-2010

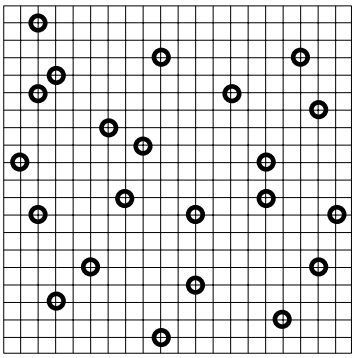

Fig. 3.3. Randomly chosen nodes of the FD grid.

the lowest frequency that can be simulated, i.e. $\omega_{MIN} \sim 2\pi / T$. The second factor is governed by the Courant stability condition. It defines the highest frequency that can be simulated, i.e. $\omega_{MAX} \sim 2\pi / \Delta t$.

The calculation is carried out for each value of the wave vector. The components of electric and magnetic fields are recorded at each step in time and after that multiplied by the Gaussian pulse to filter the noise produced by the calculation. After the multiplication has finished, the fields are Fourier transformed to the frequency domain to obtain the spectral intensities. The peaks in the spectra give the eigenfrequencies.

3.2.4 Models of the Kerr nonlinearity

In the last decades, much attention has been paid to model nonlinear media with the FDTD method. Merewether and Radasky [56] were the first who used the FDTD method in this way. Various techniques to model Kerr nonlinear media and

ISBN:978-84-593-4072-1/DL:T-1163-2010

dispersive nonlinear effects were presented independently by different authors [57-59]. With these techniques, one can investigate the propagation and scattering of femtosecond electromagnetic pulses. Alternative approaches such as the combined Maxwell-Bloch FDTD scheme and the Z-transform based FDTD scheme were later proposed [60-64] to model more complicated dispersive and nonlinear materials. Particularly, the dynamic nonlinear optical skin effect and self-induced transparency were studied. Tran in 1995 [40] was first who calculated dispersion characteristics of Kerr nonlinear photonic crystals. He did it only for the TM polarisation case and showed the problems that were encountered in the calculation. To the author's knowledge, the FDTD method has not been more used to this end. In the calculation of transmission spectra, however, the FDTD method is the absolute leader. Apart from other applications, it is used to model such optical devices as couplers, switches, splitters and modulators.

It was shown that in the linear regime the constitutive relation that relates $\vec{D}$ to $\vec{E}$ can be written as

$$\vec{D}(\vec{r},t) = \varepsilon_0 \varepsilon(\vec{r}) \cdot \vec{E}(\vec{r},t), \tag{3.31}$$

where the dielectric constant ε is connected with the refractive index n as

$$n = \sqrt{\varepsilon}. \tag{3.32}$$

In the nonlinear regime, however, Eq. (3.31) becomes more complex because it must account for the Kerr effect. Using Eq. (11), one can rewrite Eq. (3.31) as

ISBN:978-84-593-4072-1/DL:T-1163-2010

$$\vec{D}(\vec{r},t) = \varepsilon_0 \left(\varepsilon_L(\vec{r}) + \chi^{(3)} \left| \vec{E}(\vec{r},t) \right|^2 \right) \cdot \vec{E}(\vec{r},t), \tag{3.33}$$

where $\varepsilon_L(\vec{r})$ denotes an intensity independent (linear) dielectric constant, which equals to that from Eq. (3.32); $\chi^{(3)}$ is the Kerr coefficient. It should be noticed that the Kerr coefficient $\chi^{(3)}$ is measured in m^2/V^2, but in the literature it sometimes is substituted by other parameter called the nonlinear index of refraction and denoted as n_2. Unlike $\chi^{(3)}$, n_2 is expressed in terms of intensity. In order to relate them, the following formula is used

$$n_2 = \frac{\chi^{(3)}}{\varepsilon \varepsilon_0 c}. \tag{3.34}$$

The FDTD standard scheme is still valid to solve the Maxwell's equations (2.1) – (2.4) with the constitutive relation (3.33). For example, in the two-dimensional case the same equations (3.16)-(3.21) are used, but the finite-difference equation for the constitutive relation (TM polarisation) is

$$E_z^{n+1}(i,j) = \frac{D_z^{n+1}(i,j)}{\varepsilon_0 \left\{ \varepsilon(i,j) + \chi^{(3)}(i,j) \left| E_z^{n}(i,j) \right|^2 \right\}}, \tag{3.35}$$

where, following the notation used in this work, the modulus square of the electric field taken from the previous time step is used to calculate a change in the dielectric constant. Such an approach was found to be stable by the author [65] and also in the paper [66]. However, the selection of the instant in time Δt requires a special care because no stability condition was derived until now for the

UNIVERSITAT ROVIRA I VIRGILI
MODELLING OF PHOTONIC COMPONENTS BASED ON ÷(3) NONLINEAR PHOTONIC CRYSTALS
Ivan Maksymov
ISBN:978-84-593-4072-1/DL:T-1163-2010

nonlinear regime. The author found that it was possible to use a restricted Courant stability condition

$$\Delta t \le \frac{S \cdot c}{\sqrt{\frac{1}{(\Delta x)^2} + \frac{1}{(\Delta y)^2} + \frac{1}{(\Delta z)^2}}}, \tag{3.36}$$

where $0.75 \le S \le 1$ is an experimentally fitted coefficient. The smaller the instant in time, the more stable the nonlinear scheme. But the numerical errors increase as S decreases [29]. Sometimes it leads to some inconveniencies in automatization of calculations because each run of the program requires revising of the value of Δt. These inconveniencies can be avoided if the approach proposed by Tran in [40] is applied. Instead of taking the modulus square of the electric field from the previous time step, Tran proposed to analytically solve the following cubic equation, which can be obtained from Eq. (3.35)

$$\left|\chi^{(3)}\right| \cdot A^3 + 2\,\mathrm{Re}\left[\varepsilon^* \chi^{(3)}\right] \cdot A^2 + \left|\varepsilon\right| \cdot A - \frac{\left|\vec{D}\right|^2}{\varepsilon_0^2} = 0, \tag{3.37}$$

Where $A = \left|\vec{E}\right|^2$ is the modulus square of the electric field, ε^* is the complex conjugated of ε and the operator Re takes the real part of a complex number. Because the modulus square can be neither negative nor complex, only a real positive root is taken into account.

Once A is obtained, the electric field $\vec{E}$ is calculated as

UNIVERSITAT ROVIRA I VIRGILI
MODELLING OF PHOTONIC COMPONENTS BASED ON ÷(3) NONLINEAR PHOTONIC CRYSTALS
Ivan Maksymov
ISBN:978-84-593-4072-1/DL:T-1163-2010

$$\vec{E} = \frac{\vec{D}}{\varepsilon_0\left(\varepsilon_L + \chi^{(3)} \cdot A\right)}. \tag{3.38}$$

3.2.5 Simulation of radiation of oscillating dipole embedded in photonic crystals

Sakoda [54] proposed another technique to calculate dispersion characteristics of photonic crystals. It consists in simulating of the radiation of the oscillating dipole embedded into the photonic crystal by means of the FDTD method. The dipole is situated in the unit cell of the photonic crystal truncated with the periodic boundary conditions. The frequency of oscillation changes in a range of interest. For each frequency from this range the electromagnetic energy density radiated by the dipole is calculated by means of the FDTD method. The FDTD algorithm is repeated N_c times in the so-called oscillating cycle. The electromagnetic energy density radiated in each oscillating cycle is accumulated

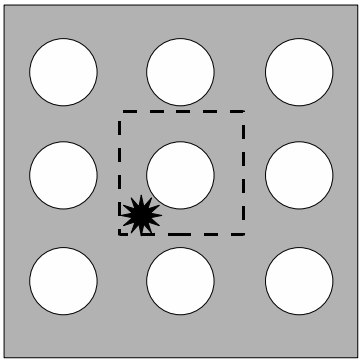

Fig. 3.4. Two-dimensional photonic crystal with an embedded oscillating dipole. The dashed line denotes the unit cell.

ISBN:978-84-593-4072-1/DL:T-1163-2010

in all nodes of the finite-difference grid and saved when the cycle is finished. This procedure is repeated for all wave vector of the first Brillouin zone. As a result, one obtains the energy density spectra for these wave vectors. The dispersion characteristics are obtained from the resonance peaks of these spectra.

Fig. 3.4 illustrates the Sakoda's idea. The 12-point star denotes the dipole situated within the unit cell (dash line). The periodic boundary conditions are imposed on the edges of the unit cell as it shown in Fig. 3.1.

In the language of formulae, the Sakoda's technique is described with the Maxwell's equations (2.1)-(2.4) together with the constitutive relations

$$\nabla \times \vec{E}(\vec{r},t) = -\frac{\partial}{\partial t}\left[\mu\mu_0 \vec{H}(\vec{r},t) + \vec{P}_M(\vec{r},t)\right], \tag{3.39}$$

$$\nabla \times \vec{H}(\vec{r},t) = \frac{\partial}{\partial t}\left[\vec{D}(\vec{r},t) + \vec{P}_E(\vec{r},t)\right], \tag{3.40}$$

where the polarisation fields $\vec{P}_M(\vec{r},t)$ and $\vec{P}_E(\vec{r},t)$ are respectively for the electric and magnetic oscillating dipole embedded into the lattice of the photonic crystal. In the explicit form the polarisation fields can be expressed as

$$\vec{P}_E(\vec{r},t) = \vec{e}_\mu \delta(\vec{r} - \vec{r}_0)\exp\left(-\hat{j}\omega t\right), \tag{3.41}$$

$$\vec{P}_M(\vec{r},t) = \vec{h}_\mu \delta(\vec{r} - \vec{r}_0)\exp\left(-\hat{j}\omega t\right), \tag{3.42}$$

where $\vec{e}_\mu(\vec{r},t)$ and $\vec{h}_\mu(\vec{r},t)$ are the amplitudes of the electric and magnetic dipoles, $\vec{r}_0$ denotes their position within the photonic crystal and ω is the angular frequency of the oscillation; $\hat{j}$ refers to the imaginary unit and $\delta(\vec{r} - \vec{r}_0)$ denotes the Dirac

ISBN:978-84-593-4072-1/DL:T-1163-2010

delta function.

The electromagnetic energy density emitted per unit time by the oscillating dipole at $\vec{r}_0$ can be calculated by using the following expression [67]

$$W = \frac{1}{2}\left[\vec{E}(\vec{r})\cdot\vec{D}(\vec{r}) + \mu\mu_0\left|\vec{H}(\vec{r})\right|^2\right]. \tag{3.43}$$

Taking into account the changes made, Eqs. (3.10)-(3.15) have now the following form

$$-\frac{\partial}{\partial t}\left[\mu\mu_0 H_z + h_{\mu_z}\delta(x-x_0)\delta(y-y_0)\exp\left(-\hat{j}\omega t\right)\right] = \frac{\partial E_y}{\partial x} - \frac{\partial E_x}{\partial y}, \tag{3.44}$$

$$\frac{\partial}{\partial t}D_x = \frac{\partial H_z}{\partial y}, \tag{3.45}$$

$$-\frac{\partial}{\partial t}D_y = \frac{\partial H_z}{\partial x}, \tag{3.46}$$

and

$$\frac{1}{c}\frac{\partial}{\partial t}\left[D_z + e_{\mu_z}\delta(x-x_0)\delta(y-y_0)\exp\left(-\hat{j}\omega t\right)\right] = \frac{\partial H_y}{\partial x} - \frac{\partial H_x}{\partial y}, \tag{3.47}$$

$$\mu\mu_0\frac{\partial H_y}{\partial t} = \frac{\partial D_z}{\partial y}, \tag{3.48}$$

$$-\mu\mu_0\frac{\partial H_x}{\partial t} = \frac{\partial D_z}{\partial x}. \tag{3.49}$$

It can be seen that only Eqs. (3.44) and (3.47) are changed. Their finite-

UNIVERSITAT ROVIRA I VIRGILI
MODELLING OF PHOTONIC COMPONENTS BASED ON ÷(3) NONLINEAR PHOTONIC CRYSTALS
Ivan Maksymov
ISBN:978-84-593-4072-1/DL:T-1163-2010

difference analogues are the following

$$H_z^{n+1/2}\left(i+\frac{1}{2,}j+\frac{1}{2}\right)=H_z^{n-1/2}\left(i+\frac{1}{2,}j+\frac{1}{2}\right)$$
$$-\frac{\Delta t}{\mu\mu_0}\cdot\left[\frac{E_y^{\,n}\left(i+1,\,j+\frac{1}{2}\right)-E_y^{\,n}\left(i,\,j+\frac{1}{2}\right)}{\Delta x}-\frac{E_x^{\,n}\left(i+\frac{1}{2},\,j+1\right)-E_x^{\,n}\left(i+\frac{1}{2},\,j\right)}{\Delta y}\right]$$
$$+\frac{\hat{j}\omega h_{\mu_z}}{\Delta x\Delta y}\cdot\delta_{ii0}\delta_{jj0}\exp\left(-\hat{j}\omega n\Delta t\right) \quad (3.50)$$

$$D_z^{n+1}(i,j)=D_z^{n}(i,j)$$
$$+\Delta t\cdot\left[\frac{H_y^{n+1/2}\left(i+\frac{1}{2},j\right)-H_y^{n+1/2}\left(i-\frac{1}{2},j\right)}{\Delta x}-\frac{H_x^{n+1/2}\left(i,j+\frac{1}{2}\right)-H_x^{n+1/2}\left(i,j-\frac{1}{2}\right)}{\Delta y}\right]$$
$$+\frac{\hat{j}\omega e_{\mu_z}}{\Delta x\Delta y}\cdot\delta_{ii0}\delta_{jj0}\exp\left(-\hat{j}\omega n\Delta t\right) \quad (3.51)$$

The expressions δ_{ii0} and δ_{jj0} denote the position of the dipole on the finite-difference grid. The energy density is calculated using the fields obtained from the Maxwell's equations. For the TE polarisation it has the following form

$$W=\frac{1}{2}\sum_{i,j=0}^{N_x,N_y}\left[E_x\left(i+\frac{1}{2},j\right)\cdot D_x\left(i+\frac{1}{2},j\right)+E_y\left(i,j+\frac{1}{2}\right)\cdot D_y\left(i,j+\frac{1}{2}\right)+\mu\mu_0 H_z^2\left(i+\frac{1}{2},j+\frac{1}{2}\right)\right] \quad (3.52)$$

ISBN:978-84-593-4072-1/DL:T-1163-2010

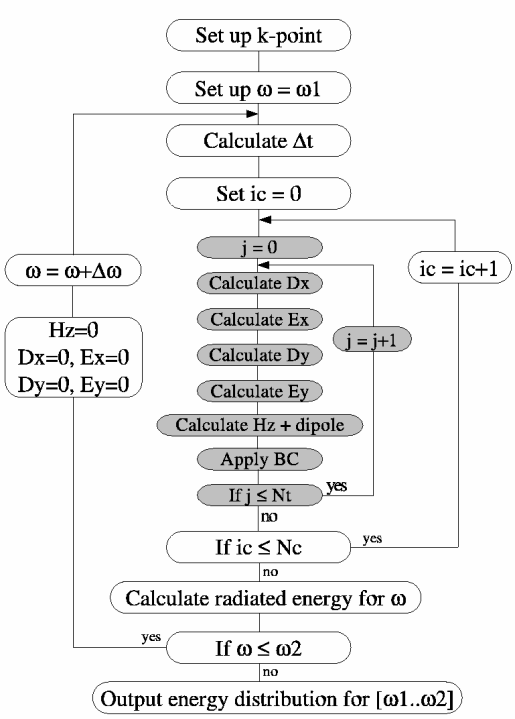

Fig. 3.5. Flow chart of the calculation process.

while for the TM polarisation it is

$$W = \frac{1}{2}\sum_{i,j=0}^{N_x,N_y}\left[E_z(i,j)\cdot D_z(i,j) + \mu\mu_0\left\{H_x^2\left(i,j+\frac{1}{2}\right) + H_y^2\left(i+\frac{1}{2},j\right)\right\}\right]. \qquad (3.53)$$

Fig. 3.5 shows the flow chart of the calculation process for a component of the wave vector $\vec{k}$ (so-called k-point). In this figure, ω denotes the angular frequency, which varies between ω_1 and ω_2 with the step $\Delta\omega$; i_c denotes the number of the current oscillating cycle, which varies between zero and the total

ISBN:978-84-593-4072-1/DL:T-1163-2010

number of oscillating cycles N_c. The grey blocks correspond to the flow chart of the sequence of operations within the main body of the FDTD algorithm for the TE polarization. If the polarization were TM, the field components D_x, E_x, D_y, E_y and H_z would be substituted for H_x, H_y, D_z and E_z, correspondingly. In the first step, the k-point is set up. All further calculations are carried out only for this k-point. In the second step, the current angular frequency ω is chosen for which the radiated energy will be calculated. In the third step, the time step Δt is calculated and the counter of the oscillating cycles i_c is zerorized. The fourth step consists of N_c of dipole's oscillating cycles. In the fifth step, the radiated energy for the current angular frequency ω set up in the second step is calculated. These steps are repeated for all angular frequencies. After this process has finished for all k-points (it is enough to take into account about 10–15 k-points for a wave vector), the accumulated electromagnetic energy density distribution W is a function of the angular frequency for the specified wave vector. The dispersion characteristic is obtained from the resonance peaks of this electromagnetic energy density distribution.

Unlike in classical FDTD approaches [29], the stability condition of the algorithm presented in Fig. 3.5 depends on the angular frequency at which the dipole oscillates. If the spatial steps Δx and Δy are normalised as $2\pi a/nx$ and $2\pi a/ny$, and the step in time is $\Delta t = 2\pi/(\omega N_t)$ (N_t is the total number of steps in time and a is period of the photonic crystal), the Courant stability condition can be written as

$$N_t \geq \frac{\sqrt{nx^2 + ny^2}}{\omega a}. \qquad (3.54)$$

UNIVERSITAT ROVIRA I VIRGILI
MODELLING OF PHOTONIC COMPONENTS BASED ON ÷(3) NONLINEAR PHOTONIC CRYSTALS
Ivan Maksymov
ISBN:978-84-593-4072-1/DL:T-1163-2010

The condition (3.54) means that one should carry out 6000 and 60 time steps to calculate the energy radiated by the dipole oscillating at $\omega = 0.01(2\pi c / a)$ and $\omega = 1.0(2\pi c / a)$, respectively.

3.2.6 Calculation of reflexion and transmission spectra

Reflexion and transmission spectra are very important characteristics of photonic crystals and optical devices based on them. Unlike the dispersion characteristics showing the complete forbidden bang gap for all directions of the first Brillouin zone, the transmission spectra are calculated for only one of the propagation directions possible in a realistic device and they suggest a frequency

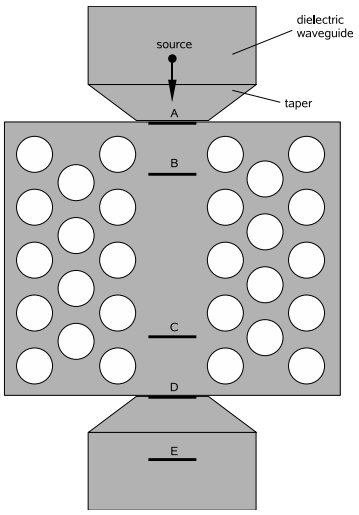

Fig. 3.6. Photonic crystal line waveguide connected with two dielectric waveguides via tapers.

ISBN:978-84-593-4072-1/DL:T-1163-2010

band where the light cannot propagate. In addition, the transmission spectra show how the propagating wave is attenuated at each frequency that is not possible with dispersion characteristics.

The calculation of a transmission spectrum can be demonstrated by the example of a photonic crystal line waveguide connected with two conventional dielectric waveguides via tapers (see Fig. 3.6).

The point at which the electromagnetic wave is originated is called the source. This wave propagates in the direction indicated by the arrow. Usually, the so-called “hard” source is used [29]. A “hard” source is set up simply by assigning a desired time function to specific components of electric or magnetic field in the FDTD grid. The time function is independent of anything else in the model. For example, in a three-dimensional FDTD grid at point with coordinates (i_s, j_s, k_s) the E_z or H_z components (TM or TE polarisation) should be excited to generate a continuous sinusoidal wave of frequency f_0 that is switched on at $n = 0$:

$$E^n{}_z(i_s, j_s, k_s) = E_0 \sin(2\pi f_0 n \Delta t). \tag{3.55}$$

The use of this source in calculating the transmission is not desired because a lot of calculation should be repeated if a wide range of frequencies are to be covered. Instead, another type of the hard source providing a bandpass Gaussian pulse with zero DC content is used

$$E^n{}_z(i_s, j_s, k_s) = E_0 \sin(2\pi f_0 n \Delta t) \exp\left(-\left[(n - n_0)/n_{decay}\right]^2\right). \tag{3.56}$$

ISBN:978-84-593-4072-1/DL:T-1163-2010

The Fourier spectrum of this pulse has even symmetry about f_0. The pulse is centred at time step n_0 and has a $1/e$ characteristic decay of n_{decay} time steps. The main advantage of this pulse is the possibility to carry out only one simulation covering a wide range of frequencies.

The observation sites A, B, C, D and E shown in Fig. 3.6 are used to save the temporal evolution of the fields. After the FDTD algorithm has finished, the field observed at these sites are Fourier transformed and the Poynting vector is calculated as [67]

$$\vec{P} = -\frac{1}{2}\mathrm{Re}\left[\int_{width} \vec{E}(\vec{r},\omega)\times\vec{H}^{*}(\vec{r},\omega)d\vec{r}\right], \tag{3.57}$$

where the $\vec{E}(\vec{r},\omega)$ and $\vec{H}^{*}(\vec{r},\omega)$ are the Fourier transformed electric and magnetic fields; the asterisk denotes the complex conjugated. Using the Poynting vectors calculated at the source point and the site E, one can calculate the transmission through the whole structure as

$$T = \frac{|P_E|}{|P_{source}|}. \tag{3.58}$$

Using Eq. (3.57) and the Pointing vector calculated at other sites, one can also calculate the efficiency of the taper used to couple the dielectric waveguides with the photonic crystal line waveguide or the transmission only through the line waveguide.

It should be noticed, that the application of the point sources like those described by Eqs. (3.55) and (3.56) instead of the total field/scattered field

ISBN:978-84-593-4072-1/DL:T-1163-2010

technique [29] is preferable because the point sources allow for the so-called waveguide source conditions. One of the main difficulties in exciting dielectric waveguides is to find a transverse distribution of the modal field in these waveguide, which is the initially unknown because the energy is not strictly bounded by the walls, but instead decays with distance from the centre of the structure. The application of point sources solves this problem. When the point source situated in the dielectric waveguide (as it is shown in Fig. 3.6) is switched on, it generates a lot of modes including undesirable ones. However, the waveguide “filters” these undesired modes which are immediately absorbed by the boundary conditions.

3.2.7 Some remarks on the nonlinear FDTD method for analysing dispersion characteristics

The previous subsections have provided detailed information on how the FDTD technique is applied for analysing the basic characteristics of photonic crystals. The purpose of this subsection is to show what kind of changes should be made in order to apply the FDTD to nonlinear problems. It also makes clear what are the contributions made by the author in this area.

First of all, unlike in [54], an oscillating dipole has been embedded in a nonlinear photonic crystal. It has resulted in the combination of the Sakoda's approach, based on simulation of radiation of oscillating dipole, with the model of the Kerr nonlinearity. To author's knowledge, it has been done for the first time.

The fact that the nonlinearity has been considered has offered a problem. In the linear regime, the amplitudes of the both electric and magnetic dipoles were

ISBN:978-84-593-4072-1/DL:T-1163-2010

not of great importance. In the nonlinear regime, however, the magnitudes of their amplitudes control the intensity that induces the nonlinearity. The relation between the amplitude of the electric dipole and the intensity is evidently direct. In the case of the magnetic dipole, however, it is not clear. It has been found that the same nonlinearity is induced when the amplitude of the magnetic dipole is lower than that of the electric dipole. The physical interpretation of such a difference in amplitudes of the electric and magnetic dipoles has not yet been clarified. It could be explained as follows. In both linear and nonlinear photonic crystals, the Purcell effect [68-69] has to be taken into account. It has been shown that for the linear photonic crystals and angular frequencies $\omega a / 2\pi c \leq 1.0$, the electric and magnetic dipoles behave like in a linear homogeneous medium [70-71]. It can be assumed that the behaviour of the dipoles in the nonlinear regime is similar to that in the linear one, i.e., in the nonlinear photonic crystal the dipoles behave like in a nonlinear homogeneous medium.

In the homogeneous Kerr-nonlinear medium, there is a growth of the transverse field components at the cost of the longitudinal one. In the TE case, the transverse electric field components play an important role in inducing the nonlinearity. The amplitudes of these field components increase at the cost of the magnetic dipole radiation. As a result of this process, the induced nonlinearity increases as the amplitudes of the electric field components increases. In the TM case, however, the transverse electric field is absent by definition. Consequently, the energy transfer mechanism from the electric dipole to the transverse magnetic field components does not facilitate the induction of the nonlinearity and, therefore, the larger amplitudes of the electric dipole should be applied to induce the same nonlinearity as with the smaller amplitudes of the magnetic dipole.

In addition to the problem with the excitation by means of the oscillating

dipoles, considering the nonlinear model has led to unfulfilling of the Courant stability condition. This situation has been repaired by decreasing the instant in time.

The calculation of dispersion characteristics in the nonlinear photonic crystal slab has also required to make some changes in the standard algorithm. Here, the Mur's absorbing boundary conditions have been combined with the periodic boundary conditions. To the author's knowledge, it has been also made for the first time. Unlike in the original Order-N method, the Dirac delta functions situated at randomly chosen nodes of the finite-difference grid have been used to create an initial field distribution. In the work, it has been investigated how many nodes of the finite-difference grid should be chosen with the random number generator to induce a considerable nonlinearity.

3.3 Conclusions

To conclude, this chapter has described and discussed the numerical methods that are employed in the dissertation. The description has been started with the presentation and discussion of the methods of theoretical investigation of photonic crystals. These methods have been compared by taking into consideration the possibility of their application to different problems. The main attention has been devoted to the finite-difference time-domain (FDTD) method. Its discussion has been commenced by outlining the basic concepts of the method, existing types of boundary conditions and also some of its modifications and extensions including models of nonlinearity.

The special attention has been paid to one of the specific applications of

the FDTD method – numerical simulation of radiation of oscillating dipoles embedded in photonic crystals. This is a new approach proposed by the author and it is intended for analysing dispersion characteristics of Kerr-nonlinear photonic crystals. It can be used to analyze the dispersion characteristics of Kerr-nonlinear one- and two-dimensional photonic crystals as a function of the intensity of the oscillating dipoles.

References

[1] C. Kittel, *Quantum theory of solids* (Wiley, 1963).

[2] L. Kahn, N. S. Almeida, L. D. Mills, "Nonlinear optical response of superlattices: multistability and soliton trains", Phys. Rev. B. **37,** 8072 (1988).

[3] E. Lidorikis, K. Busch, Q. Li, C. T. Chan, C. M. Soukoulis, "Optical nonlinear response of single nonlinear dielectric layer sandwiched between two linear dielectric structures", Phys. Rev. B. **56**, 15090 (1997).

[4] E. Lidorikis, Q. Li, C. M. Soukoulis, "Wave propagation in nonlinear multilayer structures", Phys. Rev. B. **54**, 10249 (1996).

[5] J. D. Joannopoulos, *Photonic crystals. Molding the flow of Light* (Princeton University Press, New Jersey, 1995).

[6] S. G. Johnson and J. D. Joannopoulos, *Photonic crystals. The road from theory to practice* (Kluwer, Boston, 2002).

[7] S. Guo, S. Albin, "Simple plane wave implementation for photonic crystals calculations", Opt. Express **12**, 167 (2003).

[8] K. M. Leung, M. Liu, "Photon band structures: the plane wave method", Phys. Rev. B. **41**, 10188 (1990).

ISBN:978-84-593-4072-1/DL:T-1163-2010

[9] T. Pan, F. Zhuang, Z.-Y Li, "Absolute photonic band gaps in a two-dimensional photonic crystal with hollow anizotropic rods", Solid State Commun. **129**, 501 (2004).

[10] Numerical recipes in C/C++. Freely available on-line http://www.library.cornell.edu/nr/bookcpdf.html.

[11] G. Golub and C. Van Loan, Matrix Computations (John Hopkins University Press, Baltimore, 1989).

[12] S. Johnson and J. Joannopoulos, "Block-iterative frequency-domain methods for Maxwell's equations in a planewave basis," Opt. Express **8**, 173 (2001).

[13] V. Lousse, J. P. Vigneron, "Self-consistent photonic band structure of dielectric superlattices containing nonlinear optical materials", Phys. Rev. E. **63**, 027602 (2001).

[14] P. Bienstman, R. Baets, "Optical modelling of photonic crystals and VCSELs using eigenmode expansion and perfectly mathched layers", Opt. Quantum Electron. **33**, 327 (2001).

[15] A. Modinos, N. Stefanou and V. Yannopapas, "Applications of the layer-KKR method to photonic crystals", Opt. Express **8**, 197 (2001).

[16] A. R. Baghai-Wadji, Lecture Notes (Vienna University of Technology, 1994).

[17] A. Huttunen and P. Torma, "Band structures in nonlinear photonic crystals", J. Appl. Phys. **91**, 3988 (2002).

[18] P. Lalanne and J.-P. Hugonin, "Numerical performance of finite-diffrence modal methods for thr electromagnetic analysis of one-dimensional lamellar gratings", J. Opt. Soc. Am. B. **17**, 1033 (2002).

[19] N. A. Khizhniak, *Integral equation of macroscopic electrodynamics* (Kiev, Naukova Dumka, 1968) (in Russian).

ISBN:978-84-593-4072-1/DL:T-1163-2010

[20] A. G. Nerukh, "Evolutionary approach in transient electrodynamic problems", J. Radio Science **30**, 481 (1995).

[21] A. G. Nerukh, I. V. Scherbatko and M. Marciniak, *Electromagnetics of Modulated Media with Application to Photonics* (Warsaw, 2001).

[22] F. Fedotov, A. Nerukh, T. Benson and P. Sewell, "Investigation of electromagnetic field in a layer with time-varying medium by Volterra integral equation method", IEEE J. Lightwave Technology. **21**, 305 (2003).

[23] K. Ohtaka, "Light scattering from microscopic spherical bodies. I. Integrated density of states of transverse electromagnetic fields", Phys. Rev. B. **25**, 677 (1981).

[24] N. Stefanou, V. Karathanos and A. Modinos, "Scattering of electromagnetic waves by periodic structures", J. Phys. Condens. Matter. **4**, 7389 (1992).

[25] A. Modinos, "Scattering of electromagnetic waves by a plane of spheres – formalism", Physica A **141A**, 575 (1987).

[26] K. Ohtaka and Y. Tanabe, "Photonic bands using vector spherical waves. 2. Reflectivity, coherence and local field", J. Phys. Soc. Jpn. **65**, 2276 (1996).

[27] P. Yeh*, Optical waves in layered media* (Wiley, New York, 1998).

[28] J. B. Pendry and A. MacKinnon, "Calculation of photon dispersion relation", Phys. Rev. Lett. **69**, 2772 (1992).

[29] A. Taflove ans S. Hagness, *Computational Electrodynamics. The finite-difference time-domain method* (Artech House, Boston, 2005).

[30] P. P. Silvester and R. L. Ferrari, *Finite Elements for Electrical engineers* (Cambridge, 1990).

[31] J. Jin, *The Finite Element Method in Electromagnetics* (Wiley, New York, 1993).

[32] B. Hiett, "Photonic Crystal Modelling using Finite Element Analisys", Ph. D.

ISBN:978-84-593-4072-1/DL:T-1163-2010

thesis (University of Southampton, 2002).

[33] M. N. O. Sadiku, Numerical techniques in electromagnetics (Boca Raton, 1999).

[34] D. Kremer and R. Pregla, “Method of Lines with Spectral Absorbing Boundary Conditions – Analysis of Weakly Guiding Optical Structures”, IEEE Microwave Guided Wave Lett. **28**, 1013 (1992).

[35] Y. Y. Lu and P. L. Ho, “Beam propagation method using a [(p-1)/p] Pade approximant of the propagator”, Opt. Lett. **27**, 683 (2002).

[36] A. Locatelli, D. Modotto, C. De Angelis, F. M. Rigozzo and A.-D. Capobianco, “Nonlinear bidirectional beam propagation method based on scattering operators for periodic microstructured waveguides”, J. Opt. Soc. Am. B. **20**, 1724 (2003).

[37] K. S. Yee and J. S. Chen, “The finite-difference time-domain (FDTD) and the finite-volume time-domain (FVTD) methods in solving Maxwell’s equations”, IEEE Trans. Antennas Propagat. **45**, 354 (1997).

[38] P. B. Johns and R. L. Beurle, “Numerical solution of 2-dimensional scattering problems using a transmission-line matrix”, Proc. IEEE **118**, 1203 (1971).

[39] T. Hruskovec and Z. Chen, “TLM based FDTD modeling of optical bistability”, Int. J. Num. Modelling: Electronic Networks, Devices and Fields **14**, 155 (2001).

[40] P. Tran, “Photonic-band-structure calculation of material possessing Kerr nonlinearity”, Phys. Rev. B **52**, 10673 (1995).

[41] M. Bordovsky, P. Catrysse, S. Dods, M. Freitas, J. Klein, L. Kotachka, V. Tzolov, I. M. Uzunov and J. Zhang, “Waveguide design, modeling and optimization: from photonic nanodevices to integrated photonic circuits”, Proc.

ISBN:978-84-593-4072-1/DL:T-1163-2010

SPIE **5355**, 65 (2004).

[42] BandSolve User Manual, RSoft Desing Group.

[43] N. Panoiu, M. Bahl, and R. Osgood, Jr., "All-optical tunability of a nonlinear photonic crystal channel drop filter," Opt. Express **12**, 1605 (2004).

[44] T. Fujisawa and M. Koshiba, "Finite-Element Mode-Solver for Nonlinear Periodic Optical Waveguides and Its Application to Photonic Crystal Circuits," J. Lightwave Technol. **23**, 382 (2005).

[45] K. S. Yee, "Numerical solution of initial boundary value problems involving Maxwell's equations in isotropic media", IEEE Trans. Antennas Propagat. **14**, 302 (1966).

[46] G. Mur, "Absorbing boundary conditions for the finite-difference approximation of the time-domain electromagnetic field equations", IEEE Trans. Electromagn. Compat. **23**, 377 (1981).

[47] Z. P. Liao, H. L. Wong, B. P. Yang and Y. F. Yuan, "A transmitting boundary for transient wave analyses", Scientia Sinica (series A) **XXVII**, 1063 (1984).

[48] J. P. Berenger, "A perfectly matched layer for the absorbtion of electromagnetic waves", J. Comput. Phys. **144**, 185 (1994).

[49] I. S. Maksymov, L. F. Marsal and J. Pallarès, "Band structures in non-linear photonic crystal slabs", Opt. Quantum. Electron. **37**, 161 (2005).

[50] J. A. Roden and S. D. Gedeney, "Convolutional PML (CPML): An efficient FDTD implementation of the CFS-PML for arbitrary media", Microwave Opt. Technol. Lett. **27**, 334 (2000).

[51] M. N. O. Sadiku, Numerical techniques in electromagnetics (Boca Raton, 1999).

[54] K. Sakoda*, Optical properties of photonic crystals* (Springer Verlag, Berlin,

ISBN:978-84-593-4072-1/DL:T-1163-2010

2001).

[52] D. Sullivan, *Electromagnetic simulation using the FDTD method* (Wiley-IEEE Press, 2000).

[53] K. Kunz and R. Luebbers, *The Finite Difference Time Domain method for Electromagnetics* (CRC Press, New York, 1993).

[55] C. T. Chan, Q. L. Yu and K. M. Ho, "Order-N spectral method for electromagnetic waves", Phys. Rev. B **51**, 16635 (1995).

[56] D. E. Merewether and W. A. Radasky, "Nonlinear electromagnetic fields within a cylindrical cavity excited by ionizing radiation", IEEE Trans. Nucl. Sci. **21**, 998 (1974).

[57] G. W. Zheng and K. S. Chen, "Transient analysis of dielectric step discontinuity of microstrip lines containing a nonlinear layer", Int. J. Infrared Millim. Waves **13**, 1127 (1992).

[58] P. M. Goorjian, A. Taflove, R. M. Joseph, and S. C. Hagness, "Computational modeling of femtosecond optical solitons from Maxwell's equations", IEEE J. Quantum Electron. **28**, 2416 (1992).

[59] R. M. Joseph, P. M. Goorjian, and A. Taflove, "Direct time integration of Maxwell's equations in two-dimensional dielectric waveguides for propagation and scattering of femtosecond electromagnetic solitons", Optics Lett. **18**, 491 (1993).

[60] W. Forysiak, R. G. Flesch, J. V. Moloney, and E. M. Wright, "Doppler shift of a self-reflected optical pulses at an interface: dynamic nonlinear optical skin effect", Phys. Rev. Lett. **76**, 3695 (1996).

[61] W. Forysiak, J. V. Moloney, and E. M. Wright, "Nonlinear focusing of femtosecond pulses as a result of self-reflection from a saturable absorber", Optics Lett. **22**, 239 (1997).

[62] R. W. Ziolkowski, J. M. Arnold, and D. M. Gogny, "Ultrafast pulse interactions with two-level atoms", Phys. Rev. A **52**, 3082 (1995).

[63] D. M. Sullivan, "Nonlinear FDTD formulations using Z transform", IEEE Trans. Microwave Theory Tech. **43**, 676 (1995).

[64] D. M. Sullivan, "Z-transform theory and the FDTD method", IEEE Trans. Antennas Propagat. **44**, 28 (1996).

[65] I. S. Maksymov, L. F. Marsal, M. A. Ustyantsev, and J. Pallarès, "Band structure calculation in two-dimensional Kerr non-linear photonic crystals", Opt. Commun. **248**, 469 (2005).

[66] R. W. Ziolkowski, "The incorporation of microscopic material models into the FDTD approach for ultrafast optical pulse simulations", IEEE Trans. Antennas Propagat. **45**, 375 (1997).

[67] J. D. Jackson, *Classical Electrodynamics* (Wiley, New York, 1975).

[68] E. M. Purcell, "Spontaneous emission probabilities at radio frequencies", Phys. Rev. **69**, 681 (1946).

[69] J. P. Dowling and C. M. Bowden, "Atomic emission rates in inhomogeneous media with applications to photonic band structures", Phys. Rev. A **46**, 612 (1992).

[70] I. Alvarado-Rodríguez, P. Halevi and A. S. Sánchez, "Dipole radiation in a one-dimensional photonic crystal: TE polarization", Phys. Rev. E **63**, 056613 (2001).

[71] J. R. Zurita-Sánchez, A. S. Sánchez and P. Halevi, "Dipole radiation in a one-dimensional photonic crystal. II. TM polarization", Phys. Rev. E **66**, 046613 (2002).

UNIVERSITAT ROVIRA I VIRGILI
MODELLING OF PHOTONIC COMPONENTS BASED ON ÷(3) NONLINEAR PHOTONIC CRYSTALS
Ivan Maksymov
ISBN:978-84-593-4072-1/DL:T-1163-2010

Chapter 4

Dispersion characteristics of Kerr nonlinear photonic crystals

This chapter presents and discusses the results of dispersion characteristics calculation for one- and two-dimensional Kerr nonlinear photonic crystals. First, the discussion is started with the one-dimensional structure. In the one-dimensional case, the calculation clearly shows the physicals processes that take place when the photonic crystal switches from the linear working regime to the nonlinear one. Secondly, the procedure of calculation of dispersion characteristics is generalized to deal with two-dimensional structures. Due to much practical importance, both perfect lattices and lattices with defects are considered. Another practical aspect – the influence of the light confinement in the third direction – is studied by calculating and discussing dispersion characteristics of a nonlinear photonic crystal slab.

In most of the calculations carried out in this chapter, the FDTD approach

UNIVERSITAT ROVIRA I VIRGILI
MODELLING OF PHOTONIC COMPONENTS BASED ON ÷(3) NONLINEAR PHOTONIC CRYSTALS
Ivan Maksymov
ISBN:978-84-593-4072-1/DL:T-1163-2010

based on the simulation of radiation of oscillating dipole embedded in the perfect lattice is used. When dealing with defects introduced into the perfect lattice, this approach is combined with the super cell technique. The slab structure is studied with the nonlinear Order-N method.

4.1 One-dimensional nonlinear photonic crystals

In order to calculate the dispersion characteristics of the one-dimensional nonlinear photonic crystal (1-D NLPC), the numerical approach presented in subsection 3.2.5 is used. The magnetic oscillating dipole is embedded in the unit cell and the TE polarization, for which the magnetic field is parallel to z-axis, is only considered. For one-dimensional photonic crystals in the in-plane case the TM polarisation, for which the electric field is parallel to z-axis, gives the same dispersion characteristics as that in the case of the TE polarisation. But in this case the electric dipole must be substituted for the magnetic one. In this section, the magnetic dipole is used and the TE polarisation case is considered because there is an interest in exciting the photonic crystal with the magnetic field. Unlike the excitation with the electric field, the magnetic field excitation is more complex because it is more difficult to control the incident intensity, which is a function of the electric field, not of the magnetic one. Although the polarisation and the type of the dipole are not of great importance in the one-dimensional in-plane case, they play the very important role in the two-dimensional case. It will be shown in the following sections.

The general geometry of the 1-D NLPC considered in this section is illustrated in Fig. 4.1. It consists of alternating layers of materials with high ε_1

ISBN:978-84-593-4072-1/DL:T-1163-2010

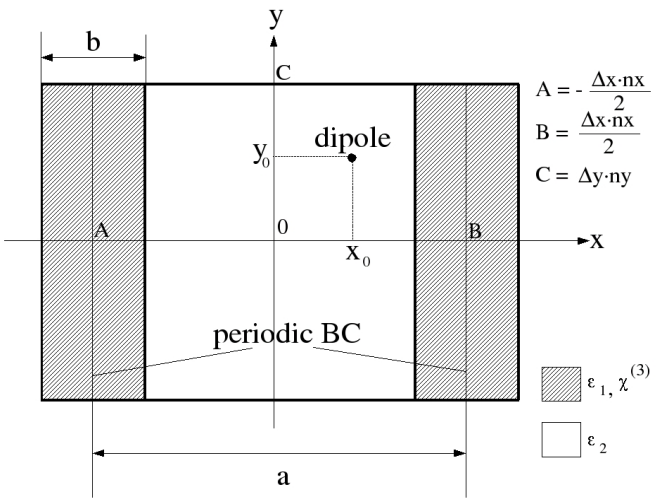

Fig. 4.1. Schematic of the 1-D NLPC

and low ε_2 dielectric constants. The optical thickness of the layers with a high dielectric constant is b and the optical thickness of the layers with a low dielectric constant is $a-b$, where a is the period. The layers with a high dielectric constant are doped with a Kerr-nonlinear material and are also characterized by the Kerr coefficient $\chi^{(3)}$. It is apparent that the structure in Fig. 4.1 is invariant when changing y to $-y$

$$\varepsilon, \chi^{(3)}(x,-y) = \varepsilon, \chi^{(3)}(x,y). \tag{4.1}$$

Therefore only the region where $0 \le y \le C$ is considered for calculation and in the y-direction the 1-D NLPC is truncated by the symmetric boundary condition (BC) that can be written as

ISBN:978-84-593-4072-1/DL:T-1163-2010

$$\vec{\Phi}(x,0) = \vec{\Phi}(x,\Delta y)\,, \tag{4.2}$$

$$\vec{\Phi}(x,C) = \vec{\Phi}(x,C-\Delta y)\,, \tag{4.3}$$

where $\vec{\Phi}$ is any field component ($\vec{E}$ or $\vec{H}$). The periodic BC truncates the structure in the x-direction. In the z-direction the structure is assumed to be infinite. The oscillating dipole is situated at $r_0 = (x_{0,} y_0)$. The parameters n_x and n_y denote the number of subcells, which divide the unit cell (the period a). The parameters Δx and Δy characterize the dimensions of the single subcell and they are defined as is suggested in subsection 3.2.5.

The parameters that will be used for all further calculations are as follows: $a = 1$, $b = 0.2$, $\varepsilon_1 = 13.0$, $\varepsilon_2 = 1$, $\frac{\omega_1 a}{2\pi c} = 0.01$, $\frac{\omega_2 a}{2\pi c} = 1.0$, $\frac{\Delta\omega a}{2\pi c} = 0.001$ and $N_t = 6000 \div 60$ (depending on the frequency). The behaviour of the band structure at $\omega = 0$ is well-known. Therefore the angular frequencies $0 \le \omega \le \omega_1$ are not taken into account because of an enormous increase in N_t. In order to calculate band structures in the 1-D NLPC the Kerr coefficient is chosen to be $\chi^{(3)} = 0.01$ [1]. For the 1-D LPC, however, it is zero. The magnetic dipole is used for excitation. It is situated in the region with a low dielectric constant. The unit cell is divided into 40×20 subcells. Information about unit cell discretization and convergence can be found in subsection 4.1.4.

4.1.1 Energy Density Spectra

Following the sequence of the operations shown in Fig. 3.5, the energy

UNIVERSITAT ROVIRA I VIRGILI
MODELLING OF PHOTONIC COMPONENTS BASED ON ÷(3) NONLINEAR PHOTONIC CRYSTALS
Ivan Maksymov
ISBN:978-84-593-4072-1/DL:T-1163-2010

density spectra must be first calculated.

Fig. 4.2 shows the accumulated electromagnetic energy density distribution calculated for the 1-D LPC (a) and 1-D NLPC (b) as a function of the number of oscillating cycles for $ka/(2\pi) = 0.5$. In both cases, the amplitude of the

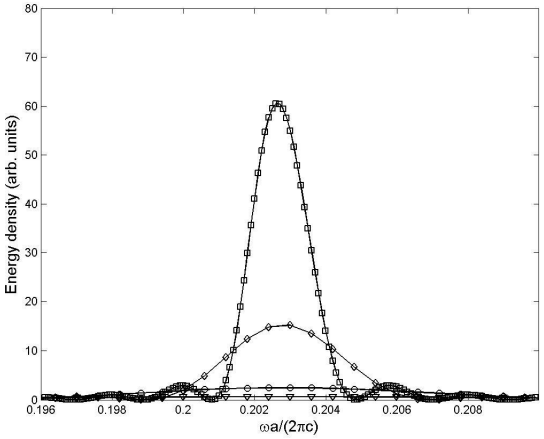

(a)

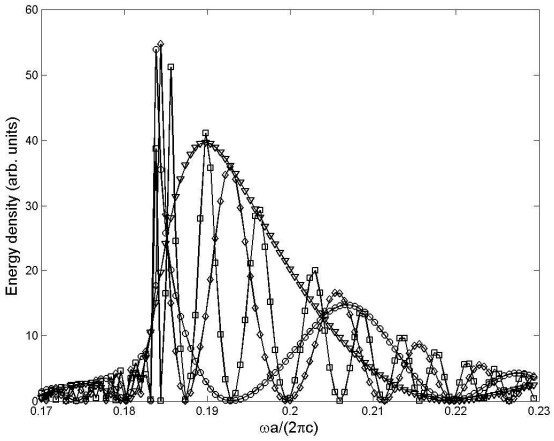

(b)

Fig. 4.2. Accumulated electromagnetic energy density distribution calculated for the 1-D LPC (a) and 1-D NLPC (b).

UNIVERSITAT ROVIRA I VIRGILI
MODELLING OF PHOTONIC COMPONENTS BASED ON ÷(3) NONLINEAR PHOTONIC CRYSTALS
Ivan Maksymov
ISBN:978-84-593-4072-1/DL:T-1163-2010

magnetic dipoles is $h_{\mu_z} = 100$ arb. units. The abscissa represents the angular frequency and ▼, ○, ◊, □ denote the accumulated electromagnetic energy density after 10, 20, 50 and 100 oscillating cycles, respectively. In Fig. 4.2 (a), a resonance is clearly observed at $\omega a/(2\pi c) = 0.203$ for all numbers of oscillating cycles. The amplitude of the peak grows as the result of energy accumulation process. Such behaviour of the energy oscillated by the dipole is well-known and described in the literature [2]. However, to the author's knowledge, the dipole's behaviour in Kerr-like nonlinear media was not yet investigated. The nonlinear simulations performed in this work reveal that the nonlinearity leads to a drift in the resonance peaks that depends on the number of oscillating cycles. For example, in Fig. 4.2 (b) a resonance peak is observed at $\omega a/(2\pi c) = 0.189$ for 10 cycles while it is at $\omega a/(2\pi c) = 0.185$ for 50 cycles. The last number of the oscillating cycles is suitable to accurately calculate dispersion characteristics. It is because any increase in this number almost does not contribute more to the shift of the resonance peaks and it makes it possible to state that the method converges.

Fig. 4.3 shows the normalized accumulated electromagnetic energy density distribution calculated for the 1-D LPC (a) and 1-D NLPC (b) as a function of the angular frequency for $ka/(2\pi) = 0.5$. The amplitudes of the magnetic dipoles used for the calculation were $h_{\mu_z} = 1$ arb. unit and $h_{\mu_z} = 100$ arb. units, respectively. There were 50 oscillating cycles.

As can be seen from Fig. 4.3 (a), in the linear regime the electromagnetic energy density distribution is very clean. No shift in the peak's position was produced because the simulation did not take into account the Kerr effect. In Fig. 4.3 (b), however, the electromagnetic energy density distribution is not clean because a noise is produced by the nonlinear calculation. Therefore, each peak in

UNIVERSITAT ROVIRA I VIRGILI
MODELLING OF PHOTONIC COMPONENTS BASED ON ÷(3) NONLINEAR PHOTONIC CRYSTALS
Ivan Maksymov
ISBN:978-84-593-4072-1/DL:T-1163-2010

the energy distribution cannot be taken as an individual mode. Tran [3] reported the same problem. He stated that in the nonlinear regime the energy distribution is very similar to that of the linear regime, which indicates that the Kerr nonlinearity, apart from shifting its angular frequency, does not drastically affect

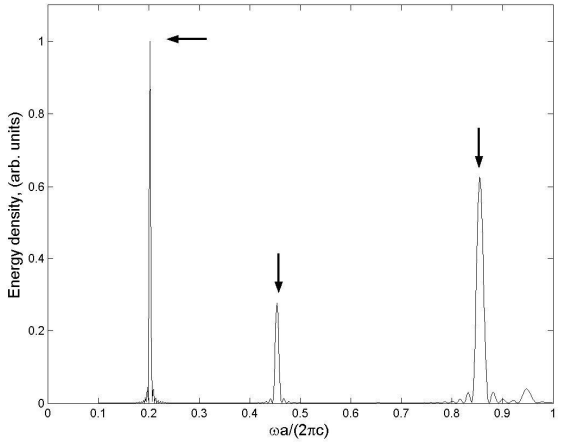

(a)

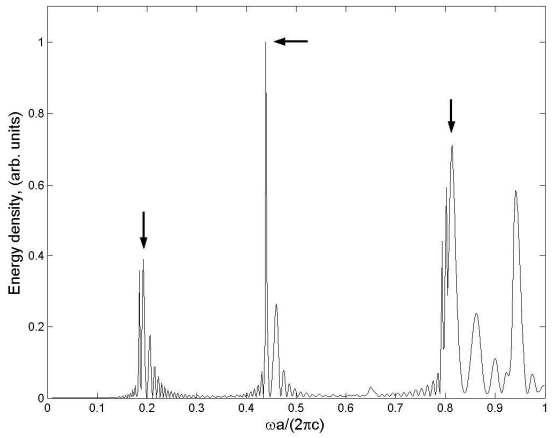

(b)

Fig. 4.3. The normalized accumulated electromagnetic energy density distribution for the 1-D LPC (a) and the 1-D NLPC (b).

UNIVERSITAT ROVIRA I VIRGILI
MODELLING OF PHOTONIC COMPONENTS BASED ON ÷(3) NONLINEAR PHOTONIC CRYSTALS
Ivan Maksymov
ISBN:978-84-593-4072-1/DL:T-1163-2010

the linear solution. Following this statement, in Fig. 4.3 (b) only the peaks indicated by an arrow are meaningful for plotting dispersion characteristics.

In accordance with the flow chart in Fig. 3.5, the energy spectra like those in Fig. 4.3 are calculated for both linear and nonlinear regimes. As it was mentioned, the dispersion characteristics are plotted by using the resonant frequencies taken from these energy spectra by means of a program for detecting local maxima. In the following subsections, the dispersion characteristics are presented for the linear and nonlinear regimes.

4.1.2 Dispersion characteristics in the linear regime

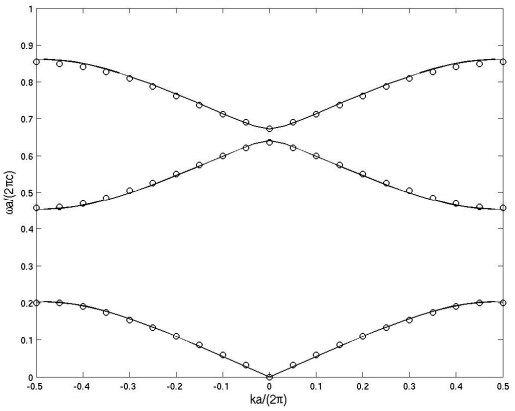

Fig. 4.4. The comparison between the band structures in the 1-D LPC calculated with the FDTD method (open circles) and the plane wave expansion method (solid line).

In this subsection, the dispersion characteristics of the 1-D LPC calculated

UNIVERSITAT ROVIRA I VIRGILI
MODELLING OF PHOTONIC COMPONENTS BASED ON ÷(3) NONLINEAR PHOTONIC CRYSTALS
Ivan Maksymov
ISBN:978-84-593-4072-1/DL:T-1163-2010

with the FDTD method are presented and compared with an etalon. The etalon used is the dispersion characteristic calculated for the same 1-D LPC but with the plane wave expansion method [4]. In Fig. 4.4, this dispersion characteristic is represented by open circles and the etalon one is represented by a solid line. As can be seen, the FDTD method provides the accurate result for the 1-D LPC.

4.1.3 Dispersion characteristics in the nonlinear regime

Fig. 4.5 shows the dispersion characteristics in the 1-D LPC (dashed line) and 1-D NLPC (solid line) calculated with the FDTD approach. In the nonlinear regime, the results are presented for the amplitudes of the magnetic dipole $h_{\mu_z} = 100$ arb. units and $h_{\mu_z} = 450$ arb. units. The open circles correspond to the dispersion characteristic calculated by Huttunen and Törmä [1], who presented dispersion characteristics in an analogical 1-D NLPC. Therefore, their results are used to validate the FDTD approach. They calculated the dispersion characteristic with the nonlinear Fourier method and, in contrast to the geometry shown in Fig. 4.1, their 1-D NLPC was surrounded by the metal. Another difference is that the additional pump wave was used to control the switching.

In Fig. 4.5, the amplitudes of the dipoles are not numerically equivalent to the amplitudes of the control waves in Huttunen's paper. Their magnitudes were fitted from the numerical experiment. In this experiment, the dispersion characteristics were calculated for the amplitudes of the magnetic dipole $h_{\mu_z} = 50 \div 500$ arb. units with the step $\Delta h_{\mu_z} = 10$ arb. units. As can be seen from Fig. 4.5, for the selected amplitudes the dispersion curves of the dispersion

UNIVERSITAT ROVIRA I VIRGILI
MODELLING OF PHOTONIC COMPONENTS BASED ON ÷(3) NONLINEAR PHOTONIC CRYSTALS
Ivan Maksymov
ISBN:978-84-593-4072-1/DL:T-1163-2010

characteristics are red-shifted. This red-shift is in good agreement with [1]. Consequently, the conclusion can be drawn that they have the same effect on the dispersion characteristic. It should be noticed that because the metal does not surround the 1-D NLPC shown in Fig. 4.1, one does not observe the flat dispersion curves, which take place in the presence of the metal.

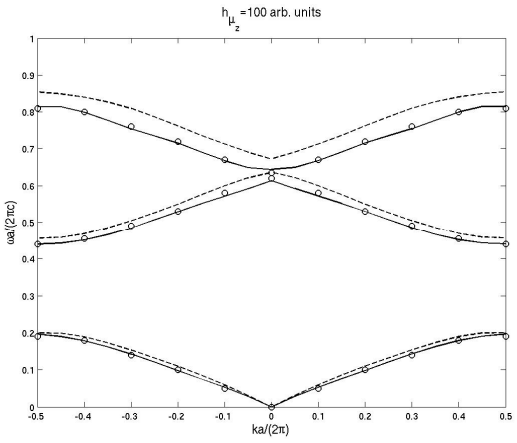

(a)

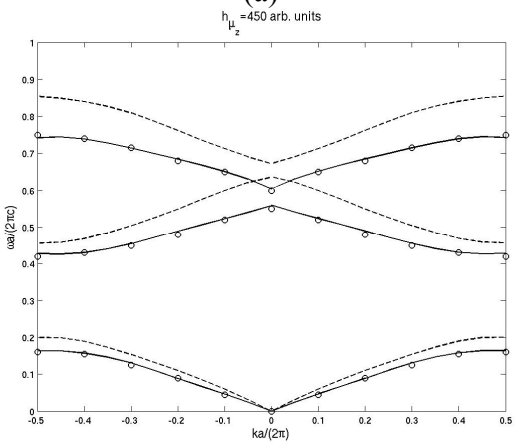

(b)

Fig. 4.5. Nonlinear dispersion characteristics calculated for different amplitudes of the oscillating dipole.

ISBN:978-84-593-4072-1/DL:T-1163-2010

The following discusses the physical origins of the red-shift of the dispersion curves. For the 1-D NLPC, the red-shift can be explained with Scalora's argumentation [5]. Because the dielectric constant depends on the field intensity, the dispersion characteristic changes dynamically with the incident field. This can be qualified by the following argument. In the frequency domain, the dispersion characteristic is determined by the difference between the dielectric constants of the materials, which form the photonic crystal. From Eq. (3.33) this difference can be expressed as

$$\Delta\varepsilon = \left[\varepsilon_1 + \chi^{(3)}\left|\vec{E}(\vec{r},t)\right|^2\right] - \varepsilon_2 \,. \tag{4.4}$$

The value of $\Delta\varepsilon$ increases as the intensity increases if $\chi^{(3)} > 0$ and decreases if $\chi^{(3)} < 0$. As the magnetic dipole excites the structure, the value of $\Delta\varepsilon$ changes and the dispersion curves of the dispersion characteristic dynamically shift. This process is the basis for intensity-driven optical limiting and all-optical switching. The results show that for the positive Kerr coefficient the value of $\Delta\varepsilon$ increases and the dispersion curves dynamically red-shift. This red-shift increases as the intensity of the oscillating dipole increases. For example, as can be seen from Fig. 4.5 (a), the intensity of the dipole just slightly shifts the dispersion curves while the more than four-time increase in the amplitude of the dipole in fact significantly shifts them. The existing difference between the amplitudes (100 arb. units and 450 arb. units) is due to need to significantly change the value of $\Delta\varepsilon$ and, consequently, significantly induce the degree of nonlinearity. It is not yet studied, which rule obeys the red-shift. At least, it is a nonlinear dependence, i.e., any uniform linear increase in the amplitude with the step Δh_{μ_z} does not mean that

ISBN:978-84-593-4072-1/DL:T-1163-2010

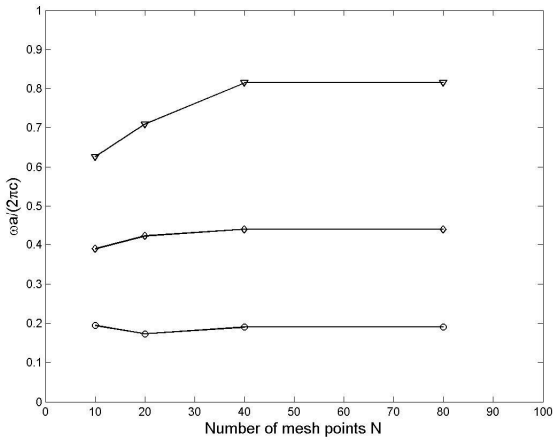

Fig. 4.6. Convergence of the FDTD method

the dispersion curves would be red-shifted on the same value of $\omega a / 2\pi c$ with regard to the previous shift. The study of the degree of the shift's nonlinear dependence on the dipole's amplitude is one of the possible directions for future investigations.

4.1.4 Unit cell discretization and convergence

Fig. 4.6 shows the convergence of the FDTD method used to the calculate dispersion characteristics. The abscissa represents the number of mesh points N in the unit cell in the x-direction. The ordinate corresponds to the angular frequency. The curves marked by ○, ◊ and ▼ correspond to the first, second and third dispersion curves of the dispersion characteristic of the 1-D NLPC. The values of the angular frequency are taken for $ka/(2\pi) = 0.5$. The parameters are the same as in Fig. 4.5 (a).

UNIVERSITAT ROVIRA I VIRGILI
MODELLING OF PHOTONIC COMPONENTS BASED ON ÷(3) NONLINEAR PHOTONIC CRYSTALS
Ivan Maksymov
ISBN:978-84-593-4072-1/DL:T-1163-2010

As can be seen, the method is convergent for $N \geq 40$. Any decrease in this number will give inaccurate results. Due to the symmetry in the y-direction, the number of parts into which the unit cell is divided in this direction can be selected as $N/2$.

4.2 Two-dimensional nonlinear photonic crystals

In this section, the two-dimensional nonlinear photonic crystal (2-D NLPC) is considered. Fig. 4.7 schematically shows the unit cell used for the calculation of dispersion characteristics. In order to demonstrate the validity of the two-dimensional numerical method, a square lattice of air holes with the same parameters that were used in [3] is considered. These parameters are: $a = 1$, $r = 0.5\text{a}$, $\varepsilon_a = 1$, $\varepsilon_b = 5.0$, $\chi_a^{(3)} = 0$, $\chi_b^{(3)} = 0.005$, $\frac{\omega_1 a}{2\pi c} = 0.01$, $\frac{\omega_2 a}{2\pi c} = 1.0$, $\frac{\Delta\omega a}{2\pi c} = 0.001$ and $N_t = 6000 \div 60$. For the two-dimensional linear photonic crystal (2-D LPC) the

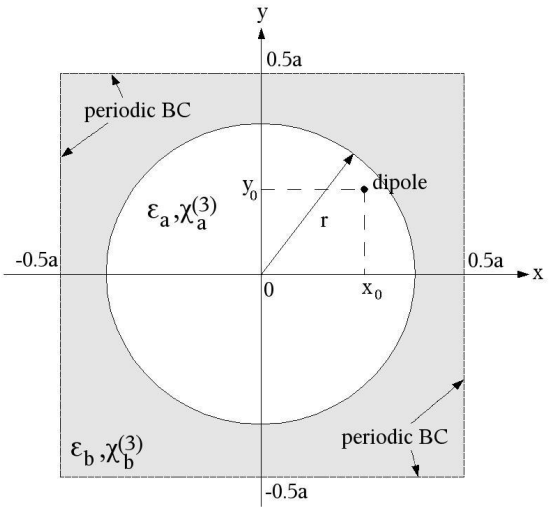

Fig. 4.7. Schematic of the 2-D NLPC.

parameters are the same, but both Kerr coefficients are zero. In the case of the TE polarization, the magnetic dipole is used for excitation while the electric one is used in the case of the TM polarization. For all calculations, 50 oscillating cycles are used. The unit cell is divided into 50x50 subcells.

4.2.1 Dispersion characteristics in the linear regime

This subsection presents the dispersion characteristics (TM and TE polarizations) in the 2-D LPC calculated with the FDTD method and compared with etalons. The etalons used for the comparison are the dispersion characteristics calculated in the same 2-D LPC for the TM and TE polarizations but with the plane wave expansion method [4]. In Figs. 4.8 (a) and (b), the dispersion characteristics calculated with the proposed FDTD method are represented by open circles and the etalon dispersion characteristics are represented by solid lines. As can be seen, the FDTD method provides the accurate result for both TE and TM polarizations.

4.2.2 Dispersion characteristics in the nonlinear regime

Figs. 4.9 (a) and (b) show the dispersion characteristics in the 2-D LPC (solid line) calculated with the plane wave method and in the 2-D NLPC (open circle) calculated with the FDTD method for TM (a) and TE (b) polarizations.

The solid circles in Fig. 4.9 (a) show the result for the TM polarization borrowed from [3] (only the first four dispersion curves were calculated there and the TE polarization was not considered). It can be seen that the FDTD method

UNIVERSITAT ROVIRA I VIRGILI
MODELLING OF PHOTONIC COMPONENTS BASED ON ÷(3) NONLINEAR PHOTONIC CRYSTALS
Ivan Maksymov
ISBN:978-84-593-4072-1/DL:T-1163-2010

provides the same result as in work [3]. Furthermore, it can be seen that the third (antisymmetric) dispersion curve in the ΓX and ΓM direction appears in the dispersion characteristic. In reference [3], Tran did not calculate it and, therefore, did not show it.

The reason why Tran did not show it can be found for example in [6]. If

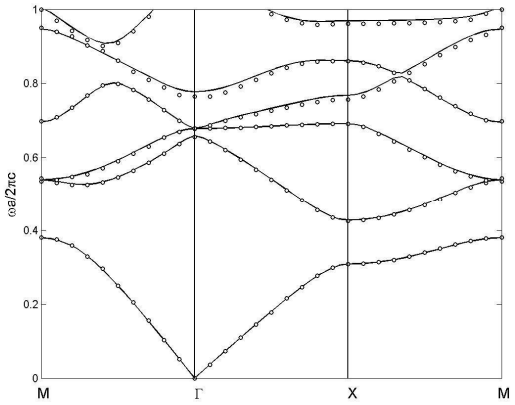

(a)

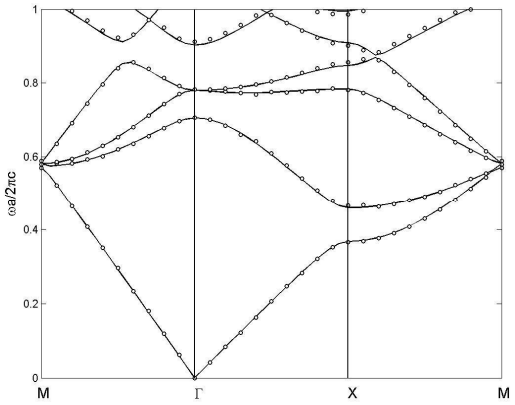

(b)

Fig. 4.8. The comparison between the dispersion characteristics for the TM (a) and TE (b) polarisations.

ISBN:978-84-593-4072-1/DL:T-1163-2010

the initial field is incident along the high-symmetry axes of the first BZ (for example ΓX-direction), it cannot excite the modes with odd parity (antisymmetric modes) with respect to the axes. This is because the initial field is even (symmetric) with respect to the axes. In general, if the oscillating dipole is situated at a point that does not coincide with the high-symmetry axes of the first

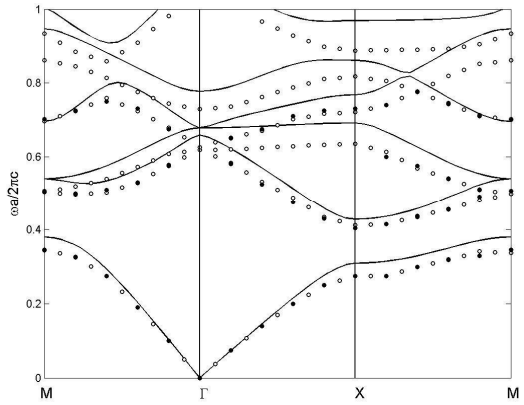

(a)

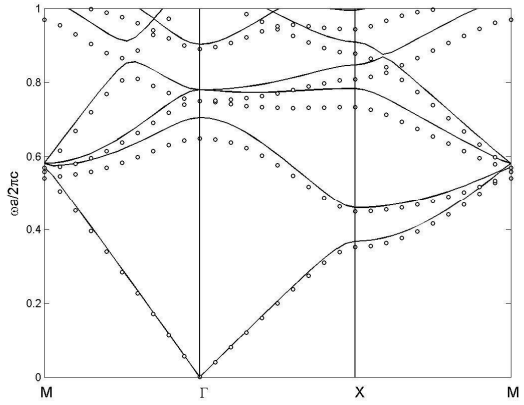

(b)

Fig. 4.9. The dispersion characteristics in the 2-D NLPC and 2-D LPC for the TM (a) and TE (b) polarisations.

UNIVERSITAT ROVIRA I VIRGILI
MODELLING OF PHOTONIC COMPONENTS BASED ON ÷(3) NONLINEAR PHOTONIC CRYSTALS
Ivan Maksymov
ISBN:978-84-593-4072-1/DL:T-1163-2010

BZ, one does not encounter any problem with the excitation of all modes. So it makes it possible to conclude that the FDTD approach with the embedded oscillating dipole is more thorough.

The amplitudes of the electric and magnetic dipole used to calculate the dispersion characteristics for the TM and TE polarizations were $e_{\mu_z} = 1500$ arb. units and $h_{\mu_z} = 225$ arb. units, respectively (see subsection 3.2.7). They were selected to obtain the same red-shift of the dispersion curves as Tran [3] did. This can be seen from Figs. 4.9 (a) and (b) where the dispersion curves of the dispersion structures are red-shifted with regard to the linear regime. The forbidden band gap that takes place in the dispersion characteristic for TM polarization is also red-shifted due to the shift of the first and the second dispersion curves which make it up. The dispersion characteristic for the TE polarization has no forbidden band gap for the range of frequencies considered.

4.2.3 Field intensity estimation

In all the calculations presented so far, both the magnetic and the electric fields are given in arbitrary units (arb. units). To estimate the feasible intensities needed to induce the nonlinearity which shifts the dispersion curves, a parallel between the arb. units and the SI units should be drawn. From the analysis of the changes in the dielectric constant [7-9], it can be deduced that after 50 oscillating cycles the magnetic dipole with an amplitude $h_{\mu_z} = 1$ arb. unit corresponds to an intensity of about $0.01 - 0.02\,\mathrm{kW/cm^2}$. After the same number of oscillating cycles, the electric dipole with an amplitude $e_{\mu_z} = 1$ arb. unit corresponds to an intensity of about $0.0015 - 0.003\,\mathrm{kW/cm^2}$.

UNIVERSITAT ROVIRA I VIRGILI
MODELLING OF PHOTONIC COMPONENTS BASED ON ÷(3) NONLINEAR PHOTONIC CRYSTALS
Ivan Maksymov
ISBN:978-84-593-4072-1/DL:T-1163-2010

There is another approach to estimate the intensity needed to induce the redshifting of dispersion characteristics, the electric field amplitude is obtained in the main body of the FDTD algorithm and taken at the angular frequency and the wave vector of interest. These values correspond to the working point of the photonic crystal device, which is modelled. The intensity is calculated as

$$I = \frac{1}{2} c\varepsilon_0 \sqrt{\varepsilon} \left| \left(\vec{E}(\vec{r},t) \right)_{\omega,k} \right|^2 , \tag{4.5}$$

where c is the light velocity in vacuum. In order to draw a parallel between the amplitude of the electric dipole $\vec{e}$ and the intensity I one should use the following rule. The dipole should be situated at the centre of the computation domain. A test calculation is carried out in which the electric field amplitude induced by the dipole is obtained. The intensity induced depends on the size of the computational domain and, if the size is changed, the amplitude of the electric dipole must be increased and the test calculation must be repeated.

4.3 Nonlinear waveguides for integrated optical circuits

4.3.1 Line-defect nonlinear photonic crystal waveguide

Fig. 4.10 (a) shows the geometry of the line-defect nonlinear photonic crystal waveguide, which is made by removing a row of rods in the ΓX direction of the first BZ. In order to calculate the dispersion characteristics of such a structure, the super cell approach is used. As Fig. 24 (a) shows, the super cell

UNIVERSITAT ROVIRA I VIRGILI
MODELLING OF PHOTONIC COMPONENTS BASED ON ÷(3) NONLINEAR PHOTONIC CRYSTALS
Ivan Maksymov
ISBN:978-84-593-4072-1/DL:T-1163-2010

(grey area) takes both the defect and the surrounding rows of rods into account. The material parameters are as follows. The intensity-independent dielectric constant of the rods is $\varepsilon = 11.56$ (AlGaAs) and the Kerr coefficient is $\chi^{(3)} = 4.4 \cdot 10^{-19} m^2 / V^2$ (see Appendix A). The background material is air with $\varepsilon = 1$ and $\chi^{(3)} = 0$. The radius of each rod is $r = 0.18a$. Fig. 4.10 (b) shows the dispersion characteristics (only the defect mode) calculated for the ΓX direction of the first BZ. It should be noticed that the defect mode no longer exists within the

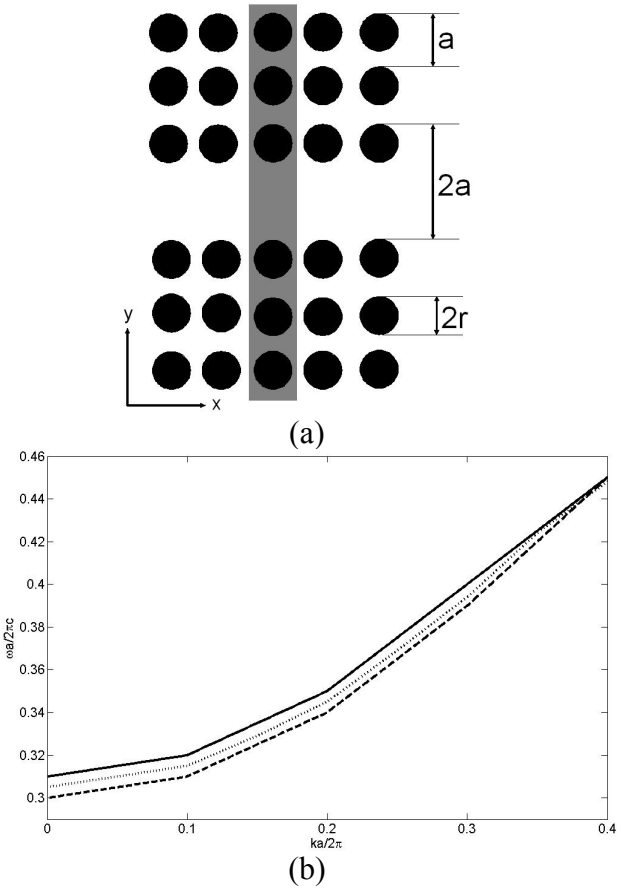

Fig. 4.10. (a) The geometry of the line-defect nonlinear photonic crystal and (b) its dispersion characteristic.

ISBN:978-84-593-4072-1/DL:T-1163-2010

forbidden band gap for $\omega a / 2\pi c > 0.4$ and, therefore, this range of frequencies is not shown. The solid line corresponds to the linear dispersion characteristic whereas the dot and dash lines correspond to the nonlinear dispersion characteristics calculated at the incident intensities of $19 GW/cm^2$ and $26 GW/cm^2$, respectively. These values have been calculated at $ka/2\pi = 0$ by using Eq. (4.5). It can be seen that in the nonlinear regime the dispersion curves are red-shifted with regard to the linear regime.

4.3.2 Coupled-cavity nonlinear photonic crystal waveguide

In this subsection, the dispersion characteristics of a coupled-cavity waveguide made in the nonlinear photonic crystal are presented. Fig. 4.11 (a) shows the geometry of this waveguide. Such a waveguide is based on evanescent coupling between modes of neighbouring resonators. As it was shown [10], in the linear regime the dispersion curve has a cosine form. The group velocity of this curve tends to be very small.

In order to carry out the calculation, the super cell is extended to take a resonator into account. The calculation usually takes less time because the dispersion curves are almost flat and therefore a small range of frequency is considered.

The dispersion curves calculated with the FDTD method are shown in Fig. 4.11 (b). The solid line corresponds to the linear dispersion characteristic whereas the dot and dash lines correspond to the nonlinear dispersion characteristics. The incident intensities are $9.5 GW/cm^2$ and $16 GW/cm^2$. These

UNIVERSITAT ROVIRA I VIRGILI
MODELLING OF PHOTONIC COMPONENTS BASED ON ÷(3) NONLINEAR PHOTONIC CRYSTALS
Ivan Maksymov
ISBN:978-84-593-4072-1/DL:T-1163-2010

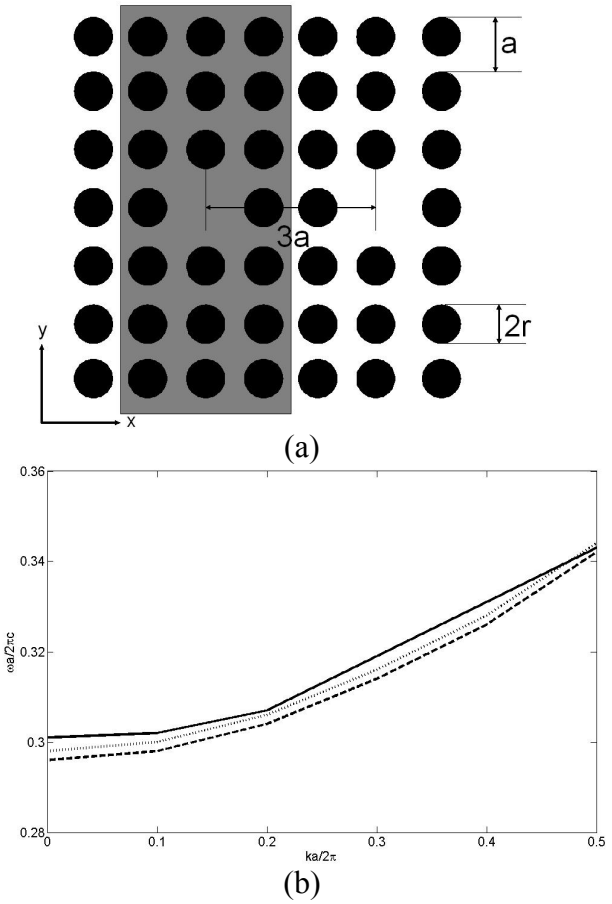

Fig. 4.11. (a) The geometry of the coupled-cavity nonlinear photonic crystal and (b) its dispersion characteristic.

values are calculated at $ka/2\pi = 0$. As it can be seen, for the nonlinear regimes there are again red-shifts. A tiny blue-shift at $ka/2\pi = 0.5$ is a numerical artefact due to a weak numerical noise that appears when calculating the electromagnetic energy density at the edge of the first BZ.

ISBN:978-84-593-4072-1/DL:T-1163-2010

4.3.3 Red-shift dependence on the group velocity

This subsection discusses the properties of the red-shift that has been obtained in calculations in the previous subsections. First, it should be noticed that the red-shift is not uniform along the ΓX direction of the first BZ (for example, in Fig. 4.10 for $k = 0$ it is larger than for $\omega a / 2\pi c > 0.4$). It can be explained by a difference in the group velocities, which correspond to different k-points. As it was shown earlier [10-11], the electric field in the waveguide mode is inverse proportional to the group velocity and the waveguide modes that correspond to lower group velocity, in turn, induce stronger nonlinear effects (for example larger red-shift). Fig. 4.12 presents the group velocities calculated by numerical differentiation of the frequency manifolds $\omega(\vec{k})$. The dash line represents the group velocity dispersion of the defect modes of the line-defect waveguide. The group velocity dispersion of the coupled-cavity waveguide is marked by the solid line. The result obtained demonstrates that the group velocities of both defect modes increase as the value of the wave vector increases. On the contrary, the red-shift

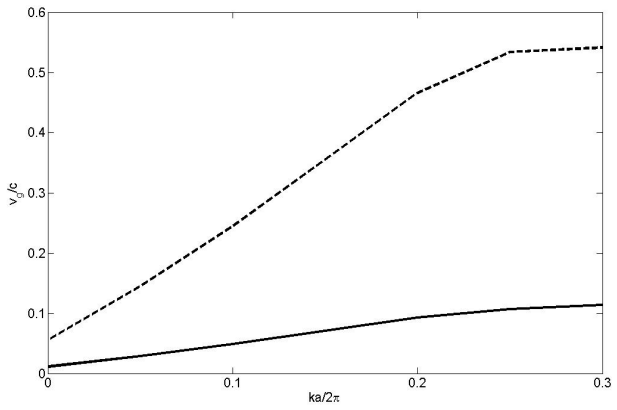

Fig. 4.12. Group velocity dispersion of the defect modes of the line-defect (dash line) and coupled-cavity (solid line) waveguides.

UNIVERSITAT ROVIRA I VIRGILI
MODELLING OF PHOTONIC COMPONENTS BASED ON ÷(3) NONLINEAR PHOTONIC CRYSTALS
Ivan Maksymov
ISBN:978-84-593-4072-1/DL:T-1163-2010

decreases as the wave vector increases. It confirms the above stated.

Second, it is seen that with the coupled-cavity waveguide one can achieve group velocities less that $0.1c$ (c denotes the light velocity), and thus a large decrease in the operating power. One can also use similar structures whose mode dispersion is specially engineered and achieve ultra small values of the group velocity [12-13]. Such structures are widely used in a variety of devices ranging from optical delay components to low-threshold lasers.

When developing optical devices, specific attention should be paid to the estimation of the intensity enhancement in the coupled-cavity waveguides. The intensity inside them is higher than that of the input pulse because the reduction of the group velocity results in the spatial compression of the pulse inside the cavities. In fact, the incident intensity applied to a coupled-cavity waveguide can be written as [14]

$$I = \frac{1}{2} v_{gr} \varepsilon_0 \varepsilon_{eff} \left| \left(\vec{E}(\vec{r},t) \right)_C \right|^2 , \tag{4.6}$$

where $\left| \left(\vec{E}(\vec{r},t) \right)_C \right|^2$ is the modulus square of the electric field inside the cavities and ε_{eff} is the effective dielectric constant, which is a function of the both the angular frequency and the intensity. Using Eq. (4.6) one obtains that the intensity inside the cavities is related to the incident intensity as

$$I_C = I \cdot S , \tag{4.7}$$

where $S = \dfrac{c}{v_{gr}\sqrt{\varepsilon_{eff}}}$ is the “slowing” or enhancement factor in accordance with the

ISBN:978-84-593-4072-1/DL:T-1163-2010

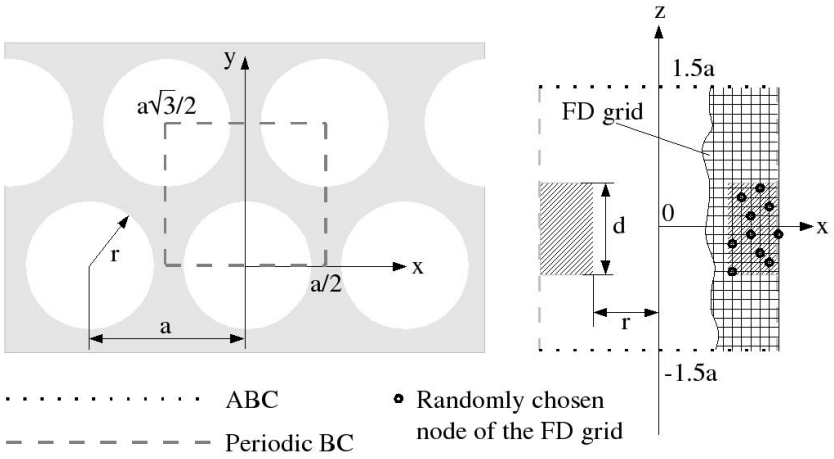

Fig. 4.13. The computational domain for the calculation of dispersion characteristics: (left) top view and (right) side section view. A part of the finite-difference (FD) grid is shown together with an example of random selection of nodes used for excitation.

definition given in section 2.2.2. The group velocities for the line-defect and the coupled-cavity waveguides taken at $ka/2\pi = 0.3$ are $0.53c$ and $0.11c$, respectively, By using these values and assuming that $\varepsilon_{eff} = 12.25$, we obtain $S = 0.54$ and $S = 2.6$, respectively.

Finally, it should be noticed that a twofold increase in the red-shift is not necessarily associated with a twofold increase in the intensity. This can be due to the nonlinear behaviour of the oscillating dipole (to author's knowledge, its behaviour in nonlinear photonic crystals is not yet studied). However, a similar result was obtained with the conventional FDTD (see the following section). It allows to draw a conclusion that the magnitude of the red-shift is increased by the intensity, but this dependence is not generally linear.

UNIVERSITAT ROVIRA I VIRGILI
MODELLING OF PHOTONIC COMPONENTS BASED ON ÷(3) NONLINEAR PHOTONIC CRYSTALS
Ivan Maksymov
ISBN:978-84-593-4072-1/DL:T-1163-2010

4.4 Nonlinear photonic crystal slabs

In this section, a photonic crystal (PC) slab with the triangular lattice of circular air rods ($a = 1$, $r = 0.24a$) in a Kerr nonlinear material ($\varepsilon' = 12$, $\chi^{(3)} = 0.01$) is considered. The PC slab, with a thickness of $d = 0.3a$ is suspended in air. Fig.

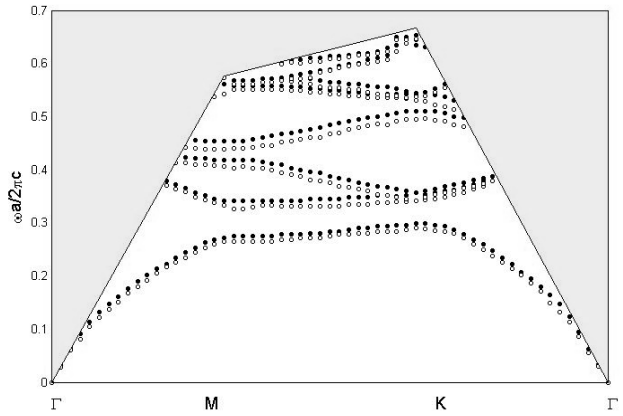

(a)

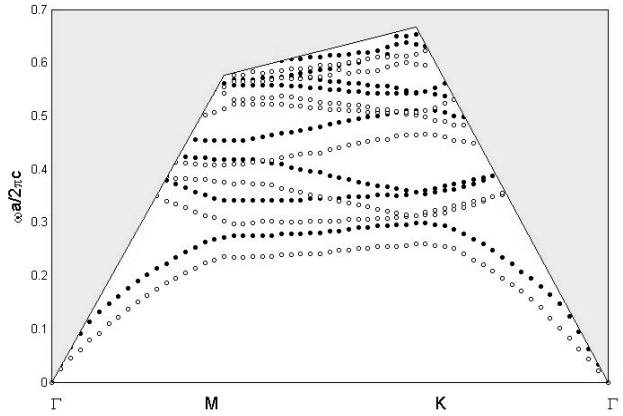

(b)

Fig. 4.14. Dispersion characteristics of the 2-D PC slab

ISBN:978-84-593-4072-1/DL:T-1163-2010

27 shows the computational domain for the calculation of the dispersion characteristic and the BC that are used to truncate it.

In the z-direction, the computational domain is divided into 70 cells. In the directions of the periodicity, it is divided into 200 cells. With this grid resolution, 3000 randomly chosen nodes are used for excitation. The total number of time steps is about $2^{14} \div 2^{15}$. On a 1.6 GHz Pentium IV processor with 512 Mb RAM, the calculation takes about 80 hours (20 values of the wave vector are taken into account in each direction of the irreducible Brillouin zone). In particular, the FDTD calculation takes about 75 percent of this time. The rest of time is used for postprocessing to obtain the spectral intensities. The postprocessing includes the field recording, filtering and fast Fourier transform routines.

Figs. 4.14 (a) and (b) show the dispersion characteristics (TE-like modes) calculated for the incident intensities $I_{inc} = 3000$ and $I_{inc} = 10000$ arbitrary units (a.u.), respectively. They are compared with the dispersion characteristic in the linear 2-D PC slab ($\chi^{(3)} = 0$, $I_{inc} = 1$ a.u.). The shaded region denotes the light cone. It can be seen that the dispersion curves of the dispersion characteristics in the nonlinear slab are red-shifted with regard to the linear regime and that the red-shift increases as the incident intensity increases. The dynamical change of the dispersion characteristic is the basis for intensity-driven optical limiting and all-optical switching and it is extremely important that it be understood if all-optical switching devices are to be modelled.

In the calculation, the incident intensities are given in the arbitrary units (a.u.). In order to make an estimation of the feasible incident intensities needed to induce the nonlinearity, a parallel between the a.u. and the SI units is drawn. It offers a problem because the incident intensity is simulated with the Dirac pulses

UNIVERSITAT ROVIRA I VIRGILI
MODELLING OF PHOTONIC COMPONENTS BASED ON ÷(3) NONLINEAR PHOTONIC CRYSTALS
Ivan Maksymov
ISBN:978-84-593-4072-1/DL:T-1163-2010

situated in the randomly chosen nodes of the FD grid. Therefore, the excitation strength depends on the chosen number of nodes, i.e. 1000 exciting nodes induce a much stronger nonlinearity than just exciting one. The solution of the problem is in comparing the results with those reported in the literature [8, 15]. In particular, the change in the dielectric constant and the incident intensity strength that has led to this change are confronted. It is obtained that using 3000 exciting nodes the intensity strength $I_{inc} = 1$ a.u. corresponds to an intensity of about $0.5W/cm^2$. A considerable decrease in the number of exciting nodes results in difficulties in finding the eigenfrequencies because of low resolution in the frequency domain. Any increase in the number of exciting nodes does not enhance this resolution.

In what follows, the results of the calculations are discussed. For the positive Kerr coefficient the value of $\Delta\varepsilon$ increases and the dispersion curves dynamically red-shift. This red-shift increases as the incident intensity increases.

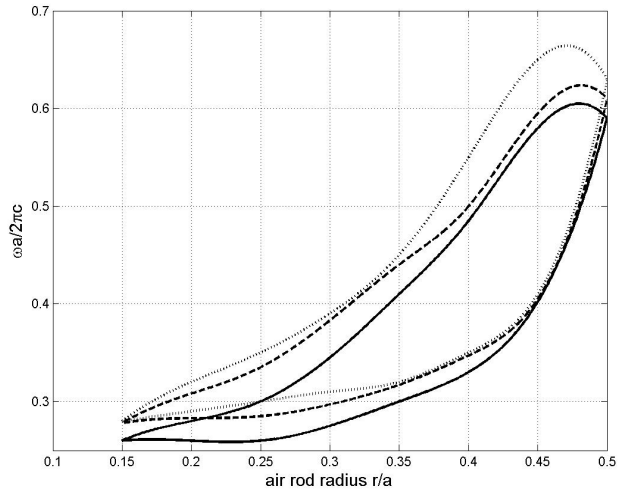

Fig. 4.15. Gap maps calculated for TE-like modes

UNIVERSITAT ROVIRA I VIRGILI
MODELLING OF PHOTONIC COMPONENTS BASED ON ÷(3) NONLINEAR PHOTONIC CRYSTALS
Ivan Maksymov
ISBN:978-84-593-4072-1/DL:T-1163-2010

For example, as can be seen from Fig. 4.14 (a), the applied intensity only shifts the dispersion curves slightly while a more than three-fold increase in the intensity (Fig. 4.14 (b)) shifts them significantly.

Fig. 29 presents the calculated gap map (TE-like modes) in the Kerr-nonlinear 2-D PC slab shown in Fig. 4.13. The dot line represents the linear gap map. The dash and solid lines represent two nonlinear gap maps calculated at the incident intensities $I_{inc} = 3000$ a.u. and $I_{inc} = 10000$ a.u., respectively. There are no band gaps in the TM-like modes for any rod radii and intensities. Therefore, there are no complete band gaps.

As can be seen from Fig. 4.15, the red-shift of the band gap is maximal when the air rod radius is in the range $0.2a$ to $0.25a$. This is because the portion of

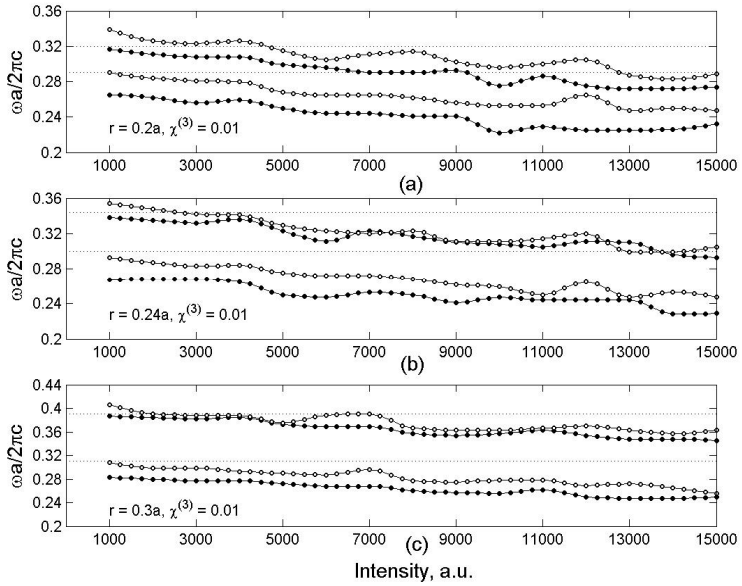

Fig. 4.16. Two lowest eigenfrequencies calculated at the K (open circle) and M (solid circle) points of the first BZ vs. incident intensity. The radius is changed. The Kerr coefficient is constant.

UNIVERSITAT ROVIRA I VIRGILI
MODELLING OF PHOTONIC COMPONENTS BASED ON ÷(3) NONLINEAR PHOTONIC CRYSTALS
Ivan Maksymov
ISBN:978-84-593-4072-1/DL:T-1163-2010

the nonlinear material decreases as the radius of the air rods increases. As a result, the red-shifting decreases. On the other hand, the portion of the nonlinear material increases as the radius of the air rods decreases. This decrease in the radius gives rise to evanescing band gaps.

In order to obtain more thorough information about the band gap, additional calculations are performed at the incident intensities which vary between 1000 and 15000 a.u. First, the value of the Kerr coefficient is fixed at $\chi^{(3)} = 0.01$ and calculations are performed for three different radii of air rods in the range $0.2a$ to $0.3a$. Secondly, the radius of air rods is fixed at $r = 0.24a$ and calculations are carried out for three different values of the Kerr coefficient.

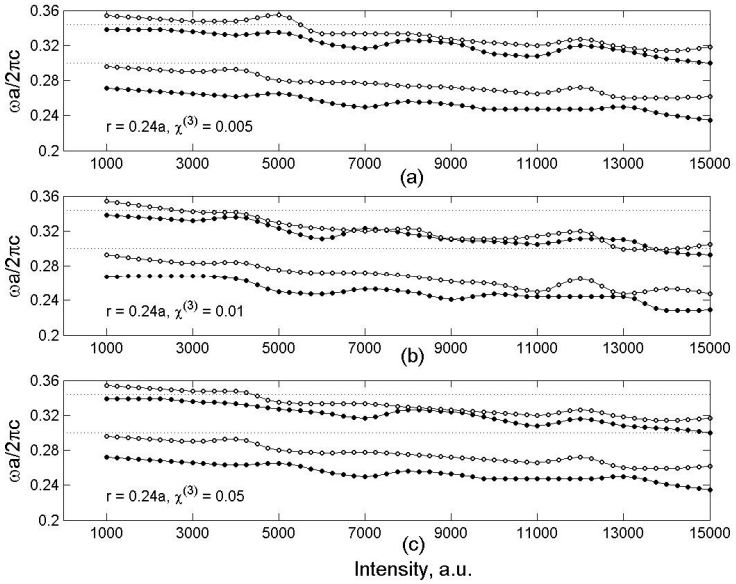

Fig. 4.17. Two lowest eigenfrequencies calculated at the K (open circle) and M (solid circle) points of the first BZ vs. incident intensity. The Kerr coefficient is changed. The radius is constant.

ISBN:978-84-593-4072-1/DL:T-1163-2010

Fig. 4.16 shows the two lowest eigenfrequencies calculated at the K (open circle) and M (solid circle) points of the Brillouin zone for the radii (a) $r = 0.2a$, (b) $r = 0.24a$ and (c) $r = 0.3a$. The Kerr coefficient is $\chi^{(3)} = 0.01$. The width of the band gap can be obtained using the information about the first and the second eigenfrequencies corresponding to the K and M points, respectively. The dot lines denote the edges of the bang gap in the linear 2-D PC slab. Fig. 30 confirms that the red-shift increases as the incident intensity increases. In addition, it shows that any uniform linear increase in the amplitude does not mean that the dispersion curves would be red-shifted on the same value of $\omega a / 2\pi c$ with regard to the previous shift.

Fig. 4.17 shows how the incident intensity influences the two lowest eigenfrequencies calculated at the same points of the Brillouine zone for the 2-D PC slab made of nonlinear materials with different values of the Kerr coefficient (a) $\chi^{(3)} = 0.005$, (b) $\chi^{(3)} = 0.01$ and (c) $\chi^{(3)} = 0.05$. The radius is $r = 0.24a$. The dot lines denote the edges of the bang gap in the linear 2-D PC slab. It can be seen that if the numerical value of $\chi^{(3)}$ is changed, the same red-shift is achieved by multiplying the incident intensity amplitude correspondingly.

Analysing the obtained results, the following conclusion is drawn. The high values of the nonlinearity lead to the instability of the field within the slab. It can be explained by the fact that the change of the permittivity is no longer linearly related to the incident intensity as it was in Kerr materials at moderate intensities [16]. It was also shown by Nerukh [17] that the instability of the field caused the oscillation of the value of the red-shift. It can explain the fluctuation of the curves in Figs. 4.16 and 4.17.

ISBN:978-84-593-4072-1/DL:T-1163-2010

4.5 Conclusions

To conclude, this chapter has presented and discusses the results of dispersion characteristics calculation for one- and two-dimensional Kerr nonlinear photonic crystals. In the one-dimensional case, the calculation has clearly shown the physicals processes that take place when the photonic crystal switches from the linear working regime to the nonlinear one. Similar results have been obtained for two-dimensional structures; both perfect lattices and lattices with defects have been considered. Another practical aspect – the influence of the light confinement in the third direction – has been studied by calculating and discussing dispersion characteristics of a nonlinear photonic crystal slab.

References

[1] A. Huttunen and P. Torma, “Band structures in nonlinear photonic crystals”, J. Appl. Phys. **91**, 3988 (2002).

[2] K. Sakoda, *Optical properties of photonic crystals* (Springer Verlag, Berlin, 2001).

[3] P. Tran, “Photonic-band-structure calculation of material possessing Kerr nonlinearity”, Phys. Rev. B **52**, 10673 (1995).

[4] S. Johnson and J. Joannopoulos, "Block-iterative frequency-domain methods for Maxwell's equations in a planewave basis," Opt. Express **8**, 173 (2001).

[5] M. Scalora, J.P. Dowling, C.M. Bowden, M.J. Bloemer, “Optical limiting and switching of ultrashort pulses in nonlinear photonic band gap materials”, Phys. Rev. Lett. **73**, 1368 (1994).

ISBN:978-84-593-4072-1/DL:T-1163-2010

[6] T. Ochiai and J. Sánchez-Dehesa, “Localized defect modes in finite metallic two-dimensional photonic crystals”, Phys. Rev. B **65**, 245111 (2002).

[7] B.Y. Soon, W. Haus, M. Scalora, C. Sibilia, “One-dimensional photonic crystal optical limiter”, Opt. Express **11**, 2007 (2003).

[8] M.D. Tocci, M.J. Bloemer, M. Scalora, J.P. Dowling, C.M. Bowden, “Thin-film nonlinear optical diode”, Appl. Phys. Lett. **66**, 2324 (1995).

[9] P. Xie and Z.-Q. Zhang, “Large enhancement of third-harmonic generation induced by coupled gap solitons in $\chi^{(3)}$ nonlinear photonic crystal”, Phys. Rev. E **71**, 026610 (2005).

[10] A. Yariv, Y. Xu, R. K. Lee, A. Scherer, “Coupled-resonator optical waveguide: a proposal and analysis”, Opt. Lett. 24, 711-713 (1999).

[11] N. Panoiu, M. Bahl, and R. Osgood, Jr., "All-optical tunability of a nonlinear photonic crystal channel drop filter," Opt. Express **12**, 1605 (2004).

[12] S. Mookherjea, “Dispersion characteristics of coupled-resonator optical waveguides”, Opt. Lett. **30**, 2406 (2005).

[13] H. Altug and J. Vuĉković, “Two-dimensional coupled photonic crystal resonator arrays”, Appl. Phys. Lett. **84**, 161 (2004).

[14] A. Yariv and P. Yeh, Optical waves in crystals (Wiley, New York, 1984).

[15] C. Lixue, D. Xiaoxu, D, Weiqiang, C. Liangcai and L. Shutian, “Finite-difference time-domain analysis of optical bistability with low threshold in one-dimensional nonlinear photonic crystal with Kerr medium”, Opt. Commun. **209**, 491 (2002).

[16] S. Trillo and W. Torruellas, *Spatial Solitons* (Springer, Berlin, 2001).

[17] A. G. Nerukh, F. V. Fedotov, T. M. Benson and P. Sewell, “Analytic-numerical approach to non-linear problems in dielectric waveguides”, Opt. Quantum Electron. **36**, 67 (2004).

UNIVERSITAT ROVIRA I VIRGILI
MODELLING OF PHOTONIC COMPONENTS BASED ON ÷(3) NONLINEAR PHOTONIC CRYSTALS
Ivan Maksymov
ISBN:978-84-593-4072-1/DL:T-1163-2010

Chapter 5

Numerical Design and Analysis of an All-Optical Switching Device

As was shown in Chapter 1, nonlinear photonic crystals [1] have been one of the most promising technologies for implementing integrated optical components. Among these components are all-optical [2-4] switches, which are fundamental components for high-speed communication systems and integrated optical circuits. The devices proposed in these studies are based on photonic crystal directional couplers originally studied in [5]. Generally, such all-optical switches can be divided into two groups. In the first group [3, 4], the switching exploits the nonlinearity of the material by controlling the intensity of the input signal. In the second group, the nonlinearity is exploited by launching a control beam but maintaining the intensity of the input signal invariable [2]. The devices in the second group seem to be more advanced and practical because they control light with light and thus take greater advantage of nonlinear optical effects.

UNIVERSITAT ROVIRA I VIRGILI
MODELLING OF PHOTONIC COMPONENTS BASED ON ÷(3) NONLINEAR PHOTONIC CRYSTALS
Ivan Maksymov
ISBN:978-84-593-4072-1/DL:T-1163-2010

In this chapter, the idea of controlling light with light is evolved and an all-optical switching device based on a nonlinear two-dimensional photonic crystal decoupler is proposed and discussed. Unlike photonic crystal couplers, photonic crystal decouplers minimize the cross-talk between two parallel photonic crystal waveguides [5-6]. Consequently, the all-optical switching device proposed is based on a concept that is in direct contrast to that of the device presented in [2]: it functions in the bar state when its working regime is linear and switches to the cross state in the nonlinear regime. In order to design the device, special care is taken to modify the coupling region between the two photonic crystal waveguides. A line of rods is introduced and the distance between them is varied. Thus, one obtains a slow wave structure (SWS) [7] that is used to enhance nonlinear effects and improve the efficiency of the device. A linear plane wave expansion (PWE) method is used to calculate dispersion characteristics and a nonlinear finite-difference time-domain (FDTD) method is applied to verify the design and analyse the device. As will be demonstrated below, the use of a linear PWE method is corroborated by a simulation with the nonlinear FDTD method.

5.1 Guided Mode Analysis of a Photonic Crystal Coupler and Decoupler

5.1.1 Conditions for Waveguide Coupling and Decoupling

Before describing the switch, the conditions required for waveguide

UNIVERSITAT ROVIRA I VIRGILI
MODELLING OF PHOTONIC COMPONENTS BASED ON ÷(3) NONLINEAR PHOTONIC CRYSTALS
Ivan Maksymov
ISBN:978-84-593-4072-1/DL:T-1163-2010

coupling and decoupling shall be discussed. Both directional couplers and decouplers consist of two line waveguides obtained by removing two rows of rods from a square lattice. The insets in Figs. 5.1 (a) and (b) schematically show the possible geometries of these devices. The radius of the rods is taken to be r = 0.2a, where a is the lattice constant. In order to operate at the wavelength $\lambda = 1.55$ μm, widely used in telecommunications, the lattice constant is taken to be a = 510 nm and the refractive index of the rods n = 3.4 (AlGaAs). If one takes AlGaAs below the half of the electronic band gap, its nonlinear refractive index is $n_2 = 1.5 \cdot 10^{-17}$ m^2/W [8]. From the dispersion characteristic shown in Fig. 5.1 (a) the coupling length of the coupler can be calculated as

$$L_C = 2\pi \left| k_{even} - k_{odd} \right|^{-1}, \tag{5.1}$$

where k_{even} and k_{odd} are, respectively, the values of the normalized wave vectors for the even and odd modes with respect to the propagation axis taken at a fixed frequency. The dispersion characteristics were calculated with the MIT MPB package [9] for the TM polarization (the electric field is parallel to the rods) and the ΓX direction of the first Brillouine zone.

The dispersion characteristic and the schematic (see inset) of the structure proposed in [5] for carrying out the waveguide decoupling are shown in Fig. 5.1 (b). A new row of rods made from the same nonlinear material was introduced into the coupling region. These rods were shifted by half a lattice constant in the direction parallel to the waveguides. This additional row of rods makes the odd and even modes cross, thus fulfilling the necessary conditions for waveguide decoupling. It can be seen that the third mode is detached from the

ISBN:978-84-593-4072-1/DL:T-1163-2010

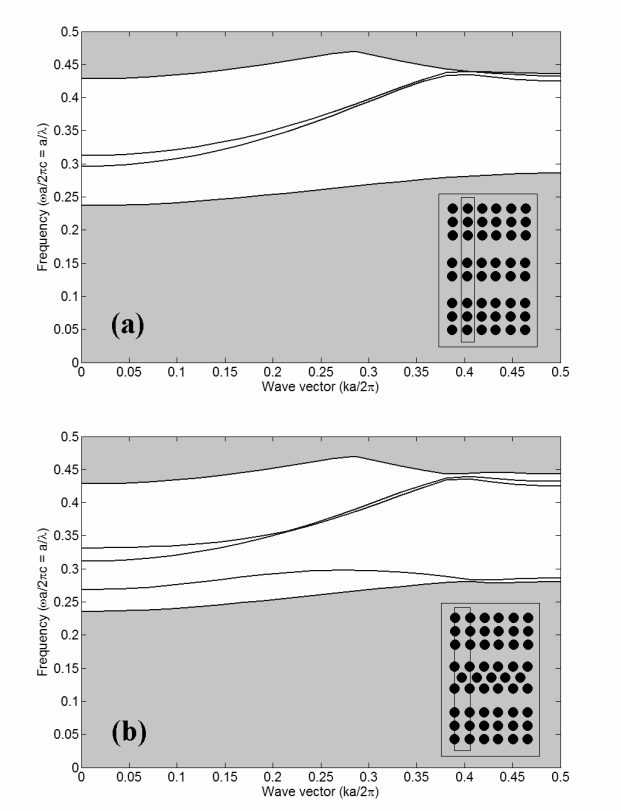

Fig. 5.1. Dispersion characteristics of the (a) coupler and (b) decoupler. The insets show the geometries and the super cells used to calculate the dispersion characteristics.

bottom of the forbidden band gap and it now lies below these two modes. This mode corresponds to the waveguide formed by the additional row of rods and it is not excited at the frequency at which the odd and even modes intersect. This waveguide can be used to dynamically control the cross-talk between the line photonic crystal waveguides by coupling or decoupling them depending on the intensity level.

UNIVERSITAT ROVIRA I VIRGILI
MODELLING OF PHOTONIC COMPONENTS BASED ON ÷(3) NONLINEAR PHOTONIC CRYSTALS
Ivan Maksymov
ISBN:978-84-593-4072-1/DL:T-1163-2010

5.1.2 Switch Architecture

When designing an all-optical switching device, one should bear in mind that the nonlinearities of materials such as AlGaAs are very weak, which means that very long devices or very high optical powers are required. This problem is solved using optical slow wave structures (SWS's) [7] similar to those used in microwave devices and masers. The main feature of SWS's is the considerable

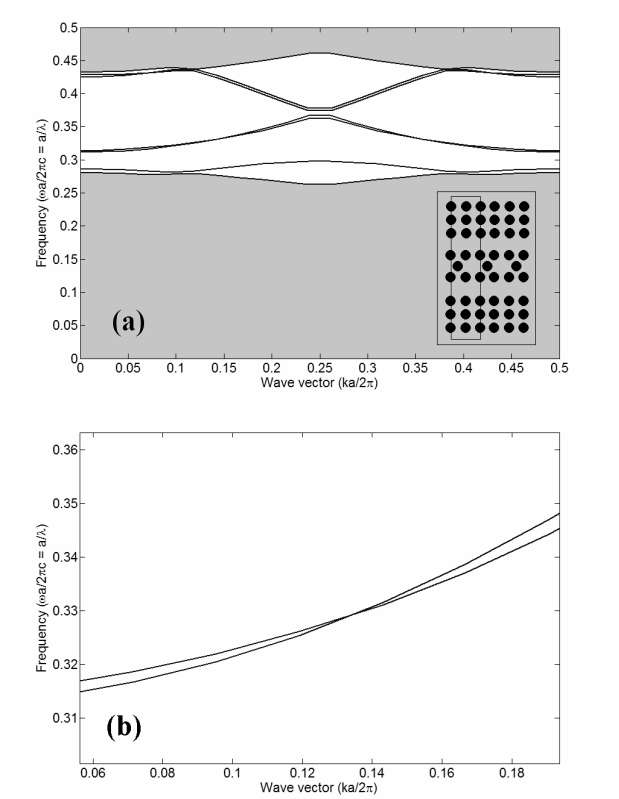

Fig. 5.2. (a) Dispersion characteristic and the schematic (inset) of the proposed device. (b) Zoomed region of the dispersion characteristic showing the intersection of the odd and even modes.

ISBN:978-84-593-4072-1/DL:T-1163-2010

reduction in the group velocity and, therefore, the enhancement of the propagation parameters by a factor called the slowing ratio $S = c/(v_{gr}\sqrt{\varepsilon_{eff}})$ [7, 10], where c is the light speed, v_{gr} is the group velocity in the SWS and ε_{eff} is the effective dielectric constant. As an example of implementation, an SWS can be made by introducing defects into a photonic crystal [11].

In this study, an SWS is implemented to control the cross-talk between the waveguides and to design an all-optical switching device. Launching the control beam into the SWS induces a considerable change in the refractive index of the dielectric rods. It makes it possible to switch the device either to the bar or the cross state. In order to create an SWS, the geometry of the additional row of rods is modified by doubling the distance between the rods. Fig. 5.2 (a) shows the schematic and the dispersion characteristic of the proposed device. Fig. 5.2 (b) shows a zoomed region of the dispersion characteristic where the odd and even modes are crossed. As can be seen from Fig. 5.2 (b), the odd and even guided modes cross at the frequency $\omega a/2\pi c = a/\lambda = 0.329$. At this frequency, the waveguides are decoupled and no wave can be propagated from one waveguide to another. This means that in the linear regime (i.e. when the refractive index of the nonlinear rods is not changed by the control beam), the device will function in the bar state. In the nonlinear regime, however, it is expected to function in the cross state.

Fig. 5.3 (a) illustrates how the dispersion characteristic changes when the device functions in the nonlinear regime. The dispersion characteristic was calculated for the same geometry, but the refractive index of the rods that make up the SWS was assumed to have increased uniformly by 10 %. Such an increase was selected only in order to demonstrate the change in the dispersion

ISBN:978-84-593-4072-1/DL:T-1163-2010

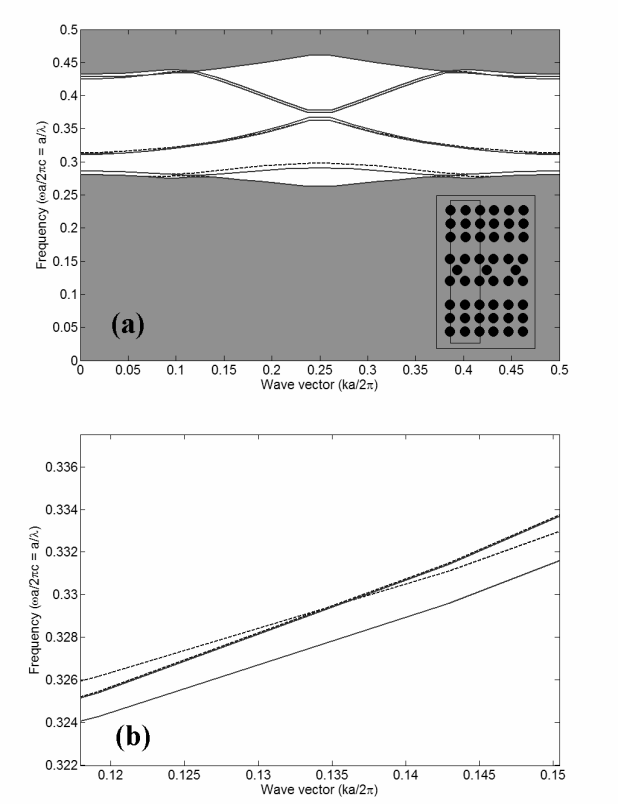

Fig. 5.3. (a) Solid lines correspond to the dispersion characteristic shown in Fig 5.2 (a). Dashed lines indicate the dispersion characteristic of the same structure, but with the changed refractive index of the defect rods. (b) Zoomed region of the dispersion characteristic showing the change caused by the uniform increase in the refractive index of the defect rods.

characteristic more clearly. The conclusions made under this assumption will be further generalized for a smaller increase in the refractive index.

Like Fig. 5.2 (b), Fig. 5.3 (b) shows a zoomed region of the dispersion characteristic presented in Fig. 5.3 (a). In the nonlinear regime, there were two important changes in the dispersion curves due to the increase in the refractive index of the rods that make up the SWS. The first change is the red-shift of the

UNIVERSITAT ROVIRA I VIRGILI
MODELLING OF PHOTONIC COMPONENTS BASED ON ÷(3) NONLINEAR PHOTONIC CRYSTALS
Ivan Maksymov
ISBN:978-84-593-4072-1/DL:T-1163-2010

guided mode of the SWS. It is very important to take this shift into account when choosing the frequency of the control beam. The second change becomes apparent if one closely examines the graph around the frequency $a/\lambda = 0.329$. It can be seen that at this frequency the two waveguides are not decoupled when the refractive index changes. In addition, it can be seen that the phase shift Δk between the odd and even modes becomes large enough to consider the device as a directional coupler. Indeed, if the values of the normalized wave vector for the even and odd modes are measured and put into (5.1), one obtains $L_c = 0.5a \cdot (0.1426 - 0.1353)^{-1} \approx 68.5a$. The device of this length will be analyzed numerically in the following section.

5.2 Numerical Analysis of the All-Optical Switching Device

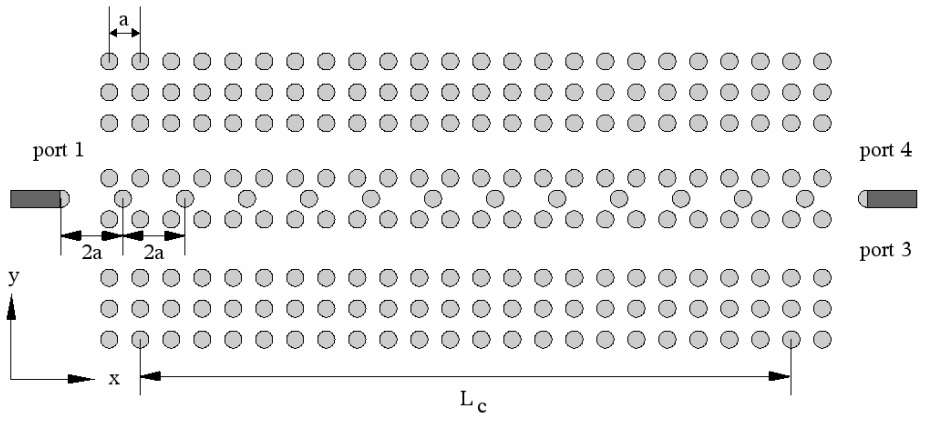

Fig. 5.4. Schematic of the device analyzed by the FDTD method.

UNIVERSITAT ROVIRA I VIRGILI
MODELLING OF PHOTONIC COMPONENTS BASED ON ÷(3) NONLINEAR PHOTONIC CRYSTALS
Ivan Maksymov
ISBN:978-84-593-4072-1/DL:T-1163-2010

In order to analyze the all-optical switching device, a 2-D nonlinear FDTD code based on the approach described in [12] and the CPML boundary conditions [13] are used. Fig. 5.4 shows the schematic of the simulated device. In the x- and y-directions, the device consists of 72 and 12 periods, respectively. In these directions, the computation domain is divided into 1600 and 240 cells. Each period consists of 20x20 cells. Here 30000 time steps are made to completely simulate the propagation of the input signal from Port 1 to Port 3 or Port 4. A taper similar to the one presented in [14] connects the optical wire waveguide that is used to inject the control beam into the SWS. The distance between the end of the optical wire and the first rod of the SWS is 2a. The input signal is launched into Port 1 and it is expected to be outputted in either Port 3 or Port 4, depending on the working regime.

The point sources are used for excitation. In both cases, the CW modulated

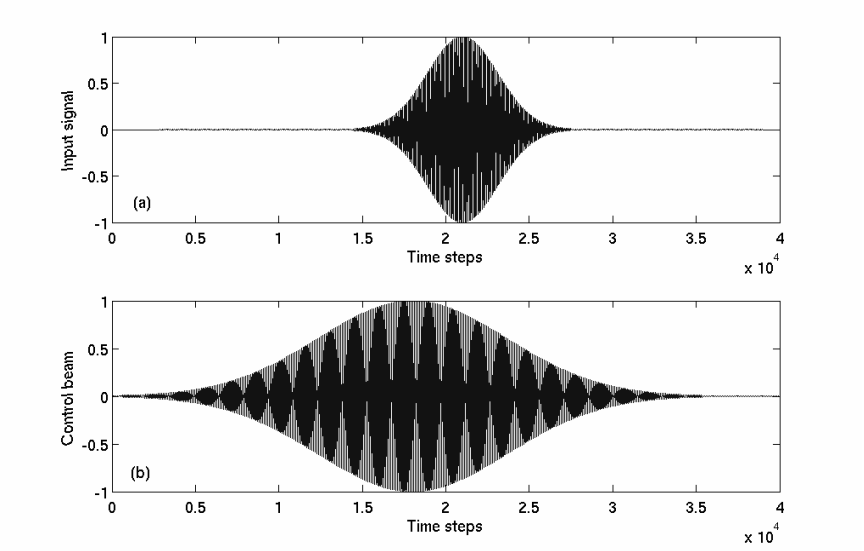

Fig. 5.5 Time delay between the input signal (a) and the control beam (b).

UNIVERSITAT ROVIRA I VIRGILI
MODELLING OF PHOTONIC COMPONENTS BASED ON ÷(3) NONLINEAR PHOTONIC CRYSTALS
Ivan Maksymov
ISBN:978-84-593-4072-1/DL:T-1163-2010

Gaussian pulses with spectra centered at the frequencies $a/\lambda = 0.329$ and $a/\lambda = 0.289$ are launched. The choice of the first frequency is explained in the second section. The second frequency is for the control beam. At this frequency the electric field localizes within the dielectric rods. The control beam and the input signal are launched at different time steps because their group velocities are different (0.05c and 0.27c, respectively). Fig. 5.5 shows the time delay between the input signal and the control beam. The amplitudes of both the signals are normalized for the sake of simplicity. This delay is intended to synchronize the coupling. In the time domain, the control beam is centered at the 18000th time step. Due to the temporal compression that this beam experiences in the SWS, its width is chosen to be greater than that of the input signal, which is launched with a delay of 3000 time steps.

Figs. 5.6 (a) and (c) show the distributions of the electric field of the all-

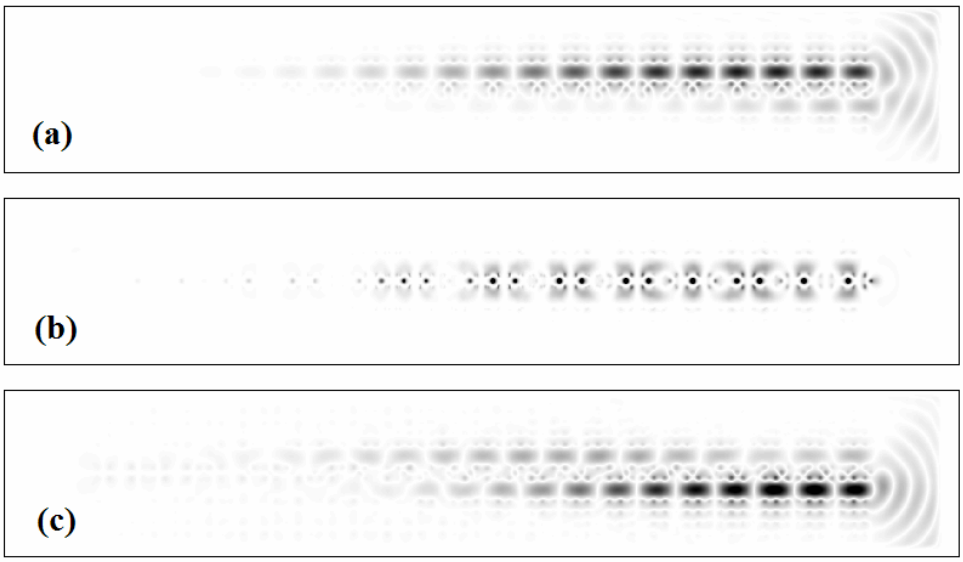

Fig. 5.6. Field distributions of the all-optical switching device simulated for the linear (a) and nonlinear (c) regimes. (b) Electric field distribution of the SWS.

UNIVERSITAT ROVIRA I VIRGILI
MODELLING OF PHOTONIC COMPONENTS BASED ON ÷(3) NONLINEAR PHOTONIC CRYSTALS
Ivan Maksymov
ISBN:978-84-593-4072-1/DL:T-1163-2010

optical switch. These field distributions are calculated for the linear and the nonlinear regimes, respectively. Fig. 5.6 (b) shows the distribution of the modulus square of the electric field injected into the SWS. All the fields presented in Fig. 5.6 are outputted after 26000 time steps.

As it can be seen from Fig. 5.6(a), the input signal is inputted in Port 1 and outputted in Port 4. This means that in the linear regime the waveguides are decoupled and the switch functions in the bar state. In Fig. 5.6(c), however, the input signal is launched in Port 1 but outputted in Port 3. This happened because the intensity of the control beam increased the refractive index of the rods that make up the SWS. This increase coupled the waveguides, which means that in the nonlinear regime the switch functions in the cross state. These results validate the switch architecture proposed and analyzed by means of the dispersion characteristic calculation in section two. The functionality demonstrated with the FDTD simulator shows that this switching device is different from those presented earlier [2-4, 21] in which the cross and the bar states are possible in the linear and nonlinear regimes, respectively.

All the computations presented so far have been made under the assumption that the device is very short and that the intensity of the control beam is very high. Here the length of a feasible all-optical switching device is estimated and the intensity of the control beam required for this length is calculated. It is evident that longer lengths will result in lower intensities being required to perform the switching. An intensity level of ~10 GW/cm^2 is frequently used in experimental work [15-18], and it can be further reduced if the length of the device is decreased. From the FDTD calculation, one can output the amplitude of the electric field taken at some nodes of the finite-difference grid situated within the rods of the SWS. The intensity of the control beam I, which is to be injected

ISBN:978-84-593-4072-1/DL:T-1163-2010

into the SWS, can be calculated by considering that it is related to the intensity inside the SWS, as in [19]

$$I = \frac{I_{SWS}}{S}, \tag{5.2}$$

where $S = c/(v_{gr} n_{eff})$ is the slowing factor [7] and v_{gr} is the group velocity in the SWS. The intensity inside the SWS is [20]

$$I_{SWS} = \frac{1}{2} c \varepsilon_0 n_{eff} |E|^2, \tag{5.3}$$

where E is the amplitude of the electric field in the SWS, ε_0 is the electric permittivity, and $n_{eff} = n + \Delta n$, where Δn is the increase in the refractive index. By substituting (5.3) into (5.2), we derive the expression that computes the intensity of the control beam that should be injected into the SWS

$$I = \frac{1}{2} v_{gr} \varepsilon_0 n_{eff}^2 |E|^2, \tag{5.4}$$

At the frequency $a/\lambda = 0.289$ the group velocity is $v_{gr} = 0.05c$ and the modulus square of the electric field is $|E|^2 = 4 \cdot 10^{18}$ V^2/m^2. These values give rise to a peak optical intensity of ~300 GW/cm^2. This result can be corroborated numerically by taking the amplitude of the electric field at the entrance point of the SWS and using (5.3). This result is in good agreement with that obtained using (5.4).

UNIVERSITAT ROVIRA I VIRGILI
MODELLING OF PHOTONIC COMPONENTS BASED ON ÷(3) NONLINEAR PHOTONIC CRYSTALS
Ivan Maksymov
ISBN:978-84-593-4072-1/DL:T-1163-2010

In what follows, it is assumed that the coupling length increases linearly as the intensity decreases. This can be checked by performing a subsidiary simulation of the structure shown in Fig. 5.4. In this simulation, the refractive index of the rods of the SWS is changed by 20 % and the coupling length achieved is roughly half of that required at a 10 % change. Therefore, in order to achieve the switching with an intensity of 10 GW/cm^2, one should make the device approximately thirty times longer (i.e. it should be about 1 mm long). This length is comparable with that of similar devices presented in [2, 21], which were also constructed on the basis of rod-type photonic crystals. The research interest that photonic crystals of this type have aroused can be seen in the numerous scientific articles published [22-24].

5.3 Conclusions

To conclude, an all-optical switching device based on a nonlinear photonic crystal decoupler has been presented and analyzed. In this device, the nonlinear effects have been enhanced with a slow wave structure embedded into the coupling region. The dispersion characteristics of the device have been calculated with the plane wave expansion method and its behaviour has been examined with the finite-difference time-domain method. Its smallness and low power consumption mean that it can be used for integrated optical circuits.

ISBN:978-84-593-4072-1/DL:T-1163-2010

References

[1] R. E. Slusher and B. J. Eggleton, *Nonlinear Photonic Crystals (*Springer-Verlag, Berlin, 2003).

[2] F. Cuesta-Soto, A. Martínez, J. García, F. Ramos, P. Sanchis, J. Blasco, and J. Martí, "All-optical switching structure based on a photonic crystal directional coupler," Opt. Express **12**, 161 (2004).

[3] A. Locatelli, D. Modotto, D. Paloshi and C. De Angelis, "All optical switching in ultrashort photonic crystal couplers," Opt. Commun. **273**, 97 (2004).

[4] I. S. Maksymov, L. F. Marsal, and J. Pallarès, "Dispersion characteristics of the nonlinear photonic crystal directional coupler," in Proc. 7th Int. Conf. Transparent Optical Networks, Barcelona, Spain, 2005, pp. 172-174.

[5] S. Boscolo, M. Midrio and C. G. Someda, "Coupling and decoupling of electromagnetic waves in parallel 2-D photonic crystal waveguides," IEEE J. Quantum. Electron. **38**, 47 (2002).

[6] T. Koponen, A. Huttunen and P. Törmä, "Conditions for waveguide decoupling in square-lattice photonic crystals", J. Appl. Phys., **96**, 4039 (2004).

[7] A. Melloni, F. Morichetti and M. Martinelli, "Linear and nonlinear pulse propagation in coupled resonator slow-wave optical structures," Opt. Quantum. Electron. **35**, 365 (2003).

[8] J. S. Aitchinson, D. C. Hutchings, J. U. Kang, G. I. Stegeman and A. Villeneuve, "The nonlinear optical properties of AlGaAs at the half band gap," IEEE J. Quantum Electron. **33,** 341 (1997).

[9] S. Johnson and J. Joannopoulos, "Block-iterative frequency-domain methods for Maxwell's equations in a planewave basis," Opt. Express **8**, 173 (2001).

ISBN:978-84-593-4072-1/DL:T-1163-2010

[10] M. Soljaĉić, S. G. Johnson, S. Fan, M. Ibanescu, E. Ippen and J. D. Joannopoulos, "Photonic-crystal slow-light enhancement of nonlinear phase sensitivity," J. Opt. Soc. Am. B **19**, 2052 (2002).

[11] A. Yariv, Y. Xu, R. K. Lee, A. Scherer, "Coupled-resonator optical waveguide: a proposal and analysis," Opt. Lett. **24**, 711 (1999).

[12] R. W. Ziolkowski, "The incorporation of microscopic material models into the FDTD approach for ultrafast optical pulse simulations," IEEE Trans. Antennas Propagat. **45**, 375 (1997).

[13] A. Taflove and S. Hagness, *Computational Electrodynamics* (Artech House, Boston, 2005).

[14] P. Bienstman, S. Assefa, S. G. Johnson, J. D. Joannopoulos, G. S. Petrich, and L. A. Kolodziejski, "Taper structures for coupling into photonic crystal slab waveguides," J. Opt. Soc. Am. B **20**, 1817 (2003).

[15] K. Al-hemyari, A. Villeneuve, J. U. Kang, J. S. Aitchinson, C. N. Ironside, and G. I. Stegeman, "Ultrafast all-optical switching in GaAlAs directional couplers at 1.55 μm without multifoton absorption," Appl. Phys. Lett. **63**, 3562 (1993).

[16] P. Millar, R. M. De La Rue, T. F. Krauss, J. S. Aitchinson, N. G. R. Broderick, and D. J. Richardson, "Nonlinear propagation effect in an AlGaAs Bragg grating filter," Opt. Lett. **24**, 685 (1999).

[17] X. Hu, Y. Liu, J. Tian, B. Cheng, and D. Zhang, "Ultrafast all-optical switching in two-dimensional organic photonic crystals," Appl. Phys. Lett. **86**, 121102 (2005).

[18] X. Hu, Q. Gong, Y. Liu, B. Cheng, and D. Zhang, "All-optical switching of the defect mode in two-dimensional nonlinear organic photonic crystals," Appl. Phys. Lett. **87**, 231111 (2005).

ISBN:978-84-593-4072-1/DL:T-1163-2010

[19] I. S. Maksymov, L. F. Marsal, and J. Pallarès, "An FDTD analysis of nonlinear photonic crystal waveguides," Opt. Quantum. Electron. **38**, 149 (2006).

[20] R. L. Sutherland, *Handbook of nonlinear optics* (Marcel Dekker, New York, 1996).

[21] F. Cuesta-Soto, A. Martínez, B. García-Baños, and J. Martí, "Numerical analysis of all-optical switching based on a 2-D nonlinear photonic crystal directional coupler," IEEE J. Select. Topic Quantum. Electron. **10**, 1101 (2004).

[22] S. Assefa, P. T. Rakich, P. Bienstman, S. G. Johnson, G. S. Petrich, J. D. Joannopoulos, L. A. Kolodziejski, E. P. Ippen, and H. I. Smith, "Guiding 1.5 μm light in photonic crystals based on dielectric rods," Appl. Phys. Lett. **85**, 6110 (2004).

[23] M. Tokushima, H. Yamada, and Y. Arakawa, "1.5-μm-wavelength light guiding in waveguides in square-lattice-of-rod photonic crystal slab," Appl. Phys. Lett. **84**, 4298 (2004).

[24] T. Tada, V. V. Poborchii, and T. Kanayama, "Channel waveguides fabricated in 2D photonic crystals of Si nanopillars," Microelectronic Engineering **63**, 259 (2002).

UNIVERSITAT ROVIRA I VIRGILI
MODELLING OF PHOTONIC COMPONENTS BASED ON ÷(3) NONLINEAR PHOTONIC CRYSTALS
Ivan Maksymov
ISBN:978-84-593-4072-1/DL:T-1163-2010

Chapter 6

Modelling of Two-Photon Absorption in Nonlinear Photonic Crystal All-Optical Switch

In Chapter 5, an all-optical switching device has been presented and simulated by means of the finite-difference time-domain (FDTD) method. A shortened model of the device has been considered and no loss has been taken into account. However, in order to model numerically a feasible all-optical switch, one should consider the two-photon absorption (TPA) because it imposes a severe limitation on the usefulness of all-optical devices that exploit the nonlinearity of materials [1]. A few papers have been published so far on studying this limitation in photonic crystal-based all-optical devices [2]. In this chapter, an approach of taking the TPA into account is proposed and applied to analyze an all-optical switch [3-4] by means of the FDTD method. Apart of presenting the approach, it is shown that although the TPA makes worse the efficiency of the device whose shortened model is considered, it does not impede its operation under realistic

ISBN:978-84-593-4072-1/DL:T-1163-2010

conditions.

6.1. Numerical details

This section is started with the formulae relating the conductivity σ to the intensity I. As is well known, the conductivity term is used to consider the absorption of materials when solving the Maxwell's equations. Naturally, it adds to the FDTD algorithm. The expressions relating the complex dielectric constant ($\varepsilon = \varepsilon_r + i\varepsilon_i$) to the complex refractive index ($\varepsilon = n_r + ik$) at the given wavelength λ [5] are:

$$\varepsilon_r = \varepsilon_0\left(n_r^2 - k^2\right), \tag{6.1}$$

$$\varepsilon_i = \varepsilon_0\left(2n_r k\right), \tag{6.2}$$

where ε_0 denotes the electric permittivity of free space ($8.854 \cdot 10^{-12}$ F/m). In the presence of the TPA the absorption coefficient can be written as [6]

$$\alpha = \alpha_0 + \alpha_2 I, \tag{6.3}$$

where α_0 and α_2 are respectively the linear and nonlinear absorption coefficients. For the most of materials commonly used in fabricating nonlinear photonic crystals (e.g. AlGaAs or Si), $\alpha_0 \approx 0$ at the wavelengths widely used in telecommunication systems [7]. The imaginary part of the refractive index is related to the absorption coefficient as $k = \lambda\alpha/(4\pi)$. Following the reasoning

ISBN:978-84-593-4072-1/DL:T-1163-2010

above, one can express it as

$$k = \frac{\alpha_2 I \lambda}{4\pi}. \tag{6.4}$$

After that we write the conductivity σ as

$$\sigma = \frac{2\pi c}{\lambda}\varepsilon_i \tag{6.5}$$

where c is the light speed in free space. Knowing that $I = \frac{1}{2} c \varepsilon_0 n_r \left|\vec{E}\right|^2$ where $\vec{E}$ is the electric field vector, Eqs. (6.2) and (6.4) are then used and the following formula for the conductivity is derived

$$\sigma = \frac{\alpha_2}{2} c^2 \varepsilon_0^2 n_r^2 \left|\vec{E}\right|^2. \tag{6.6}$$

Eq. (6.6) is then used together with the nonlinear FDTD algorithm. For example, for the TM polarization (the electric field is parallel to the rods) the finite-difference equations are written as

$$E_z^{n+1}(i,j) = \frac{\varepsilon_r^I(i,j) - \sigma^I(i,j)\frac{\Delta t}{2}}{\varepsilon_r^I(i,j) + \sigma^I(i,j)\frac{\Delta t}{2}} E_z^n(i,j)$$

UNIVERSITAT ROVIRA I VIRGILI
MODELLING OF PHOTONIC COMPONENTS BASED ON ÷(3) NONLINEAR PHOTONIC CRYSTALS
Ivan Maksymov
ISBN:978-84-593-4072-1/DL:T-1163-2010

$$+\frac{\Delta t}{\varepsilon_r^I(i,j)+\sigma^I(i,j)\frac{\Delta t}{2}}\cdot\left[\frac{H_y^{n+1/2}\left(i+\frac{1}{2},j\right)-H_y^{n+1/2}\left(i-\frac{1}{2},j\right)}{\Delta x}-\frac{H_x^{n+1/2}\left(i,j+\frac{1}{2}\right)-H_x^{n+1/2}\left(i,j-\frac{1}{2}\right)}{\Delta y}\right], \quad (6.7)$$

$$H_x^{n+1/2}\left(i,j+\frac{1}{2}\right)=H_x^{n-1/2}\left(i,j+\frac{1}{2}\right)-\frac{\Delta t}{\Delta y\mu_r}\cdot\left[E_z^n(i,j+1)-E_z^n(i,j)\right], \quad (6.8)$$

$$H_y^{n+1/2}\left(i+\frac{1}{2},j\right)=H_y^{n-1/2}\left(i+\frac{1}{2},j\right)+\frac{\Delta t}{\Delta x\mu_r}\cdot\left[E_z^n(i+1,j)-E_z^n(i,j)\right]. \quad (6.9)$$

$$\sigma^I(i,j)=\frac{\alpha_2(i,j)}{2}c^2\varepsilon_0^2\left\langle n_r^I(i,j)\right\rangle^2\left|E_z^{n+1}(i,j)\right|^2. \quad (6.10)$$

Similar expressions are obtained for the TE polarization.

In Eqs. (6.7) and (6.10), the superscript *I* means a dependence on the intensity because of the optical Kerr effect and the TPA. The dielectric constant and the refractive index with this superscript should be updated by using one of the existing nonlinear FDTD approaches. The Courant stability condition is still valid for Eqs. (6.7)-(6.10).

6.2. Results and discussion

The next step is to analyze an all-optical switch. Fig. 6.1 shows the schematic of the device [3, 4]. This is the same device considered in the previous chapter. In Fig. 6.1, all the rods of the square lattice are made from AlGaAs whose refractive index is $n_r = 3.4$, the nonlinear refractive index is $n_2 = 1.5\cdot10^{-17}$ m^2/W and the nonlinear absorption coefficient is $\alpha_2 = 10^{-13}$ m/W [6]. The radius of the rods is taken to be $r = 0.2a$, where $a = 510$ nm is the lattice constant. In the

UNIVERSITAT ROVIRA I VIRGILI
MODELLING OF PHOTONIC COMPONENTS BASED ON ÷(3) NONLINEAR PHOTONIC CRYSTALS
Ivan Maksymov
ISBN:978-84-593-4072-1/DL:T-1163-2010

x- and y-directions, the device consists of 72 and 12 rods, respectively. In these directions, the computation domain is divided into 1600 and 240 cells giving the resolution of 20x20 cells per period. The control beam of high intensity is inputted into the waveguide made by doubling the distance between the rods introduced into the coupling region. The input signal is inputted in Port 1 and outputted to Port 3 or Port 4 depending on the working regime. The point sources are used for excitation. In both cases, the CW modulated Gaussian pulses with spectra centred at the frequencies $a/\lambda = 0.329$ (input signal) and $a/\lambda = 0.289$ (control beam) are launched.

It should be stressed, that all the computations presented in this papers will be made under the assumption that the device modelled is very short and that the intensity of the control beam is very high. The application of a shortened model is required because the length of feasible photonic-crystal all-optical switches tends to be longer than that of photonic-crystal Mach-Zehnder interferometers [2] and thus their simulation becomes more time and memory consuming. It is evident that longer lengths will result in lower intensities being required to perform the

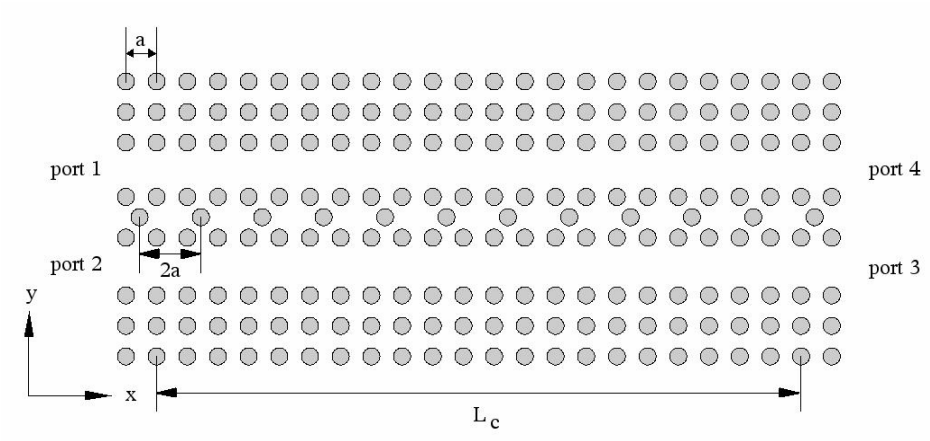

Fig. 6.1 Schematic of the analyzed device.

UNIVERSITAT ROVIRA I VIRGILI
MODELLING OF PHOTONIC COMPONENTS BASED ON ÷(3) NONLINEAR PHOTONIC CRYSTALS
Ivan Maksymov
ISBN:978-84-593-4072-1/DL:T-1163-2010

switching. Under the condition that the width of the switch is of 70 periods, the intensity required to perform the switching is of about 300 GW/cm^2 [3-4]. This intensity is not used in experimental work and therefore the impact of the TPA on the efficiency of the device will be overestimated. However, it was found convenient to demonstrate the viability of the approach.

As reported in [3, 4], in the linear regime, when the intensity of the control beam is low, the device functions in the bar state because the photonic crystal waveguides are decoupled. Here only the results for the nonlinear regime are presented. Figs. 6.2 and 6.3 show the electric field distributions of the all-optical switch calculated respectively for $\alpha_2 = 0$ and $\alpha_2 = 10^{-13}$ m/W. As we can see from Fig. 6.2 (a), the input signal is inputted in Port 1 and outputted in Port 3. This

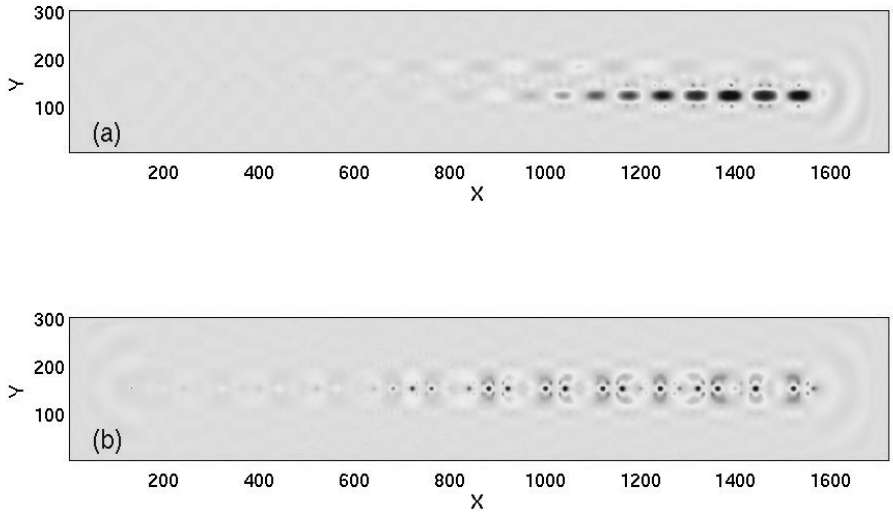

Fig. 6.2 Electric field distribution of the all-optical switch without the impact of the TPA: (a) input signal and (b) control beam.

ISBN:978-84-593-4072-1/DL:T-1163-2010

happened because the intensity of the control beam increased the refractive index of the rods that make up the waveguide over which the control beam propagates. This increase coupled the photonic crystal waveguides, which means that in the nonlinear regime the switch functions in the cross state. Fig. 6.2 (b) shows the distribution of the control beam for this case. From Fig. 6.3 (a), however, it can be seen that the input signal is inputted in Port 1 but is not completely outputted in Port 3. This happened because the control beam losses some of its energy due to the TPA. This loss can be seen in Fig. 6.3 (b) as a decreasing of the amount of the electric field concentrated within the rods that make up the waveguide for the control beam.

Transmission characteristics can also help to comprehend the impact of the TPA on the functionality of the device. Fig. 6.4 shows the normalized

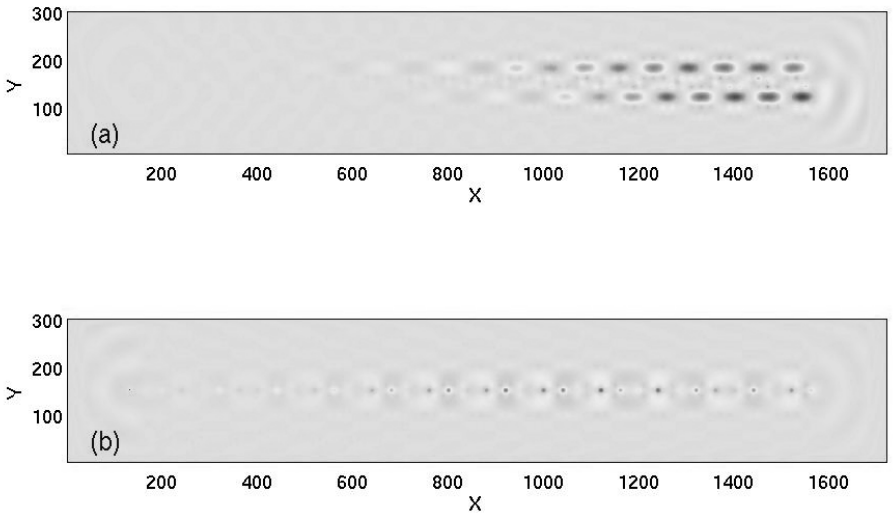

Fig. 6.3 Electric field distribution of the all-optical switch with the impact of the TPA: (a) input signal and (b) control beam.

ISBN:978-84-593-4072-1/DL:T-1163-2010

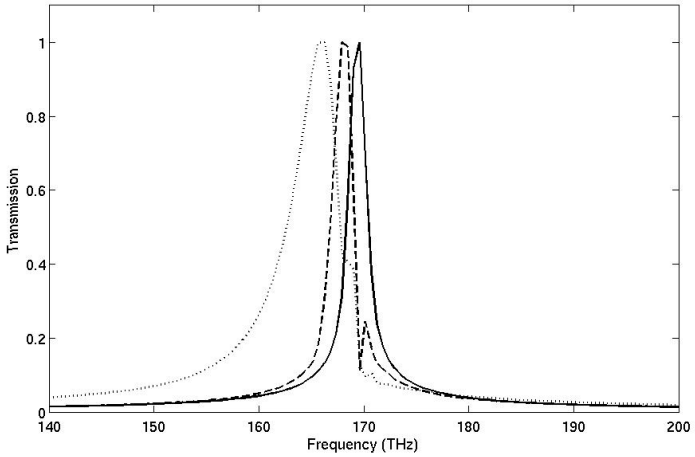

Fig. 6.4 Normalized transmission characteristics calculated for the linear (solid line), nonlinear without (dot line) and with the TPA (dash line) regimes

transmission characteristics of the waveguide for the control beam calculated for the linear (solid line) and nonlinear regimes. In the nonlinear regime, the dot and the dash lines correspond respectively to the transmission curves calculated for $\alpha_2 = 0$ and $\alpha_2 = 10^{-13}$ m/W. A technique for calculating the transmission characteristic of nonlinear photonic crystals was described in Ref. 8. The width of the Gaussian pulse launched into the waveguide covered a narrow band of wavelength at which the nonlinear absorption coefficient was assumed to be invariable.

As it can be seen from Fig. 6.4, in the nonlinear regime (in the both cases with and without TPA) the transmission curves are red-shifted with respect to that calculated for the linear regime. It can be explained by the typical shift of the waveguide mode that lies within the forbidden photonic band gap [3-4, 9]. In the presence of the TPA, however, this shift is weaker because a smaller amount of

the electric field is concentrated within the rods and therefore the strength of the nonlinear effect is reduced. It ensues that the shift of the transmission curve can measure the impact of the TPA. In particular, it is of importance when choosing the frequency of the control beam.

6.3 Conclusions

To conclude, an approach of taking into account the effect of the two-photon absorption has been presented and examined by the example of analyzing an all-optical switching device. A shortened model of the device has been used because the full-length simulation would require much computational cost. Due to the high intensity applied in the simulations, the impact of the two-photon absorption on the shortened model of the device is severe enough to impede the correct functionality. Therefore, the two-photon absorption should be borne in mind when designing practicable all-optical devices.

References

[1] J. S. Aitchison, M. K. Oliver, E. Kapon, E. Colas, and P. W. E. Smith, “Role of Two-Photon Absorption in Ultrafast Semiconductor Optical Switching”, Appl. Phys. Lett. **56**, 1305 (1990).

[2] T. Fujisawa and M. Koshiba, “Finite-element modeling of nonlinear Mach-Zehnder interferometers based on photonic-crystal waveguides for all-optical signal processing”, IEEE J. Ligthwave Techn. **24**, 617 (2006).

[3] I. S. Maksymov, L. F. Marsal and J. Pallares, “An all-optical switching

ISBN:978-84-593-4072-1/DL:T-1163-2010

structure based on the decoupling property of two parallel photonic crystal waveguides", in: Proceedings of the 15th International Workshop on Optical Waveguide Theory and Numerical Modelling, Varese, Italy, 2006.

[4] I. S. Maksymov, L. F. Marsal, and J. Pallarès, "Modelling of two-photon absorption in nonlinear photonic crystal all-optical switch", Opt. Commun. (accepted for publication).

[5] R. del Coso and J. Solis, "Relation between nonlinear refractive index and third-order susceptibility in absorbing media", J. Opt. Soc. Am. B **21**, 640 (2004).

[6] J. S. Aitchinson, D. C. Hutchings, J. U. Kang, G. I. Stegeman and A. Villeneuve, "The nonlinear optical properties of AlGaAs at the half band gap," IEEE J. Quantum Electron. **33,** 341 (1997).

[7] E. D. Palik, *Handbook of optical constants of solids* (Academic Press, New York, 1985).

[8] I. S. Maksymov, L. F. Marsal, and J. Pallarès, "Transmission spectra of 2D Kerr-nonlinear photonic band gap structures", in: Proceedings of the 2005 Spanish IEEE Conference on Electron Devices, Tarragona, Spain.

[9] I. S. Maksymov, L. F. Marsal, and J. Pallarès, "An FDTD analysis of nonlinear photonic crystal waveguides", Opt. Quantum. Electron. **38**, 149 (2006).

UNIVERSITAT ROVIRA I VIRGILI
MODELLING OF PHOTONIC COMPONENTS BASED ON ÷(3) NONLINEAR PHOTONIC CRYSTALS
Ivan Maksymov
ISBN:978-84-593-4072-1/DL:T-1163-2010

Chapter 7

Summary and conclusions

The work presented in this dissertation has dealt with the following subjects:

- development of the FDTD-based numerical approach for analysing dispersion characteristics of Kerr nonlinear photonic crystals;
- analysis of the basic characteristics of nonlinear one- and two-dimensional structures;
- design of an all-optical switching device and its analysis.

Since much potential applications of nonlinear photonic crystals are based on the dynamically tuneable shift of the forbidden band gap, the main attention has been paid to the analysis of dispersion characteristics. For this purpose, a novel finite-difference time-domain approach has been developed. The basics of the developed approach have been outlined in Chapter 3. In Chapter 4, the approach has been tested and used to calculate dispersion characteristics of Kerr nonlinear photonic crystals. First, one-dimensional structures have been

ISBN:978-84-593-4072-1/DL:T-1163-2010

considered. Secondly, two-dimensional structures have been considered for which the same calculations as those made in the one-dimensional case have been performed for both TE and TM polarisations. The investigation of these structures has allowed to gain understanding of how the nonlinearity affects the properties of photonic crystals and how one can make use of it in designing optical devices.

Thinking of optical devices, dispersion characteristics of such two-dimensional photonic crystal structures with defects as line-defect and coupled-cavity waveguides have been calculated and the impact of the group velocity has been discussed. In addition, the discussion has been extended to consider the influence of the confinement effect in nonlinear photonic crystal slabs.

In what follows, in Chapter 5, a novel all-optical switching device based on a nonlinear two-dimensional photonic crystal decoupler has been presented and analysed. When designing this device, the information on the possibility to dynamically control the properties of nonlinear photonic crystal waveguides has been used. In particular, an enhancement of nonlinear effects has been achieved with a slow wave structure embedded into the coupling region. The behaviour of the device has been examined by means of the FDTD method.

Chapter 6 shows how the two-photon absorption effect can be modelled with the FDTD method. An example of application is provided where the all-optical switch from Chapter 5 is modelled in presence of the two-photon absorption.

UNIVERSITAT ROVIRA I VIRGILI
MODELLING OF PHOTONIC COMPONENTS BASED ON ÷(3) NONLINEAR PHOTONIC CRYSTALS
Ivan Maksymov
ISBN:978-84-593-4072-1/DL:T-1163-2010

Future work

There are many possibilities for the future work. In author's opinion, one of the most interesting of them is the solution of the so-called inverse problem. Regarding to photonic crystal devices, this problem consists in the reconstruction or optimal design of the geometry of the photonic crystal. The inverse problem is closely related to the direct problem that has been solved in this dissertation. The solution of the direct problem consists in analysing or simulating a device with a previously defined geometry. In the inverse problem, the direct problem is included to be solved for many times within the main body of an optimization method.

The second possible direction consists in advancing as much as possible the FDTD source code. The design and analysis of feasible optical devices require to take into consideration lots of nonlinear effects such as, for example, the second-order nonlinearity, the Raman effect, etc. It also would be very interesting to mix nonlinear materials with metals or left-hand materials and thus try to achieve new possibilities of controlling light.

The third but very important thing that could be made is to perform full-dimensional 3-D FDTD simulations. The results of these simulations could be directly compared with those obtained in experiments.

UNIVERSITAT ROVIRA I VIRGILI
MODELLING OF PHOTONIC COMPONENTS BASED ON ÷(3) NONLINEAR PHOTONIC CRYSTALS
Ivan Maksymov
ISBN:978-84-593-4072-1/DL:T-1163-2010

Publications related to the thesis

Papers in international journals

I. S. Maksymov, L. F. Marsal and J. Pallarès, "Finite-difference time-domain analysis of band structures in one-dimensional Kerr non-linear photonic crystals", Opt. Commun. **239**, 213 (2004).

I. S. Maksymov, L. F. Marsal, M. A. Ustyantsev, and J. Pallarès, "Band structure calculation in two-dimensional Kerr non-linear photonic crystals", Opt. Commun. **248**, 469 (2005).

I. S. Maksymov, L. F. Marsal and J. Pallarès, "Band structures in non-linear photonic crystal slabs", Opt. Quantum. Electron. **37**, 161 (2005).

I. S. Maksymov, L. F. Marsal and J. Pallarès, "An FDTD analysis of nonlinear photonic crystal waveguides", Opt. Quantum. Electron. **38**, 149 (2006).

I. S. Maksymov, L. F. Marsal and J. Pallarès, "Numerical design and analysis of an all-optical switching device based on a nonlinear photonic crystal decoupler", IEEE Trans. Nanotechnology (submitted).

I. S. Maksymov, L. F. Marsal and J. Pallarès, "Modeling of two-photon

absorption in a nonlinear photonic crystal all-optical switch", Opt. Commun. (accepted for publication).

International conferences

I. S. Maksymov, L. F. Marsal and J. Pallarès, "Band structures in non-linear photonic crystal slabs", Proceedings of the 12th International Workshop on Optical Waveguide Theory and Numerical Modelling, Ghent, Belgium, March 22–23, 2004.

I. S. Maksymov, L. F. Marsal and J. Pallarès, "Non-linear photonic crystal waveguide analysis for integrated optical circuits", Proceedings of the 13th International Workshop on Optical Waveguide Theory and Numerical Modelling, Grenoble, France, April 8–9, 2005.

I. S. Maksymov, L. F. Marsal and J. Pallarès, "FDTD analysis of non-linear PBG waveguides for optical circuit applications", Proceedings of PECS-VI: International Symposium on Photonic and Electromagnetic Crystal Structures, June 19-24, Crete, Greece.

I. S. Maksymov, L. F. Marsal, and J. Pallarès, "Dispersion characteristics of the nonlinear photonic crystal directional coupler," in Proceedings of 7th IEEE International Conference on Transparent Optical Networks, (Barcelona, 2005), pp. 172-174.

I. S. Maksymov, L. F. Marsal and J. Pallarès, "An all-optical switching structure based on the decoupling property of two parallel photonic crystal waveguides", Proceedings of the 15th International Workshop on Optical Waveguide Theory and Numerical Modelling, Varese, Italy, April 19–21, 2006.

ISBN:978-84-593-4072-1/DL:T-1163-2010

National Spanish conferences

I. S. Maksymov, L. F. Marsal and J. Pallarès, "Transmission spectra of 2D Kerr non-linear photonic band gap structures", Proceedings of the 2005 Spanish Conference on Electron Devices, Tarragona, Spain, 2–5 February 2005.

I. S. Maksymov, L. F. Marsal and J. Pallarès, "A non-linear FDTD approach for dispersion characteristic calculation", Abstracts Book of the 3th Nanoelectronic and Photonic Systems Workshop, Tarragona, Spain, June 27-28, 2005.

I. S. Maksymov, L. F. Marsal and J. Pallarès, "Design and modelling of a nonlinear photonic crystal all-optical switch", XXII Trobades Científiques de la Mediterrània (accepted).

Other publications related to the thesis

National Ukrainian journals

G. I. Churyumov, **I. S. Maksymov** and D. B. Eremeev, "Mathematical modelling of electromagnetic phenomena by means of the finite-difference time-domain method. Part 1: Theory", Radiotechnika 135, 7 (2003) (in Russian).

G. I. Churyumov, **I. S. Maksymov** and D. B. Eremeev, "Mathematical modelling

of electromagnetic phenomena by means of the finite-difference time-domain method. Part 2: Boundary conditions and practical applications", Radiotechnika 136, 21 (2004) (in Russian).

International conferences

I. S. Maksymov and G. I. Churyumov, "2D computer modelling of waveguiding in 2D photonic crystals", Proceedings of the 4th International Laser and Fibre-Optical Network Modelling Conference (LFNM 2002), Kharkov, Ukraine, 2002.

I. S. Maksymov, G. I. Churyumov, "Modelling of light propagation in photonic crystals", 12th International Crimean Conference "Microwave & Telecommunication Technology", Sevastopol, Ukraine, 2002.

UNIVERSITAT ROVIRA I VIRGILI
MODELLING OF PHOTONIC COMPONENTS BASED ON ÷(3) NONLINEAR PHOTONIC CRYSTALS
Ivan Maksymov
ISBN:978-84-593-4072-1/DL:T-1163-2010

Appendix A

Maxwell's equations in SI and Gaussian systems of units

This appendix deals with some issues connected with the definition of the Maxwell's equations in the SI and Gaussian systems of units. In Table A.1, the Maxwell's equations are presented in the SI and Gaussian systems of units. Table A.2 presents the conversion factors for the first, second and third order nonlinear optical susceptibilities in the SI and Gaussian units. The basic SI and Gaussian electromagnetism units are compared in Table A.3. In the conclusive part, the intensity defined in the Gaussian system is related to that in the SI.

UNIVERSITAT ROVIRA I VIRGILI
MODELLING OF PHOTONIC COMPONENTS BASED ON ÷(3) NONLINEAR PHOTONIC CRYSTALS
Ivan Maksymov
ISBN:978-84-593-4072-1/DL:T-1163-2010

Table A.1. Maxwell's equation in the SI and Gaussian units.

Equation	Gaussian system	SI system
Electromagnetic energy density	$\frac{1}{8\pi}\left(\varepsilon\vec{E}^2+\mu\vec{H}^2\right)$	$\frac{1}{2}\left(\varepsilon\varepsilon_0\vec{E}^2+\mu\mu_0\vec{H}^2\right)$
Pointing vector	$\frac{c}{4\pi}\vec{E}\times\vec{H}$	$\vec{E}\times\vec{H}$
Maxwell's equations	$\nabla\times\vec{E}=-\frac{1}{c}\frac{\partial\vec{B}}{\partial t}$ $\nabla\times\vec{H}=\frac{1}{c}\frac{\partial\vec{D}}{\partial t}+\frac{4\pi}{c}\vec{J}$ $\nabla\cdot\vec{B}=0$ $\nabla\cdot\vec{D}=4\pi\rho$	$\nabla\times\vec{E}=-\frac{\partial\vec{B}}{\partial t}$ $\nabla\times\vec{H}=\frac{\partial\vec{D}}{\partial t}+\vec{J}$ $\nabla\cdot\vec{B}=0$ $\nabla\cdot\vec{D}=\rho$
Constitutive relations	$\vec{D}=\varepsilon\vec{E}=\vec{E}+4\pi\vec{P}_E$ $\vec{B}=\mu\vec{H}=\vec{H}+4\pi\vec{P}_M$	$\vec{D}=\varepsilon\varepsilon_0\vec{E}=\varepsilon_0\vec{E}+\vec{P}_E$ $\vec{B}=\mu\mu_0\vec{H}=\mu_0\vec{H}+\vec{P}_M$

Table A.2. Conversion factors for the first, second and third order nonlinear optical susceptibilities in the SI and Gaussian units.

Susceptibility	SI units	Gaussian units	Conversion factor (SI→Gaussian)
$\chi^{(1)}$	--	--	$\chi^{(1)} = 12.56\,\chi^{(1)}$
$\chi^{(2)}$	m/V	cm/statvolt	$\chi^{(2)} = 4.19\cdot10^{-4}\,\chi^{(2)}$
$\chi^{(3)}$	m^2/V^2	$cm^2/statvolt^2$	$\chi^{(3)} = 1.4\cdot10^{-8}\,\chi^{(3)}$

ISBN:978-84-593-4072-1/DL:T-1163-2010

Table A.3. SI and Gaussian electromagnetism units.

Name of quantity	**Symbol**	**SI system**	**Gaussian system**
Energy	W	1 J (joule)	10^7 erg
Intensity (power)	P	1 W (watt	10^7 erg·sec^{-1}
Current	I	1 A (ampere)	$3\cdot10^9$ cm$^{3/2}$·g$^{1/2}$ sec^{-2}
Electric charge	q	1 C (coulomb)	$3\cdot10^9$ cm$^{3/2}$·g$^{1/2}$ sec^{-1}
Electric field strength	$\vec{E}$	1 V/m (volt per meter)	$1/3\cdot10^{-4}$ g$^{1/2}$·cm$^{-1/2}$·sec^{-1}
Polarization	$\vec{P}$	1 C/m^2 (coulomb per squared meter)	$3\cdot10^5$ g$^{1/2}$·cm$^{-1/2}$·sec^{-1}
Electric field displacement	$\vec{D}$	1 C/m^2 (coulomb per squared meter)	$12\cdot10^5$ g$^{1/2}$·cm$^{-1/2}$·sec^{-1}
Conductivity	Σ	1 S/m (siemens per meter)	$9\cdot10^9$ sec^{-1}
Magnetic flux	$\vec{\Phi}$	1 Wb (weber)	10^8 M (maxwell)
Magnetic flux density	$\vec{B}$	1 T (tesla)	10^4 G (gauss)
Magnetic field strength	$\vec{H}$	1 A/m (ampere per meter)	$4\cdot10^{-3}$ Oe (Oersted)

UNIVERSITAT ROVIRA I VIRGILI
MODELLING OF PHOTONIC COMPONENTS BASED ON ÷(3) NONLINEAR PHOTONIC CRYSTALS
Ivan Maksymov
ISBN:978-84-593-4072-1/DL:T-1163-2010

Table A.4. Intensity in the SI and Gaussian units.

Conventional	Gaussian system		SI system	
I	I (erg/cm^2·sec)	E (statvolt/m)	I (W/m^2)	E (V/m)
1 W/cm^2	10^7	0.0458	10^4	$1.37\cdot10^3$
1 kW/cm^2	10^{10}	1.45	10^7	$4.34\cdot10^4$
1 MW/cm^2	10^{13}	45.8	10^{10}	$1.36\cdot10^6$
1 GW/cm^2	10^{16}	$1.45\cdot10^3$	10^{13}	$4.34\cdot10^7$
1 TW/cm^2	10^{19}	$4.85\cdot10^4$	10^{16}	$1.37\cdot10^9$

In the Gaussian system of units, the intensity associated with the field

$$\widetilde{E}(t) = Ee^{-i\omega t} + c.c \tag{A.1}$$

is

$$I = \frac{nc}{2\pi}|E|^2, \tag{A.2}$$

where n is the refractive index, c = $3\cdot10^{10}$ cm/sec is the speed of light in vacuum, I is measured in erg/cm^2, and E is measured in statvolts/cm.

In the SI system, the intensity of the field is given by

UNIVERSITAT ROVIRA I VIRGILI
MODELLING OF PHOTONIC COMPONENTS BASED ON ÷(3) NONLINEAR PHOTONIC CRYSTALS
Ivan Maksymov
ISBN:978-84-593-4072-1/DL:T-1163-2010

$$I = 2n\left(\frac{\varepsilon}{\mu_0}\right)^{1/2}|E|^2 = \frac{2n}{Z_0}|E|^2, \qquad \text{(A.3)}$$

where $\varepsilon_0 = 8.854\cdot10^{-12}$ F/m, $\mu_0 = 4\pi\cdot10^{-7}$ H/m, and $Z_0 = 377\Omega$. I is measured in W/m^2, and E is measured in V/m.

Table A.4 is obtained by using these relations. As a numerical example, a pulsed laser of modest energy might produce a pulse energy of Q=1mJ with a pulse duration of T=10nsec. The peak laser power would then be of the order of P=Q/T=100kW. If this beam is focused to a spot size of w_0=100μm, the pulse intensity will be $I=P/\pi w_0^2 \approx 0.3$GW/cm^2.

ISBN:978-84-593-4072-1/DL:T-1163-2010